

THE NEURAL RETINA IN PHOTORECEPTOR DEGENERATIONS

by

Bryan William Jones

A dissertation submitted to the faculty of
The University of Utah
in partial fulfillment of the requirements for the degree of

Doctor of Philosophy

Department of Physiology

The University of Utah

December 2003

Copyright © Bryan William Jones 2003

All Rights Reserved

THE UNIVERSITY OF UTAH GRADUATE SCHOOL

SUPERVISORY COMMITTEE APPROVAL

of a dissertation submitted by

Bryan William Jones

This dissertation has been read by each member of the following supervisory committee and by majority vote has been found to be satisfactory.





Chair: Robert Marc, Ph.D.



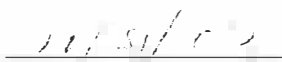


Thomas Parks, Ph.D.





Scott Rogers, Ph.D.





Mary Lucero, Ph.D.





Edward Levine, Ph.D.


THE UNIVERSITY OF UTAH GRADUATE SCHOOL

FINAL READING APPROVAL


To the Graduate Council of the University of Utah:


I have read the dissertation of Bryan William Jones in its final form and have found that (1) its format, citations, and bibliographic style are consistent and acceptable; (2) its illustrative materials including figures, tables, and charts are in place; and (3) the final manuscript is satisfactory to the supervisory committee and is ready for submission to The Graduate School.

Date 6.11.08


Chair: Supervisory Committee

Approved for the Major Department


Approved for the Graduate Council


David S. Chapman
Dean of The Graduate School

ABSTRACT

The mammalian retina is comprised of 55-60 cell types mediating transduction of photic information through visual preprocessing channels. These cell types fall into six major cell superclasses including photoreceptors, horizontal, amacrine, Müller and ganglion cells. Through computational molecular phenotyping, using amino acids as discriminands, this dissertation shows that the major cellular superclasses of the murine retina are subdivisible into the following natural classes: 1 retinal pigment epithelium class, 2 photoreceptor, 2 bipolar cell, 1 horizontal cell, 15 amacrine cell, 1 Müller cell, and 7 ganglion cell classes.

Retinal degenerative diseases like retinitis pigmentosa result in loss of photoreceptors, which constitutes deafferentation of the neural retina. This deafferentation, when complete, is followed by retinal remodeling, which is the common fate of all retinal degenerations that trigger photoreceptor loss. The same strategy used to visualize cell classes in wild type murine retina was applied to examples of retinal degenerative disease in human tissues and naturally and genetically engineered models, examining all cell types in 17 human cases of retinitis pigmentosa (RP) and 85 cases of rodent retinal degenerations encompassing 13 different genetic models. Computational molecular phenotyping concurrently visualized glial transformations, neuronal

translocations, and the emergence of novel synaptic complexes, achievements not possible with any other method. The fusion of phenotyping and anatomy at the ultrastructure level also enabled the modeling of synaptic connections, illustrating that the degenerating retina produces new synapses with vigor with the possibility that this phenomenon might be exploited to rescue vision. However, this circuitry is likely corruptive of visual processing and reflects, we believe, attempts by neurons to find synaptic excitation, demonstrating that even minor rewiring seriously corrupts signal processing in retinal pathways leaving many current approaches to bionic and biological retinal rescue unsustainable.

The ultimate conclusion is that the sequelae of retinal degenerative disease are far more complex than previously believed, and schemes to rescue vision via bionic implants or stem/engineered cells are based on presumed beliefs in preservation of normal wiring and cell population patterning after photoreceptor death. Those beliefs are incorrect: retinal neurons die, migrate, and create new circuitries. Vision rescue strategies will need to be refined.

TABLE OF CONTENTS

| | |
|-----------------------------------------------------------|------|
| ABSTRACT | iv |
| LIST OF FIGURES | viii |
| ACKNOWLEDGMENTS | x |
| INTRODUCTION | 1 |
| BACKGROUND AND SIGNIFICANCE | 8 |
| Normal retinal structure and cell populations | 9 |
| Amino acids and computational molecular phenotyping | 16 |
| Degenerate retinal structure and physiology | 20 |
| RESEARCH DESIGN AND METHODS | 31 |
| General | 32 |
| Terminology | 32 |
| Fixation and embedding | 32 |
| High performance immunohistochemistry | 36 |
| Embedding and sectioning | 34 |
| Digital image acquisition and analysis | 37 |
| Image analysis | 38 |
| Computational molecular phenotyping | 41 |
| Tissues and animal models | 47 |
| Electron microscopy | 49 |
| NORMAL MURINE EYE | 52 |
| Wild type CMP retinal atlas background | 53 |
| Normal eye structure and cell populations | 55 |
| Sclera | 55 |
| Uveal tract | 56 |

| | |
|--------------------------------------------------------|-----|
| Iris | 61 |
| Lens | 61 |
| Ciliary body | 64 |
| Choroid | 65 |
| Retina proper and the retinal pigment epithelium | 68 |
| Retinal pigment epithelium..... | 78 |
| Müller cells..... | 81 |
| Photoreceptors | 85 |
| Horizontal cells | 87 |
| Bipolar cells | 93 |
| Inner plexiform layer | 96 |
| Amacrine cells | 97 |
| Ganglion cells | 110 |
| Summary | 118 |
| | |
| DEGENERATE RETINA..... | 129 |
| | |
| Abstract..... | 130 |
| Introduction | 131 |
| Results..... | 134 |
| Discussion | 166 |
| | |
| SUMMARY DISCUSSION/FUTURE DIRECTIONS | 173 |
| | |
| BIBLIOGRAPHY | 178 |

LIST OF FIGURES

| <u>Figure</u> | <u>Page</u> |
|---------------------------------------------------------|-------------|
| 1. Eyeball cross-section with retina | 10 |
| 2. Fundoscopic image of RP with dissected retina | 22 |
| 3. Normal retinal amino acid immunohistochemistry | 24 |
| 4. Abnormal immunohistochemistry from RP retina | 26 |
| 5. Sectioning techniques | 35 |
| 6. Mosaicking and registration..... | 39 |
| 7. Univariate histograms..... | 42 |
| 8. Bivariate scale..... | 46 |
| 9. Vertical extra-retinal theme map | 57 |
| 10. Univariate extra-retinal histogram matrix..... | 59 |
| 11. Iris and lens image matrix | 62 |
| 12. Image matrix of ciliary body | 66 |
| 13. Theme map of rodent retina..... | 69 |
| 14. TQE→RGB vertical retinal section | 72 |
| 15. TQE→RGB whole retina horizontal section | 74 |
| 16. Whole retina histogram matrix..... | 76 |
| 17. Horizontal section through RPE | 79 |
| 18. TQE→RGB of human RP fovea | 83 |

| | | |
|-----|----------------------------------------------------------------|-----|
| 19. | Univariate signature matrix of the inner nuclear layer | 88 |
| 20. | Image matrix of classified murine retina | 90 |
| 21. | Image matrix with horizontal cell | 94 |
| 22. | Immunoreactivity of GABAergic amacrine cells..... | 99 |
| 23. | Glycine and taurine in the glycinergic amacrine cells..... | 100 |
| 24. | Image matrix with All amacrine cell..... | 102 |
| 25. | Univariate histogram matrix of GCL | 105 |
| 26. | Univariate histogram matrix of glycinergic amacrine cells..... | 108 |
| 27. | Univariate histogram matrix of GABAergic amacrine cells | 111 |
| 28. | Aspartate and GABA in the ganglion cell layer..... | 116 |
| 29. | Bivariate plots cell classes 1 | 125 |
| 30. | Bivariate plots cell classes 2 | 127 |
| 31. | Normal rat immunohistochemistry matrix | 135 |
| 32. | RGB and theme map of normal rat retina..... | 137 |
| 33. | Degenerate rat RGB matrix..... | 140 |
| 34. | Theme maps of normal and degenerate retina | 144 |
| 35. | EM synaptic images | 157 |
| 36. | EM overlay displaced amacrine cells | 161 |
| 37. | EM overlay microneuroma fascicle | 164 |

ACKNOWLEDGMENTS

Robert E. Marc, mentor and friend. Robert accepted me into his lab, helped me formulate ideas and made possible this educational experience through his intellect, teaching and patience.

Carl B. Watt, friend and electron microscopist extraordinaire who made possible all of the electron microscopic images in this dissertation either through his teaching, assistance or direct work.

Maggie Shaw, friend, teacher of laboratory etiquette and immunohistochemistry. Maggie has always been able to provide a much needed reality check, helping me up at times when I was feeling down, and checking me at times when I was feeling too full of myself.

Jia-Hui Yang, friend, an amazing anatomist and teacher of ultramicrotomy who once said after teaching me how to cut thin sections, "I was pretty good.....for a boy". Jia-Hui, together with Maggie Shaw, made possible much of the data in this dissertation through their teaching, patience and hard work.

To my committee members, Tom Parks, who suggested I talk with Robert Marc when I was looking for a basic science lab, setting in motion the rest of this story. To Scott Rogers, who helped me develop a protocol for exploring the hippocampus in epilepsy models for an earlier project. and who said he would serve on my committee after I successfully identified a trilobite eye embedded in

matrix. To Bud Brown and subsequently Mary Lucero who graciously agreed to serve on my committee and helped navigate the vagaries of getting through graduate school as our Physiology Dept. graduate advisors. To Ed Levine, whose easy-going manner, humor and sharp intellect has, along with Robert Marc, helped me to define future directions for research and investigation. I owe you all a great many thanks and my unending gratitude.

All my family and friends, without whom I certainly would not be here, literally or figuratively. You have given me a sense of peace, happiness, love and...

Last, but certainly not least, my best friend, teammate and wife Hilari who has supported me through late nights and long hours with her love and patience. Life with you is more fulfilling, happier, and to you I owe you perhaps the most of all, a great debt of gratitude and my unending love. Thank you.

Chapter 5 is reprinted by permission of John Wiley & Sons, Inc. Retinal remodeling triggered by photoreceptor degenerations. Bryan W. Jones, Carl B. Watt, Jeanne M. Frederick, Ching-Kang Chen, Edward M. Levine, Ann H. Milam, Matthew M. LaVail and Robert E. Marc. Copyright 2003, *Journal of Comparative Neurology* 464(1): 1-16.

INTRODUCTION

Societies have long been concerned with the concept of restoring lost vision, and historical records are replete with references to blindness and healing blindness. Historic, indeed current practice for the prevention of blindness focuses on environmental and lifestyle causes of blindness such as trachoma, xerophthalmia, onchocerciasis, hypertension and diabetes. However, the search for a cure for retinal blindness once vision has been lost has a more modern history and requires more intimate interventions than simple alterations in sanitation, exercise or diet.

Vision loss has a number of forms and aside from environmental or traumatic causes, may occur as a result of cataracts, glaucoma, presbyopia, macular degeneration, diabetic retinopathy or other degenerative diseases of the retina such as retinitis pigmentosa (RP). Some forms of blindness have surgical or optical interventions that may restore sight, such as lenses that adjust the focal plane properly upon the retina or surgeries to replace diseased or damaged corneas or even lenses within the eye, but many forms of blindness, particularly the retinal degenerative ones, do not have any satisfactory resolution resulting in and inspiring work in visual prosthetics and are currently an area of intense study.

The retina does not intrinsically deconstruct itself over time and is capable of remaining intact for the lifetime of an organism. However, there are degenerative diseases in addition to environmental or genetic insults that can

alter the function of the retina and cause architectural deterioration with consequent changes in physiology that are reflected by loss or degradation of vision. The loss of photoreceptors in retinal degenerative diseases effectively deafferents the neural retina, leaving the organism functionally blind. This visual impairment has inspired many groups to develop visual transduction surrogates based on bionic and/or biological implants. Of the retinal degenerative diseases, retinitis pigmentosa (RP) is the best characterized (Bird, 1995) of the inherited retinal degenerations with an incidence of approximately 1 in 3500 to 4000 (Bunker et al., 1984) and involves more than 40 known genes, with many mutations in the rhodopsin gene (<http://www.sph.uth.tmc.edu/RetNet/>) alone. RP clinically manifests itself often in the subject's early 20s, progressively starting with night blindness and peripheral vision loss, and often advancing to complete loss of vision often by the age of 40. Much current literature argues that retinal degenerations such as RP affect only the sensory retina, and approaches to retinal rescue are engineered around this assumption.

Several strategies to restore vision with silicon based implants in human subjects have been proposed (Humayun et al., 1996; Chow and Chow, 1997; Zrenner, 2002) along with tissue based approaches (Li and Turner, 1988; Lund et al., 1997), the use of survival promoting factors (Faktorovich et al., 1990; Levine et al., 2000), and gene therapy (Bennett et al., 1996) (Kumar-Singh and Farber, 1998).

A number of approaches to a visual prosthesis have been proposed, but the implant and transplant strategies depend explicitly upon preservation of the neural retinal architecture. The first transplant approach conceptually functions as a retinal transplant for the retinal pigment epithelium (RPE), in disorders where this tissue degenerates. The RPE functions as the outer blood-retinal barrier and plays a supportive role in maintaining the photoreceptor function. When this structure fails or degenerates, photoreceptor loss ensues. Therefore, attempts to restore the RPE through surgical transplants are being developed (Sauve et al., 2002), but as we show in this dissertation, these attempts must be made prior to photoreceptor loss and the ensuing changes to the neural retina that inevitably occur.

Of the other transplant therapies in development, including photoreceptor transplants, fetal retinal transplants and stem cell transplants, potentially with the exception of the stem cell transplants, all techniques explicitly depend upon the preservation of the neural retina underlying the photoreceptors.

Implant therapies are also a consideration and an area of active research and development. Bionic implants or silicon-based photodetectors fall into two categories, but both are conceptually built around the proposition that a photosensitive device will transduce the photons falling upon the chip into electrical currents that will subsequently stimulate the surviving retina followed by

the cortex in a retinotopic fashion generating phosphenes (Brindley and Lewin, 1968b; Brindley and Lewin, 1968a; Dobbelle and Mladejovsky, 1974; Humayun et al., 1996; Chow and Chow, 1997). Subretinal implants are being engineered with the goal of replacing the function of the photoreceptors and stimulating surviving neural circuits while epi-retinal implants placed on the vitreal surface of the retina would theoretically detect photons and directly drive the ganglion cell populations. Hypothetically, both approaches will stimulate the remnant neural retina, but these approaches also depend explicitly upon the preservation of the remaining neural retina for proper functioning, all technical, optical and engineering considerations aside. In essence, subretinal implants depend upon the existence of a normal neural circuitry in the retina to mediate the inputs from the surrogate bionic implants into the proper visual channels and then to activate the ganglion cells. Epi-retinal implants depend upon the existence of ganglion cell populations in approximately the same numbers as in normal retina. This dissertation demonstrates that both of these situations are likely untenable in degenerate retina. An alternative that bypasses the retina entirely is conceptualized by a CCD camera connected to an array of electrodes that provide direct stimulation of visual cortex (Normann et al., 1999).

The impetus for this dissertation arose from an analysis of a number of aged human retinal tissue samples, which demonstrated confusing and profound alterations in neural retinal structure when analyzed by computational molecular

phenotyping (CMP). After examining all of the human tissue available, the question arose as to whether or not the neural retina in other retinal degenerations maintains its neural structure and thus circuitry in light of the assumptions in the literature that the human neural retina is maintained in structure and function after photoreceptors have degenerated.

To date, a number of mouse and rat models in addition to human RP tissues have been evaluated by various labs to a limited extent, but a normative computational molecular phenotypic database or atlas was not available and is needed to establish baseline values for cell classes and to establish homologies with other mammalian species. Therefore, the purpose of this dissertation was to create a wild type murine metabolic phenotypic atlas and test the hypothesis that the neural retina is preserved in retinal degenerations.

To accomplish these goals, this dissertation includes the following specific aims: 1) determine normal amino acid signatures and create a metabolic phenotypic atlas of the wild type mouse and, based upon the normal metabolic phenotypic atlas, test the hypothesis that the neural retina is preserved in retinal degenerations; 2) establish timelines and the sequelae for retinal degeneration across human, naturally occurring and engineered mouse lines through small molecular signature analysis or computational molecular phenotyping; 3) based upon evidence in the literature that suggests neuronal sprouting may occur in degenerate retina, test the hypothesis that the circuitry of the retina is corruptive

by looking for the presence of synapses from sprouting neurons and within the plexiform layers and in subretinal space via EM overlay and attempt to characterize the circuitry on the ultra structural level.

Ultimately, this dissertation documents the normal populations of the murine retina according to their small molecular amino acid phenotypes and then, through the use of these same techniques, demonstrates that the neural retina does not remain in stasis after the photoreceptors degenerate. To accomplish this, we used naturally occurring and engineered models of retinal degeneration in addition to human tissue from patients with retinal degenerative diseases. These data challenge commonly held beliefs in the literature that the neural retina remains unchanged after photoreceptor death and show that the neural retina is highly plastic, reacting to deafferentation via photoreceptor loss in modes similar to cells of the central nervous system.

CHAPTER 2

BACKGROUND AND SIGNIFICANCE

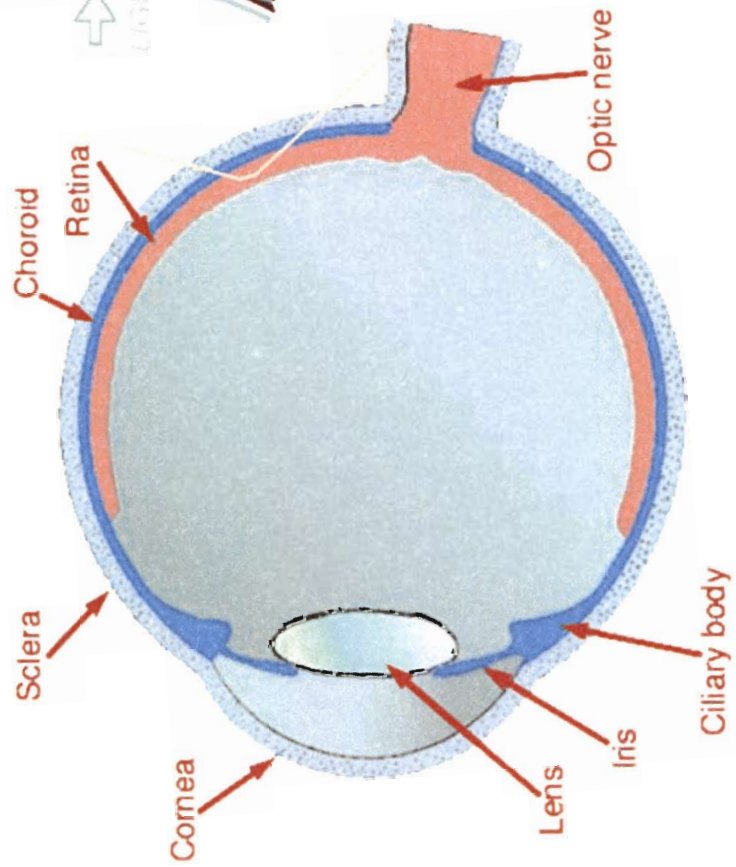
Normal retinal structure and cell populations

The retina is a thin sheet of cells that lies at the back of the eye and functions as the neural preprocessing element of the visual system. It is a multi-laminar structure unique within the nervous system and is subdivided into two primary anatomical and functional layers, the sensory retina and the neural retina. Light enters the eye through the cornea and lens and impinges upon the retina where it is transduced into electro-chemical signals by photoreceptor cells. Those signals are preprocessed by the intrinsic retinal circuitry comprising bipolar, horizontal, amacrine and ganglion cells (Figure 1).

From there, information is sent primarily to the lateral geniculate nuclei and then on to area V1 of visual cortex. Other nuclei within the visual system subserving nonvisual functions such as the superior colliculus and the supra-chiasmatic nucleus also receive inputs from retina.

Closer examination of the retina reveals two synaptic layers and three cellular or nuclear layers (inset Figure 1). The mammalian retina is composed of six major cell types (photoreceptor, horizontal, bipolar, amacrine, ganglion, and Müller cells), and several types are further divisible, yielding \approx 55-60 classes (Kolb et al., 1981; 1992; Masland, 2001a).

Figure 1: Eyeball cross section with retina. Adapted from Webvision (<http://webvision.med.utah.edu/>). Representation of a typical cross section through the human eye showing the major structures and their relationships including the cornea, sclera, lens, iris, ciliary body, choroid and retina. A magnified portion of the retina is shown in cartoon form at right, illustrating the multilaminar structure of the retina with some of the representative circuitry including five of the six major superclasses of retinal cells.



Photoreceptors are the light sensitive cells and transduce light into neural signals (Schneeweis and Schnapf, 1995). Photoreceptors in the retina include both rods and cones with cones being subdivided into typically two classes in mammalian vertebrates, while primates exhibit three classes of cones. Both rods mediating scotopic (low light) vision and cones mediating photopic (bright light) vision have their cell bodies in the outer nuclear layer with their axon terminals in the outer plexiform layer where they synapse on horizontal and bipolar cell dendrites (Dowling and Boycott, 1966). Light impinging upon photoreceptors photo-activates rhodopsin, a visual pigment, and generates a biochemical cascade that ultimately leads to graded hyperpolarizing potentials. This causes a decrease in the release of glutamate inducing the ON bipolar cells to depolarize whereas OFF bipolar cells respond by hyperpolarizing. The loss of photoreceptors in the case of the retinal degenerative diseases leaves the sensory retina unable to signal the neural retina, thus leaving the organism functionally blind and inspiring many groups to develop artificial methods of visual transduction based on bionic and biological implants.

Bipolar cells are positioned in the inner nuclear layer with their dendrites and axons in the outer and inner plexiform layers respectively. Bipolar cells can be separated into ON rod bipolar cells, ON cone bipolar cells and OFF cone bipolar cells. Bipolar cells can be further anatomically and functionally subdivided into a number of subtypes termed rod, cone (4 ON cone diffuse, 4

OFF cone diffuse, S types), and Midget (OFF and ON). ON and OFF varieties of cone driven bipolar cells respond to glutamate application from cone photoreceptors differently. While the OFF bipolar cells respond to glutamate by activation of ionotropic channels with subsequent depolarization, the ON bipolar cells hyperpolarize via activation of mGluR6 receptor coupled G protein pathways (Nawy and Jahr, 1990a; 1990b; 1991).

Horizontal cell bodies are found at the distal edge of the inner nuclear layer and extend their dendritic processes into the outer plexiform layer. These cells can be divided into two basic subtypes in primates. Type 1 horizontal cells or H1 cells contact rods and two types of cones while type 2 or H2 horizontal cells contact exclusively cones of all three types. H1 and H2 horizontal cells also form syncytium within each subtype via gap junctions to increase each cell's receptive area. However, in mice, there is only one type of horizontal cell (Masland, 2001b). This horizontal cell is axon bearing and contacts cones at its soma and rods at its axon terminal where the horizontal cell axon terminals are electrically isolated from their somas. Horizontal cells generate graded, sustained hyperpolarization that follows photoreceptor responses via sign conserving AMPA receptors. Their function is believed to be one of enhancing contrast between areas of light and dark impinging upon the retina.

Amacrine cells are predominantly found in the inner nuclear layer, with displaced subtypes found in the ganglion cell layer, and approximate 40% of all

neurons in the INL (Strettoi and Masland, 1995; Jeon et al., 1998). Mammals express at least 26 amacrine cell classes based on Golgi impregnation, dye injection and photofilling technologies (MacNeil et al., 1999), while teleosts are known to harbor at least 70 classes (Wagner and Wagner, 1988). Amacrine cells receive information from bipolar cells and other amacrine cells and send their outputs to bipolar cells and other amacrine cells in addition to providing inhibitory feed-forward inputs onto ganglion cells, which comprise the majority of inputs onto ganglion cells (Freed and Sterling, 1988; Calkins et al., 1994; Jacoby et al., 1996).

Ganglion cells are separable into approximately 14 classes (Marc and Jones, 2002b) and are the output cells of the retina. Ganglion cell dendrites send their processes to the inner plexiform layer and their axons to the fiber cell layer on their way to thalamic and collicular targets and are typically classified according to their diverse morphologies (Oyster et al., 1980; Rodieck et al., 1985; Buhl and Peichl, 1986; Freed and Sterling, 1988; Kolb et al., 1992; Stone et al., 1992; Dacey and Lee, 1994) and molecular contents (Massey and Redburn, 1987; Marc et al., 1990; 1995; 1998a; 1998b; 2001; Marc, 1999a; 1999b; Kalloniatis and Fletcher, 1993; Kalloniatis et al., 1996; Kalloniatis and Napper, 1996; Kalloniatis and Tomisich, 1999; Jones et al., 2000; Marc and Cameron, 2001; Marc and Jones, 2002a).

Müller cells are the primary glial cells in the retina, functioning both as architectural support, filling spaces between the neural cells, and serving as metabolic support for neuronal cell classes within the retina while interacting physiologically with all of the neuronal cell types in the retina (Reichenbach and Wohlrab, 1986; Newman and Reichenbach, 1996). Anatomically, Müller cell nuclei lie in the inner nuclear layer and their processes span the entire neural retina, forming both the inner and outer limiting membranes via intermediate junctions.

The vascular cells of the retina are also important due to the high metabolic requirements of the retina which has been estimated to have the highest oxygen consumption (per weight) of any tissue (Anderson, 1968). Vascular circulatory systems of the retina have two forms. One is the choroidal vascular system, which is served by fenestrated capillaries that enables the RPE to function as the blood retinal barrier for the retina. The other is direct retinal vascularization, which are nonfenestrated and act as another blood retinal barrier. The choroidal vascular system both perfuses the RPE and is essential for photoreceptor function given their high metabolic needs. The retinal vascular system perfuses the neural retina and is essential for proper functioning of the neural elements.

Amino acids and computational molecular phenotyping

The application of multispectral analysis to quantitative immunocytochemistry, which we term computational molecular phenotyping (CMP), has proven useful in determining cell populations in normal and pathologic retinal tissue (Kalloniatis et al., 1994; 1996; Marc et al., 1995; 1998a; 1998b; 2001; Jones et al., 2001; 2003a; Marc and Jones, 2002a) and is a formal test of the signature hypothesis originally posited by Lam et. al., (1985).

Computational molecular phenotyping depends upon quantitatively tracking the colocalizations and concentrations of small molecules in tissues to determine cellular identity with IgGs generated against amino acids, which have proven to be good class discriminants for cell populations. The determination of cell classes or populations of cells based upon the small molecular contents are not visualized per se under the microscope. The datasets are constructed of individual labels of immunocytochemically labeled sections of slides that are then realized as hyperdimensional data-sets.

Amino acids are used by various cellular machinery for biosynthesis, regulation and signaling. Glutamate, glutamine, alanine, and aspartate are all involved in either the citrate cycle or involved in metabolism of pyruvate. Glutamate is incorporated into peptides and proteins, serves as an excitatory neurotransmitter, and is a precursor to glutamine production as well as GABA, succinate, proline, ornithine and arginine. Glutamate functions as an activator of

the urea cycle and is important for reactions of transamination. Glutamine is incorporated into proteins and is important in transamination reactions for synthesis of other amino acids, amino sugars and nucleotides. Alanine is an important contributor in muscular metabolism, while aspartate is a glutamate precursor via transamination, as well as a reactant for pyrimidine and arginine synthesis. Glycine is an inhibitory neurotransmitter, and glutathione is important in reducing reactions to quench free radicals and to conjugate with toxic compounds, thus playing important roles in cellular protection. Glutamate, glycine and cysteine are all glutathione precursors as well. Additionally, taurine likely functions as an osmolyte (Dominguez et al., 1989; Huang and Karwoski, 1992; Marc et al., 1995; Kalloniatis and Tomisich, 1999) and potentially may function as a possible weak neurotransmitter analog of glycine (Han et al., 1997). Three of the amino acids glutamate, GABA and glycine, have long been recognized as molecules involved in fast neurotransmission (Storm-Mathisen et al., 1983; Iversen, 1984; Massey and Redburn, 1987; Ehinger et al., 1988; Hendrickson et al., 1988; Maycox et al., 1988; Carlson et al., 1989; Kish et al., 1989a; 1989b; Muller and Marc, 1990; Jojich and Pourcho, 1996).

The use of small molecules to identify cell classes provides for a more sophisticated means of identification than relying solely upon cell size, shape, location, connectivity and neurotransmitter content. Indeed, it can also be used in conjunction with the previous more traditional techniques to more precisely

identify cellular cohorts. Tracking cellular content of amino acids and establishing normative values in tissues of various animal models important to medical research is important because of the role amino acids play or reveal in signaling, metabolism, osmoregulation, development, pathology and cell identity (Orr et al., 1976; Grunert and Wassle, 1990; Murashima et al., 1990; Davanger et al., 1991; Crooks and Kolb, 1992; Kalloniatis and Fletcher, 1993; Kalloniatis et al., 1994; 1996; Barnett and Osborne, 1995; Kalloniatis, 1995; Marc et al., 1995; 1998a; 1998b; 2001; Fletcher and Kalloniatis, 1996; Pourcho, 1996; Fletcher, 2000; Gadea and Lopez-Colome, 2001; Jones et al., 2001; 2003a; Marc and Jones, 2002a). Specifically, amino acid phenotypes or fingerprints are useful due to the ability to establish a set of unique multidimensional signatures associated with individual cell classes that are stable across preparations and over time in adult retinal tissues, pathological insults notwithstanding.

Progressing beyond simple binary immunolabeling of amino acids, the ability to quantitatively track a higher dimensionality of amino acid content in cells has proven useful in retinal research to establish unified identities and distributions for cell populations (Marc et al., 1995; 1998a; 1998b; 2001; Jones et al., 2001; 2003a; Marc and Jones, 2002a) and to identify physiologic responses further facilitating cellular cohort identification (Marc, 1999a; 1999b; Marc and Jones, 2002a). All retinal space can be accounted for by amino acid immunolabeling, and in particular, using the amino acids glutamate, GABA and

glycine, which label neuronal populations with taurine and glutamine labeling glial populations (Marc et al., 1995; Kalloniatis et al., 1996). Glycine and GABA are primarily the neurotransmitters of the horizontal pathway of information flow through the retina, which includes horizontal cells (GABA), amacrine cells (GABA and glycine), and glutamate is primarily responsible for the vertical flow of information through the retina including photoreceptors and bipolar cells. Multispectral classification can occur with just these three immunolabels allowing quick discrimination of bipolar cells, amacrine cells, and ganglion cells, but not with the degree of resolution that may be obtained with seven or more small molecular labels.

Phenotyping using small molecules, particularly amino acids is constant over normal preparations, but can be altered after pathological insults including retinal detachment (Marc et al., 1998a) and hypoxia (Barnett and Osborne, 1995; Fletcher and Kalloniatis, 1996), which induces alterations in the amino acid immunolabeling of the inner plexiform layer and neuronal cell bodies. GABA immunolabeling in the plexiform layers appears to be a good early indicator of retinal ischemia and may correlate with reports of high oxygen consumption requirements of the plexiform layers of the retina (Yu and Cringle, 2001). Amino acid content in cells also changes during development as retinas mature and cell classes are born (Fletcher, 2000). Additionally, studies appear to reveal early abnormalities in Müller cell populations during development of RCS rat retinas

(Fletcher and Kalloniatis, 1996) and dystrophic retina (Orr et al., 1976; Murashima et al., 1990), which may presage cell death and indicate fates for retinal degeneration earlier than previously thought.

Degenerate retinal structure and physiology

The retinal degenerative diseases including retinitis pigmentosa (RP) (Figure 2A), age related macular degeneration (AMD) and Usher's syndrome are a prevalent cause of blindness and there currently is no cure for any of them.

Therefore investigations and potential interventions to arrest retinal degeneration or rescue retinas that have already undergone degeneration are an area of intense study. To this end, a number of animal models have been developed that mimic the retinal degenerative diseases found in human patients with the goal of using these models to help understand mechanisms of degenerative blindness, and to assist the development of strategies to regenerate the retina or develop retinal biological and/or bionic prosthesis to assist vision.

Current dogma holds that the neural retina in these genetic models and indeed human retina remains relatively intact after the photoreceptors of the sensory retina have degenerated despite some evidence in the literature that this belief may not reflect the true status of degenerate retina. Because of this, most strategies to rescue vision may be engineered around incorrect assumptions.

Clinical observations observed in fundoscopic examinations of the retina of patients with retinal degeneration reveal an ischemic appearance with a waxy, pale optic nerve head with brown or black pigmented “bone spicules” observed in the periphery (Figure 2A, Figure 2B). An example of a foveal to peripheral whole mount histological examination of the tissue reveals hypopigmentation in the periphery and dark pigmented “bone spicules” mid retina (Figure 2B). However, this level of examination, indeed even nuclear stains like Toluidine blue are impoverished methodologies for examination of the changes that take place in these tissues. Computational molecular phenotyping (CMP) or even the use of multiple IgG’s generated against small molecules of interest reveal dramatic changes in these tissues from normal retina (Figure 3) to degenerate retina (Figure 4).

Figure 2. Fundoscopic image of RP with dissected retina. This image shows a representative fundoscopic image from a patient with retinitis pigmentosa 2A, showing the hypopigmented appearance of the retina with a waxy, pale optic nerve head. Also visible in the peripheral retina are the typically observed "bone spicules" or hyperpigmented areas signifying areas of retinal degeneration. A section of human retina in 2B shows a temporal to nasal strip (left to right respectively) with the fovea at right and a broad strip of pigmented bone spicules in the middle portion of the retina. While clinical observation of these diseased retinas can certainly reveal some of the hallmarks of retinitis pigmentosa, it should be noted that traditional histologic techniques do not reveal the status of neuronal populations or intrinsic retinal circuit properties.

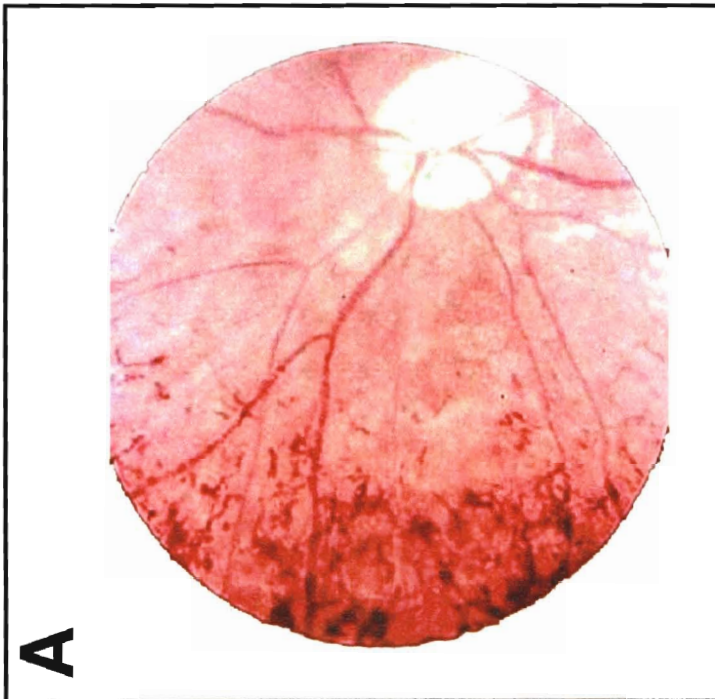


Figure 3. Normal retinal amino acid immunohistochemistry. This set of images is a representative section of mid-peripheral retina from the mouse. These images represent the eight IgG labels used for the construction of the computational molecular phenotypic atlas of the murine retina. Small molecules are good indications of cell state and metabolic status. Alanine, aspartate, glutamate, glycine, glutathione, glutamine, taurine and GABA are used to discriminate cell populations, revealing natural classes that separate according to differences in amino acid concentration.

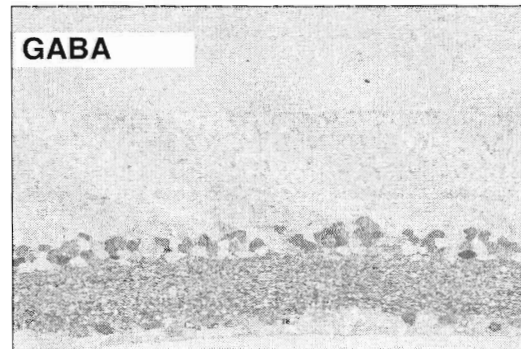
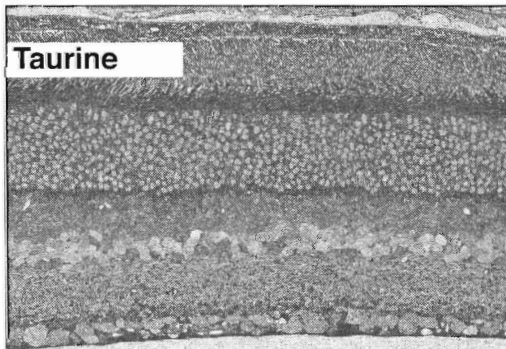
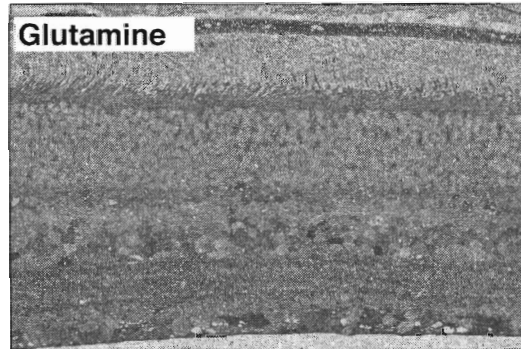
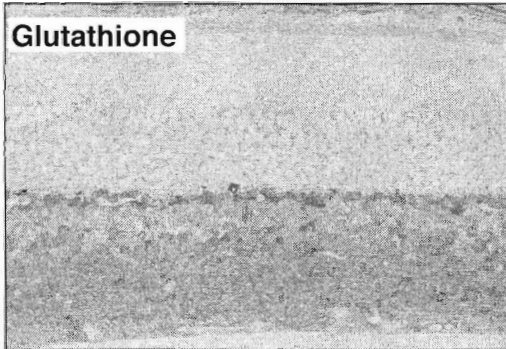
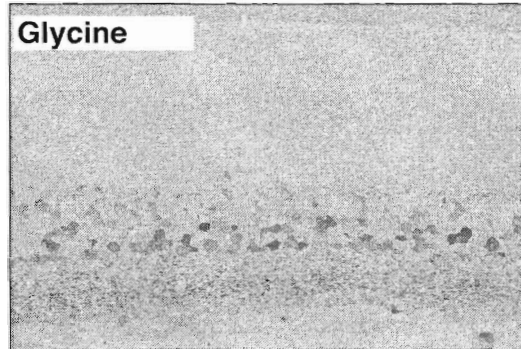
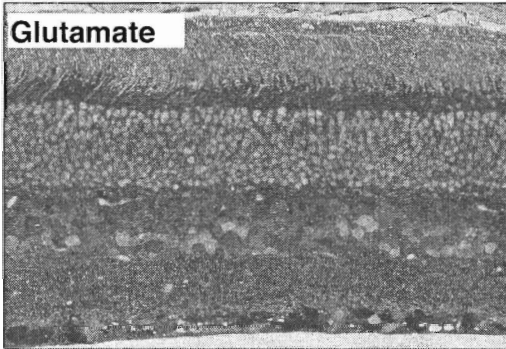
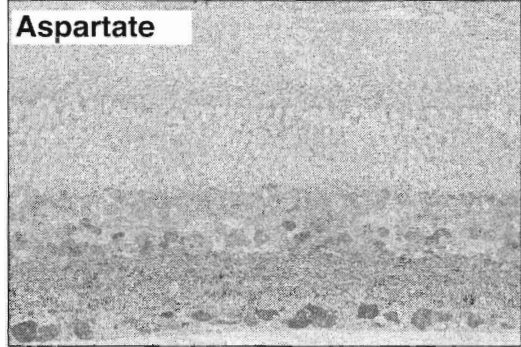
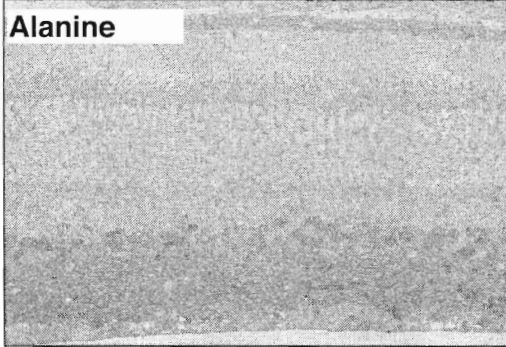
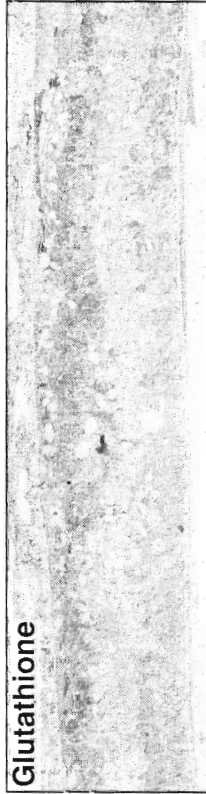
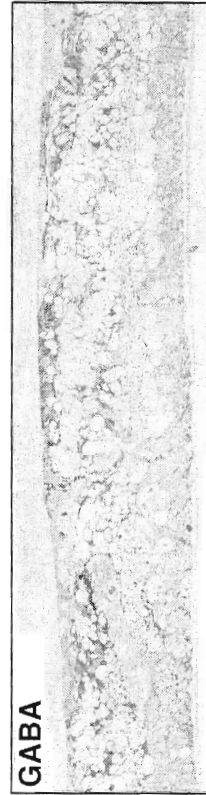
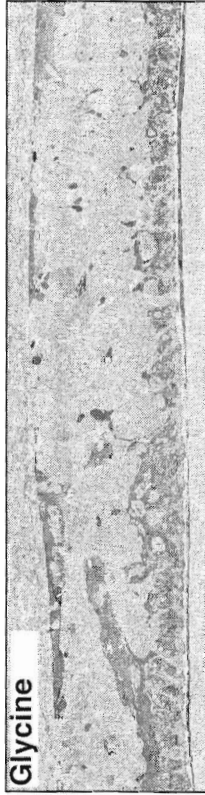
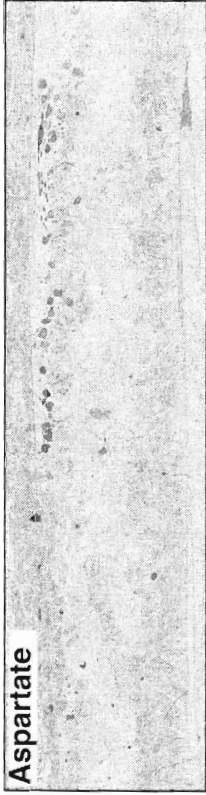


Figure 4. Abnormal immunohistochemistry from RP retina. A corresponding image to Figure 3 to represent the differences seen in retinal structure in normal retina (Fig 3) versus degenerate human retina (this image). These images represent 250 nm sections with the same eight IgG labels against alanine, aspartate, glutamate, glycine, glutathione, glutamine, taurine and GABA are used as in Figure 3 showing the dramatic morphological differences in the degenerate versus normal retina. From this image, it should be apparent that there is a significant rate of cell death in these retinas with the remaining populations of cells becoming involved in retinal remodeling. Also apparent in this image at left are large intrusions into the neural retina of a structure immunoreactive for alanine, slight aspartate immunoreactivity, glutamate immunoreactivity as well as glutamine and glycine. The identity of this structure is unknown, but it could represent astrocytic invasion and hypertrophy.



Ultimately, this work indicates that in both the human and rodent models of retinal degeneration, photoreceptor cell death is followed by continued neural retinal degeneration and remodeling, ultimately rendering the retina radically altered. In short, after retinal photoreceptor loss, a set of dramatic, identifiable stereotypical sequelae can be found in models of degenerative retinas. These include, but are not limited to, changes to the inner plexiform layer, Müller cell hypertrophy, and migration of remaining cell classes including ganglion cells and amacrine cells into regions of retina where they are not found in normal functioning retina. Additionally, neurons that survive display unexpected plasticity, rewiring the remnant inner plexiform layer and forming thousands of novel ectopic microneuromas in the remnant inner nuclear layer with bipolar, amacrine and likely horizontal cells engaging in new circuit topologies and assembling novel presynaptic architectures. The implications of plasticity in the neural retina may preclude the use of biological implants, but may also prove advantageous to retinal rescue.

Therefore, it was essential to document the level of functional and structural viability of degenerate retinas to determine windows of opportunity for restorative therapies. Several studies have attempted to do just this by examining the preservation of the ganglion cells in retinas from patients with RP including those diagnosed with moderate and severe forms of the disease (Stone et al., 1992; Santos et al., 1997; Humayun et al., 1999). Of these studies, one

found approximately 20% of inner nuclear layer cells are lost in the macula of late stage RP patients (Santos et al., 1997) and another documented 20% survival in regions peripheral to the macula (Humayun et al., 1999), yet both studies concluded that the retina is essentially normal allowing retinal transplant studies to go forward. Some earlier studies suggest the possibility of early abnormal changes in the inner retina. Machida et al. (2000), imply that photoreceptor synaptic remodeling may occur during photoreceptor degeneration and Strettoi and Pignatelli demonstrate specific changes occurring in the bipolar and horizontal cell populations in the rd mouse after photoreceptor loss (Strettoi and Pignatelli, 2000). Others have indicated that pathological features in human RP correlate with similar features in the RCS rat (Milam et al., 1998).

Despite these few studies there appears to be a common assumption that the neural retina remains largely intact in retinal degenerations. The preservation of the neural retina in advanced RP and allied diseases is central to the designs of cellular and bionic rescue, and is often asserted in the literature (Scarlatis, 2000; Zrenner, 2002). However, there are indications that the neural retina in human RP is highly remodeled (Fariss et al., 2000) and severely depleted of neurons in regions devoid of cones. Anatomical surveys of the macula in human RP (Stone et al., 1992; Santos et al., 1997; Humayun et al., 1999) document variable ganglion cell loss, from mild to severe, but well-preserved regions of the neural retina invariably possess surviving sensory retina harboring cones,

suggesting that cone loss and subsequent neuronal loss are related. Analyses of acquired (de Raad et al., 1996) and inherited (Fletcher and Kalloniatis, 1996) rodent degeneration models reveal subtle changes in cellular molecular phenotypes in the neural retina, some even preceding rod degeneration (Fletcher and Kalloniatis, 1996). Subtle remodeling of rod pathways emerges rapidly in the *rd1* mouse (Strettoi and Pignatelli, 2000; Strettoi et al., 2002), where a phototransduction defect evokes death of rods by postnatal day pnd 21. Rod-driven bipolar cells and horizontal cell axon terminals retract their fine dendrites, and rod bipolar cell axon terminals assume immature synaptic structures. Defects extend to cone circuits with both cones (Fei, 2002) and cone horizontal cells (Strettoi et al., 2002) in the young *rd1* mouse sprouting new neurites. During human rod degeneration, surviving rods, horizontal and amacrine cells similarly extend anomalous neurites throughout the retina (Fariss et al., 2000). But many human and rodent retinal degenerations progress slowly, and no consensus on the fate of the inner retina has emerged as aged rodent retinal degeneration specimens are rare and studies rarely extend beyond pnd 90. Furthermore, standard histology and *ad hoc* immunocytochemistry, where small sets of probes are employed, are ineffective tools for tracking cell the 55-60 classes of cells (Masland, 2001b) in the mammalian retina.

CHAPTER 3

RESEARCH DESIGN AND METHODS

General

This dissertation has one central hypothesis. Specifically, we set out to test the hypothesis that the neural retina is preserved in retinal degenerations. To accomplish this and set the foundation for future work in retinal degeneration, a normative atlas of the murine retina was constructed so as to provide a baseline of cell classes.

Terminology

Each major type of cell, photoreceptors, bipolar cells, horizontal cells, amacrine cells, ganglion cells and Müller cells traditionally defined in terms of retinal position and morphology in the retina is defined as being comprised of statistical subgroupings termed superclasses and classes. An ultimate class is defined as the one in which no further subclasses can be resolved. We assume, based on prior studies, that this is also a cell's natural class.

Amino acids are often represented by their single letter codes: (A) alanine, (D) aspartate, (E) glutamate, (G) glycine, (J) glutathione, (Q) glutamine, (T) taurine, (γ) GABA.

Fixation and embedding

For this work, retinas to be examined with light microscopy were fixed in 1% paraformaldehyde/2.5% glutaraldehyde in phosphate buffer and dehydrated

in graded methanols and acetone, followed by embedding in plastic epoxide resin. Tissues to be examined with electron microscopy were prepared with 1% paraformaldehyde/2.5% glutaraldehyde in cacodylate buffer followed by dehydration and osmication to reveal membrane structure. Sections of tissues employed as the silver intensified light microscopy components in electron microscopy overlay were deosmicated for 10 min with fresh 1% Na metaperiodate to eliminate nucleation sites for silver deposition prior to immunocytochemistry.

Fixation is aldehyde trapping and rapid fixation with glutaraldehyde/paraformaldehyde ensures capture of the small molecules desired for high performance immunocytochemistry. Small molecules with free amino groups are trapped by glutaraldehyde. Glutaraldehyde is a five-carbon dialdehyde that forms Schiff's-base linkages with primary amino groups of free amines or proteins. Reactions continue with imines from the Schiff's base reactions thus polymerizing dialdehydes into sequential chains with side chains being composed of amino acids, amino sugars and peptides. Through these reactions, it is estimated that approximately 86-95% of free amines may be trapped through glutaraldehyde mediated covalent bonding. Architecturally, through glutaraldehyde linking, the meshwork of aldehyde cross-linked amino acid side chains from proteins leaves spacings of approximately 1nm in diameter, which prevents many macromolecule from binding and also creates an

environment where IgGs cannot penetrate into the tissue. This seeming disadvantage in actuality allows for the molecular phenotypic strategy to work in that all binding in these tissues is a surface phenomenon explaining how sections as thin as 40nm can exhibit the same amino acid binding levels as much thicker sections and allows for superimposition of sections for classification.

Embedding and sectioning

Dehydration and embedding within epoxy plastic resins provides the structural support to section the tissues at dimensions thin enough for digital superimposition and reconstruction of serial sections in later steps of computational molecular phenotyping. An added benefit of using the epoxy resins is that their properties make them compatible in both light and electron microscopy paradigms.

After fixation, all samples were dehydrated in graded methanols followed by acetone and processed in resin matrices as single specimens, stacks or mosaics (Marc, 1999b) for thin sectioning at 40-250nm into serial arrays depending upon application and mounted on 12 spot Teflon® coated slides (Cell-Line, Fisher Scientific) (Figure 5).

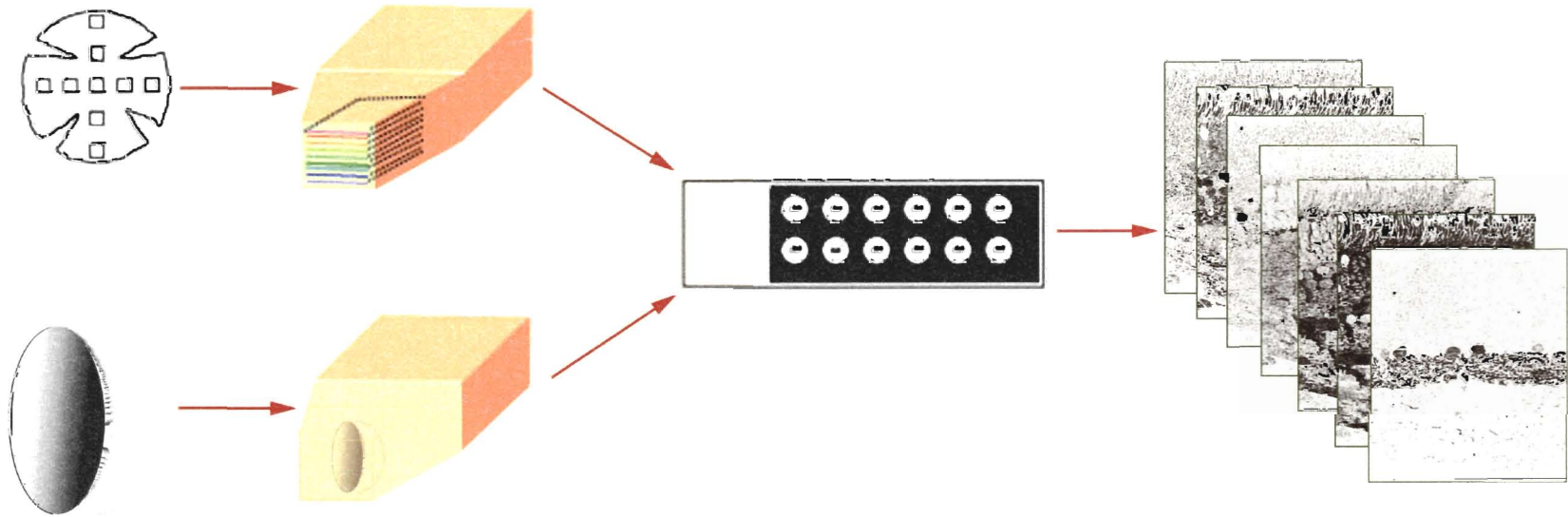


Figure 5. Sectioning techniques. Tissues are either scribed out of retinal flat mount preparations and embedded in stacks or whole eyes are embedded for vertical or horizontal sectioning onto 12-well Teflon coated slides for sectioning at 40-250 nm. Following sectioning, the slides are processed for immunocytochemistry using a library of 8 primary antibodies to alanine, aspartate, glutamate, glutathione, glutamine, taurine, glycine and GABA. Primary antibody exposure is followed by secondary antibodies with 1nm gold adsorbed to them for silver intensification. After silver development of the slide, each section of tissue is digitally scanned into a computer as 8-bit images to create a calibrated image that scales with concentration of amino acids. Each image is then digitally registered/warped to match the alignments of all others. Thus, each pixel in a series of images will represent a chemical vector in N-dimensional space for image classification.

High performance immunocytochemistry

High performance immunocytochemistry is the only method developed to date that routinely allows for the quantitative discrimination of cellular small molecular signatures at the individual cellular resolution within large fields of cells. The technique is based upon quantitative immunocytochemistry using IgGs directed against a hapten conjugate of the target amino acid and glutaraldehyde (Storm-Mathisen et al., 1983). Because small molecule targets of interest are conjugated to the fixation agent (glutaraldehyde), dialdehyde fixation of tissues mimics the hapten required for binding of the IgG allowing for detection in the thin sections. IgG binding in these sections is a surface phenomenon (Marc et al., 1995), and IgG binding is proportional to antigen concentration on sections up to the maximum packing density of the IgGs. Therefore, section thickness is irrelevant to the density of the IgG molecules. However, thin sections (40-250 μm) are required to achieve precise alignment of cellular structures and will report the same concentration of IgG as sections that are dimensionally thicker (Marc et al., 1990).

High performance immunocytochemistry was performed as described previously (Marc et al., 1995). Briefly, slides were deplasticized with sodium ethoxide, washed and rinsed in de-ionized water before drying. Sections were probed for 12 hours with primary antibodies in 1% goat serum directed towards the molecule of interest. After washing for 10 minutes in phosphate buffer, slides

were serially surface probed (Marc et al., 1995) with antibodies targeting L-alanine, L-aspartate, L-glutamate, L-glutamine, glutathione, glycine, taurine, GABA obtained from Signature Immunologics Inc. (Salt Lake City, Utah) and the Marc Laboratory. Because of the need to assign macromolecules to specific locations or domains within cells, post-embedding high performance immunocytochemistry is followed by silver intensification as described by Kalloniatis and Fletcher (Kalloniatis and Fletcher, 1993) via a secondary antibody bound to (typically 1 nm) (Pharmacia-Amersham) colloidal gold allowing for high resolution identification of immunolabeling within structures down to the electron microscopy level (Marc and Liu, 2000) (Figure 5). Secondary antibodies bound to gold particles are then silver intensified for visualization allowing for quantitative imagery that has a wide dynamic range and is archival.

Digital image acquisition and analysis

All images of silver intensified immunoreactivity were captured with a CCD camera as 8-bit high-resolution images (Marc and Jones, 2002a). These images can be calibrated by comparison with amino acid standards bound to protein. Image acquisition was accomplished with a MTI DC 330 E CCD camera and LG-3 scientific frame grabber board and CFW-1310M Firewire© cameras from Scion Corporation (Scion Corp, Frederick, Maryland). Images were visualized as high-resolution (243 nm/pixel) images, mosaicked and registered (PCI Geomatica

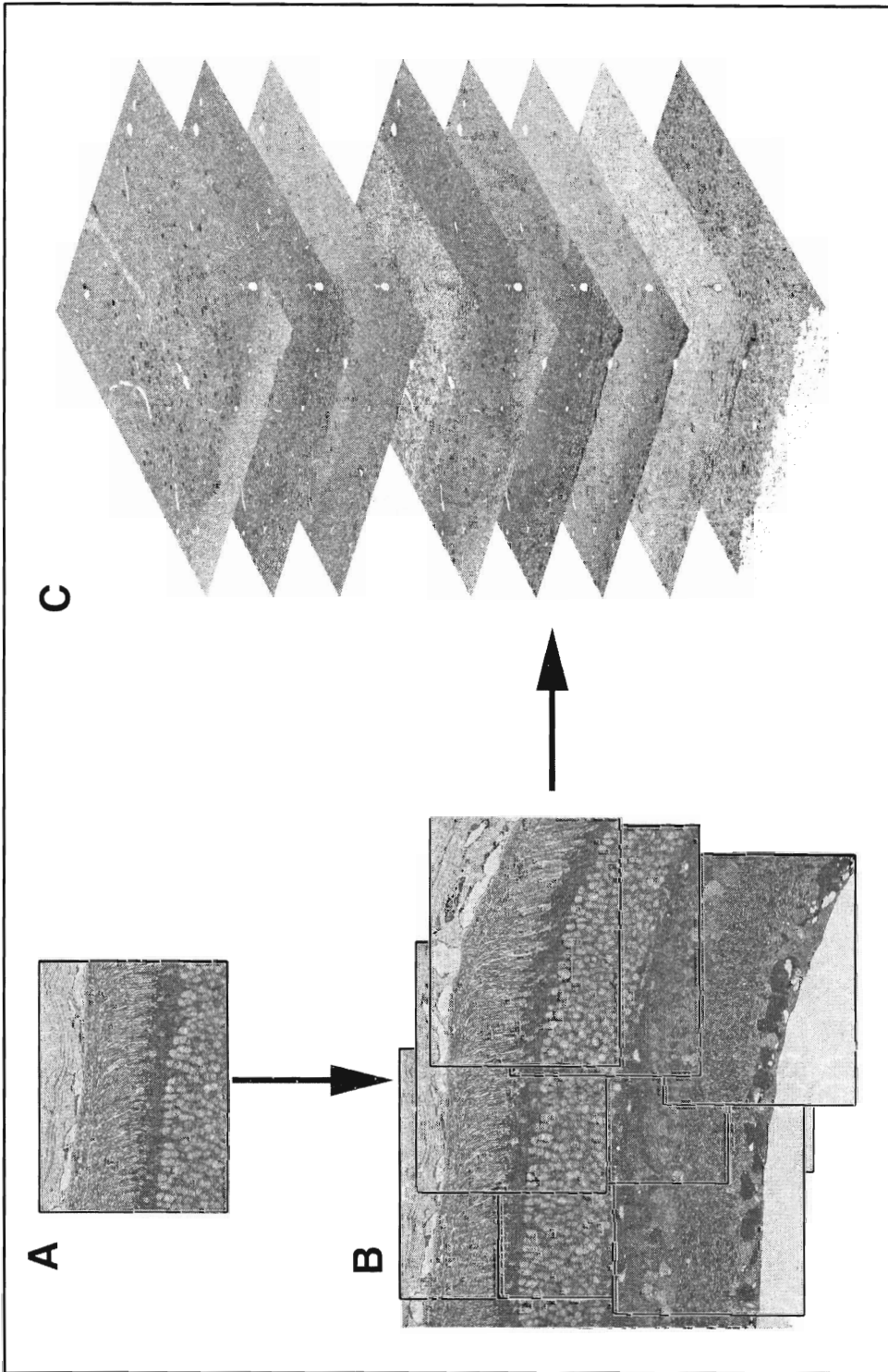
V8.2 PCI Geomatics, Richmond Hill, Ontario Canada) into large image databases, often ≈ 2 Gb/sample (Figure 6).

Since each section is physically removed from the adjacent sections by ~ 40 -250 nm, each image needs to be registered or warped to match a selected master image using common reference points selected in each image (Marc and Cameron, 2001) to correct for rotation, shear and scaling. Each image, digitally registered to one another using polynomial image transformations becomes a layer within an N-dimensional database where each pixel represents a chemical or molecular vector in N-space (Figure 6). These vectors can then be combined and compared with other vectors to create a mathematical classification or fingerprint of cellular identity for all pixels in the image.

Image analysis

A useful multidimensional approach, termed amino acid \rightarrow RGB mapping, assigns a molecular signal to a color within RGB space allowing for a visual color discrimination of classes. RGB reconstruction and histogramming are useful in limited cases, but are not statistical tools.

Figure 6. Mosaicking and registration. This image illustrates the processing of immunohistochemical data after digital capture via CCD. Each individual image (6A) is mosaicked into larger data-sets (6B) providing sample densities sufficient for proper image classification. Each large mosaic (6B) is then digitally registered or warped to a selected master image (typically glutamate or taurine) to create a hyperdimensional database (6C) where each pixel in a representative section is registered to pixels in adjacent images.



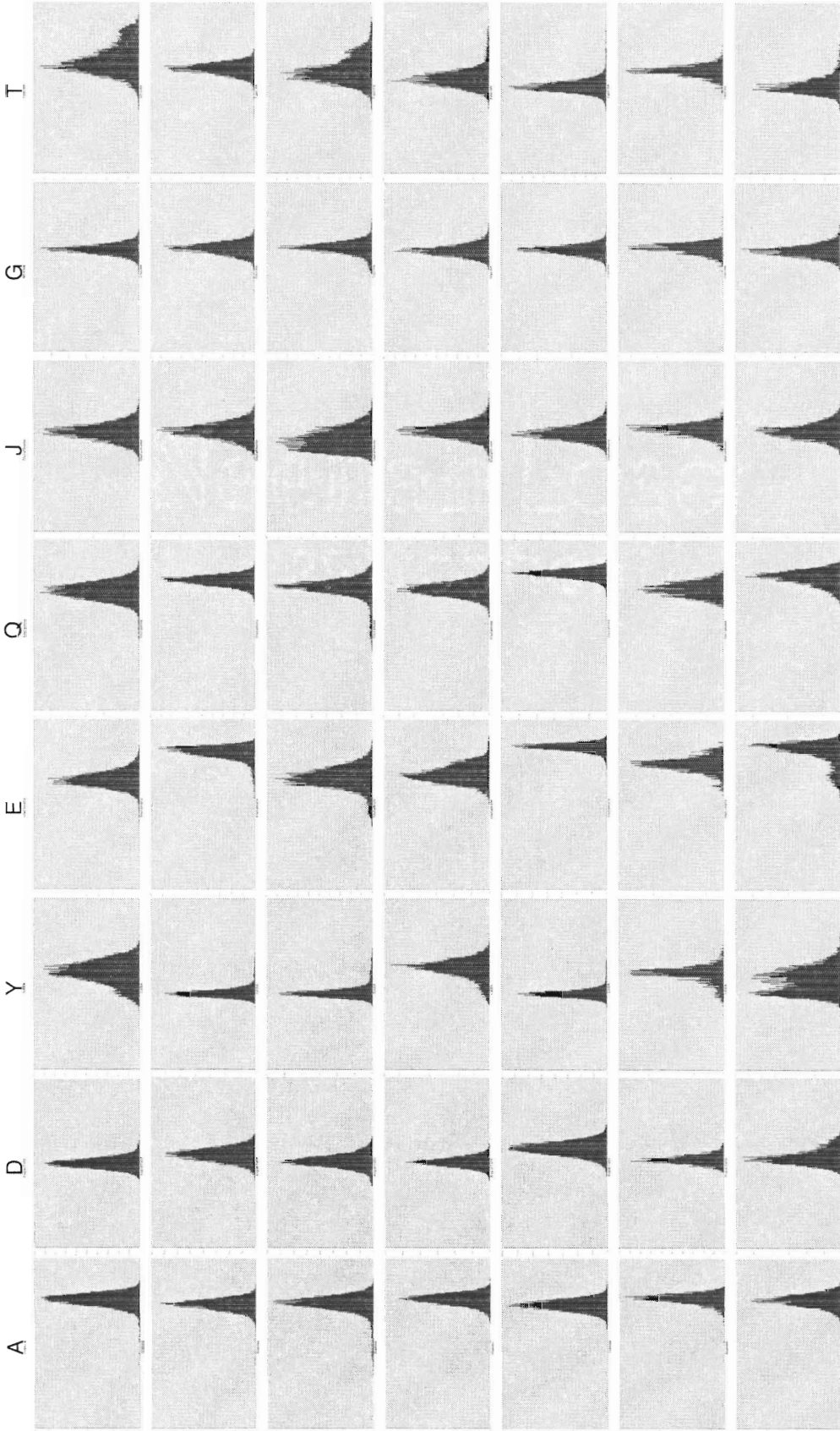
To properly manage the numbers of classes of cells encountered in these tissues, pattern recognition, or classification algorithms are needed (Marc et al., 1995; Marc and Cameron, 2001; Marc and Jones, 2002a). These techniques allow for a more precise discrimination of classes than can be achieved visually and provides a statistical measure of separability.

Images can also be explored, and classes refined, using a limited form of image analysis, histogramming. This unidimensional analysis of each amino acid within classes reveals probability distributions for amino acids within each class and can be useful for determining class separability and refining classifications (Figure 7).

Computational molecular phenotyping

Computational molecular phenotyping transforms cellular anatomical data into multidimensional molecular signatures, which can be parsed by classification algorithms to formally classify all cells into the major neuronal types, subtypes and, ultimately, natural classes (Marc and Cameron, 2001; Marc and Jones, 2002a). Unlike other immunocytochemical strategies, computational molecular phenotyping classifies all cell space and tracks the fates of the major retinal cell types and subtypes across different models and species with constant performance.

Figure 7. Univariate histograms. This graph is comprised of univariate signatures of classified cells. Univariate signatures are used to refine classifications and explore differences in molecular phenotypes between classes of cells. Histograms of each amino acid concentration reveal probability distributions for amino acids within each class. In this example, there are seven classes of cells represented by each row. The single letter amino acid code for individual amino acids are on top representing A (alanine), D (aspartate), Y (GABA), E (glutamate), Q (glutamine), J (glutathione), G (glycine), T (taurine). Histograms should be interpreted as probability distributions of cell classes derived from N-space image classifications. The y-axis is the probability of finding a particular small molecular concentration with the x-axis representing the range of concentration observed in the cell class on a logarithmic scale in mM. Each histogram is a log scale showing distributions from .1-10 mM of each respective amino acid. Each row represents a class that was separated out of the whole image based upon its unique N-dimensional small molecular fingerprint. Multiple peaks within some univariate histograms in this image reveal possible additional classes hidden within these distributions or subcellular inhomogenities (e.g., mitochondrial, ER, lysosomal partitioning).



Classifications were performed on raw data channels using the k-means and isodata clustering algorithms (Marc and Jones, 2002a) with PCI Geomatica (PCI Geomatics) and data explored with custom code written in IDL (Research Systems Inc., Boulder, CO) on Apple Macintosh and Windows computers. Isodata is similar to the simpler and computationally faster k-means clustering method but adds a further step of class splitting within clusters with high variance. Conceptually, both k-means and isodata clustering techniques allow one to iteratively work through large sets of apparently randomly distributed and weighted data points to find smaller sets of cluster centers that minimize the sum of the squared distances between each data point and the nearest cluster center point. The basic concept is that one assigns data points to clusters by finding the nearest cluster mean and assigning a data point to that cluster that is represented by a single vector. One then iteratively “steps” through an image migrating the means until the sum of the squared distances no longer migrates. These techniques can be useful in a variety of applications from data analysis, digital image processing, and pattern recognition in fields as disparate as remote sensing of intelligence and military targets of interest, medical imaging, forestry management and ecology among other applications (Fu et al., 1969; Gordon, 1980; Burgess, 1993; Taxt and Lundervold, 1994).

The multidimensional signatures of classes were surveyed and visualized as selected *rgb* maps, univariate histograms and as superimposed bivariate 2N-

plots. Single bivariate plots (Marc et al., 1995) display the area of concentration space occupied by a class in a two-dimensional chemical space (Figure 8). 2N-plots superimpose several bivariate plots in an N-space allowing for easier discrimination of the cell classes. Pairs of signals are displayed as class means bounded by 2 SD margins. The XY axes span 0.1-10 mM with logarithmic scaling and the [X,Y] pairs are color-coded: [E, γ] orange; [D,Q] cyan; and [G, τ] magenta (Marc and Jones, 2002a) (Figure 8).

Detailed theme map generation first involved production of raw classification theme maps (Marc et al., 1995; Kalloniatis et al., 1996), which is equivalent to the spatial logical AND of all the classified channels. Thus no single channel completely matches the raw theme map, and there is an error kerf surrounding classified structures (Marc et al., 1995). Refined theme maps were produced by assigning all cells and structures in a single channel (e.g., the toluidine blue channel) to their aligned classes in the theme map (Marc and Cameron, 2001; Marc and Jones, 2002a). All theme maps displayed in this manuscript are refined. For display only, raw data channels were linearly contrast stretched over a 30-220 pixel value range and sharpened with unsharp masking. Monochrome images as density mapped and rgb images are intensity mapped (Marc et al., 1995). All images were prepared in Adobe Photoshop® V7.01 (Adobe Systems Inc., San Jose CA).

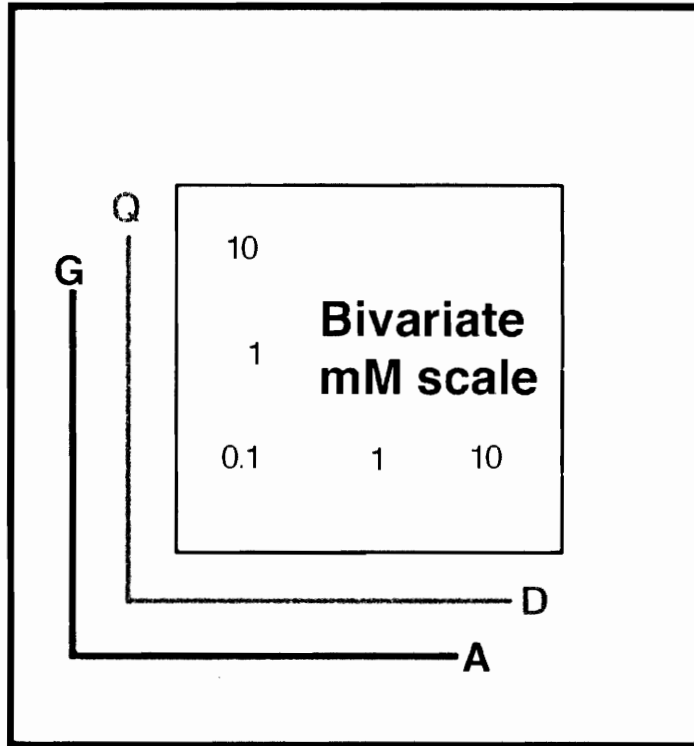


Figure 8. Bivariate scale. A bivariate scale used to examine the small molecular fingerprint of cells in a compact notation with all eight small molecular labels overlaid on top of one another to render colored data clouds of probability where each cell class contains a particular small molecular composition on a log scale from 0.1 to 10 mM. Clouds are bounded by 1 standard deviation limits and are rendered as unique "pawprints" enabling quick analysis of cell classes.

Tissues and animal models

Wild type atlas

CB-57 pigmented mice were used for WT controls in these studies due to the substantial physiologic differences in the sleep architecture that light mediates in pigmented versus albino mice (Benca et al., 1998). These differences possibly indicate alterations in retinal structure and cell populations. Additionally, light tends to enhance retinal degeneration in albino mice (Naash et al., 1996).

Degenerate retina studies

Specimens. Human RP tissue was obtained from The Foundation Fighting Blindness Retina Donor Program. Institutional approval for use of human eyes was obtained from the University of Utah and University of Pennsylvania and followed the tenets of the Declaration of Helsinki. Twenty samples of advanced RP included 16 simplex, one X-linked, one autosomal dominant (ad) RP, and two Usher's syndrome. All were fixed in phosphate buffered aldehydes, (pH 7.4) including 0.5-2% glutaraldehyde with postmortem intervals of 0.5-6.5 hours, and were stored in 2% Paraformaldehyde in 0.1M phosphate buffer at pH 7.4 (1988-2000) until they were resin embedded in 2000. Sixty-seven samples, mostly of advanced ages (pnd 150-900) from 13 rodent models of retinal degeneration were analyzed. All animal experiments were conducted according to the ARVO

Statement for the Use of Animals in Ophthalmic and Vision Research, with approval of the Institutional Animal Care Committee at the University of Utah. Animal tissues were harvested after halothane or intraperitoneal barbiturate anesthesia, followed by perfusion with or enucleation and immersion in buffered 0.5-2.5% glutaraldehyde / 1% paraformaldehyde. Some tissues were postfixed in 1% buffered osmium tetroxide pH 6.0, and all were resin embedded over the interval of 1987-2002. All were processed for computational molecular phenotyping and electron microscopy as previously described (Marc et al., 1995; Marc and Liu, 2000; Marc and Jones, 2002a). Specific models included the transgenic S334ter rat expressing a truncated rhodopsin at Ser334 (Steinberg et al., 1996); the transgenic P23H rat model of autosomal dominant (ad) RP with an N-terminal rhodopsin H mutation at P23 (Steinberg et al., 1996; Machida et al., 2000); the natural RCS rat with a *merlk* defect impairing rod outer segment phagocytosis (LaVail et al., 1975; D' Cruz et al., 2000); the natural *rd1* mouse model of autosomal recessive (ar) RP with a *pde6 β* nonsense mutation (Keeler, 1966; Pittler et al., 1993); the transgenic GHL mouse model of adRP, with a triple V20G, P23H, P27L rhodopsin mutation (Frederick et al., 2001); the transgenic TG9N mouse, expressing the N-terminal fragment of mouse RGS9 (Chen et al., 1993); the natural *nr* mouse, with a chromosome 8 defect causing Purkinje cell and rod degeneration (Landis, 1975; LaVail et al., 1993; Campbell and Hess, 1996); the natural *or* mouse model of human microphthalmia, with a null mutation

in the *chx10* homeobox gene (Robb et al., 1978; Burmeister et al., 1996); the *Chx10/p27^{Kip1}* mouse - *p27^{Kip1}* knockout rescue model of the *or* mouse (Green et al., 2003); the natural *Agtpbp1* (formerly *pcd*) mouse with Purkinje cell and slow rod degeneration (Mullen and LaVail, 1975; Blanks et al., 1982; Fernandez-Gonzalez et al., 2002); the natural *rd2* (formerly *rds*) mouse with a partial dominant *prph2* defect and slow rod degeneration (van Nie et al., 1978); the *rho*^{-/-} knockout mouse model of human RP (Humphries et al., 1997); the transgenic *rho* Δ CTA mouse with truncated rhodopsin at Ser334. Genomic DNA is extracted from mouse tails for use as polymerase chain reaction (PCR) templates. Genotypes are determined via the use of two primer pairs with the transgene and wild-type genes being distinguished by differential restriction digestions.

Electron microscopy

As will be illustrated in Chapter 5, we observed a number of changes in degenerate retinas that suggested cellular circuitries and established patterns of retinal information flow may be compromised. In order to examine these potential changes, we employed a fusion of techniques termed electron microscopy overlay that digitally superimposes light microscopic data on top of electron microscopy structural images revealing cellular identities.

Conventional transmission electron microscopy was performed at 80 Kv on 90 nm lead stained sections of aldehyde fixed retinal tissue on single-hole

grids. Sections were carbon coated and supported on Formvar film (Pelco) on single-hole grids. Sections on either side of the section reserved for electron microscopy were used for conventional light microscopy and standard silver intensified immunocytochemistry for EM Overlay as per (Marc and Liu, 2000). In short, single 90-nm gold sections immediately previous and immediately consecutive to each electron microscopic section are collected onto a glass spot slide (HTC slide, Cel-Line, Inc.), deplasticized in sodium methoxide, deosmicated with sodium periodate, and processed for postembedding immunocytochemistry with anti-IgGs followed by silver intensified immunogold visualization as described by Marc et al. (1995) and Marc and Liu (2000). Sections were then imaged for ultrastructure and light microscopy signals by overlay microscopy where light microscopy images are digitally registered to EM images and examined for aberrant synaptic activity within the microneuromas. Both high and low magnification montages were captured as conventional electron micrographs and scanned as 8-bit monochrome channels at 300-600 dpi. Large databases were assembled from the ultrastructural images as described in (Marc and Liu, 2000) and then registered to scaled optical microscope data. This process resolves one of the difficulties of EM level analysis, namely, identifying cell types that may be in inappropriate locations. Identifying cells based upon characteristic cytology and high vesicular content could lead one to conclude that one cell type is actually another in the absence of characteristic features that may not be

available in all sections. Multichannel overlays of light microscopy upon EM data allows the precise definition and identification of cells and their molecular signatures.

CHAPTER 4

NORMAL MURINE EYE

Wild type CMP retinal atlas background

A common ancestor of mice and humans, *Eomaia scansoria*, gave rise to all placental mammals. However the common mouse, *Mus musculus* did not appear until approximately 8,000 B.C. (Ji et al., 2002). Fast forward a few thousand years and beginning in the 1800s, mice were bred by fanciers, and by the 1900s mice were being used for the first experiments in genetic inheritance. Currently, mice are recognized as ideal research animals because of their small size, short generation times and prolific reproductive abilities. The genome of the the C57 BL strain used in many experimental systems and originally bred by Clarence Little, was recently sequenced (Waterston et al., 2002). This has implications for all of medical science because homologies with many human genes exist within the mouse genome (Mural et al., 2002). Thus the mouse has rapidly become a model of choice for discovering pathologies in retinal disorders (Thomas et al., 2003). The creation of a metabolic phenotypic atlas of the murine retina to identify all cell cohorts for comparison with other taxa and pathologies in retinal research was thus undertaken.

The use of transgenic mice to investigate the pathogenesis of human retinitis pigmentosa is an accepted and powerful tool (Lem and Makino, 1996). However, the use of genetic constructs has the potential of altering normal retinal cell populations and physiology (Chen et al., 1995; Masu et al., 1995; Bonfanti et al., 1996; Xu et al., 1997) including metabolic amino acid concentrations (Yazulla

et al., 1997; Jones et al., 2001), so the existence of a normative baseline with which to compare suspect or altered signatures may provide some insight into metabolic pathologic mechanisms. It has not been possible to map all the consequences of gene defects induced by either transgenic, or knock-out/knock-in strategies. The molecular phenotype atlas of the mouse retina would provide a stronger basis than simple individual cell counting, morphology or biochemistry for tracking both the cell autonomous changes induced in cells expressing altered genes and the secondary changes induced in other cells as part of a homeostatic system.

Previous attempts have been made to identify the major cell populations in the murine retina (Jeon et al., 1998), but these relied on classical morphological approaches that failed to distinguish many classes of neurons in the retina. Other studies were able to survey individual populations of neurons to a limited extent (Vaney, 1980; Martin and Grunert, 1992; Grunert et al., 1994; MacNeil and Masland, 1998; MacNeil et al., 1999), based upon a number of differing metrics including cell counts, shapes axonal and dendritic morphologies, locations and limited physiological recordings. The ability of computational molecular phenotyping to parse the entire retina into a comprehensive assembly of superclasses and classes (Marc and Jones, 2002a) renders it a far more powerful tool for tracking genetic and acquired disease differences than conventional visualization strategies.

Normal eye structure and cell populations

The implementation of classification partitions the eye into separate chemical classes that can be discriminated through classification. Individual class assignments for all ocular tissues, retina and extra-retinal are shown as univariate histograms allowing for comparison of amino acid concentration within neural and non-neural classes and across amino acid categories. Interestingly, almost all non-neural tissues in the eye contain significant amounts of glutamate that approach or even exceed that of some neural classes.

Sclera

The murine eye, indeed the eye in all mammals possesses a multilaminar, nested architecture to the globe of the eye which is enveloped at the outermost layers within a hard covering called the sclera (*gr. Skleros*). The sclera is composed of dense connective tissue, providing shape, and functions as the protective covering for the more delicate structures contained within as well as providing a platform with which to attach the ocular muscles and move the eyeball. Most of the sclera is a dense connective fibrous tissue composed of extracellular matrix and sparse, finely branched fibroblasts with only a small rind of vascular elements on the outer surface called the epi-sclera. The sclera is continuous with the anterior portion of the eye, the transparent cornea, but contains less well-ordered collagenous fibers.

Little is known of the metabolism or small molecules of the cells comprising the sclera. The sclera in the murine retina expresses two classes of cellular signatures differentiated primarily by differences in their expression of glutathione, glutamate and glutamine. Most other intrinsic amino acids do not appear in measurable quantities in the free state in the most populous class in the sclera, although the outer epithelia and endothelium of the cornea are strongly immunoreactive for taurine and slightly immunoreactive for glutathione. Deeper past Bowman's membrane, which lies immediately beneath the epithelium of the cornea, and the much thicker stromal layer, small lamellated isolated fibers immunoreactive for taurine, glutamine, glutamate and glutathione appear interwoven within the thick stromal layer (Figure 9, Figure 10). Scleral class 2 is essentially negative for all amino acids examined with the exception of a very low glutamate signal and a low glutamine signal.

Uveal tract

Progressing inward from the sclera, the next layer apparent is the uveal tract, comprising the choroid, the ciliary body and the iris. While not involved in the processing of light information, these structures are essential to the functioning of the visual system.

Figure 9. Vertical extra-retinal theme map. This image mosaic of 10 panels represents classification of the extra retinal components of the eye including the vascular choroid, sclera, musculature and connective tissue. All images are digital composites superimposed upon Toluidine blue labeled sections for clarity and orientation. Image A is a classified image with major clusters representing the vascular spaces (black), choroid (orange), sclera (light blue), three classes of musculature (light yellow, blue and purple) and connective tissues (aqua and browns). Image B (alanine), shows moderate levels of alanine in the choroid and musculature with very low levels in the sclera. Aspartate immunolabeling (image C) shows high levels of aspartate in one type of connective tissue (aqua) and in vascular elements in the connective tissue layers along with moderate levels in the choroid. Glutamate immunolabeling (image D), demonstrates very high levels of glutamate in one class of myocytes (purple in image A), and in connective tissue (aqua) with moderate levels in other myocyte classes and in choroid. Low levels of glutamate are present in the sclera. Glycine immunolabeling (image E) is largely absent from the ocular tunic with the exception of moderate levels in connective tissue vascular elements and in the choroid. Glutathione levels (image F) are moderate in connective tissue and high in the choroid. Glutamine immunolabeling (image G) reveals saturating levels in two myocyte classes (purple and blue in image A), and moderate levels in the other class. High levels of glutathione are also found in the vascular elements of the choroid with low levels present elsewhere in the tunic and connective tissue. Taurine immunolabeling (image H) is absent in the sclera but present at moderate to high levels in the musculature and in the choroid with low levels found in the myofascia surrounding the musculature. GABA immunolabeling (image I) is largely absent, save low levels in the choroid. Toluidine blue labeling of these tissues (image J), allows one to make structural discrimination, but class memberships are impossible to determine within structural classes

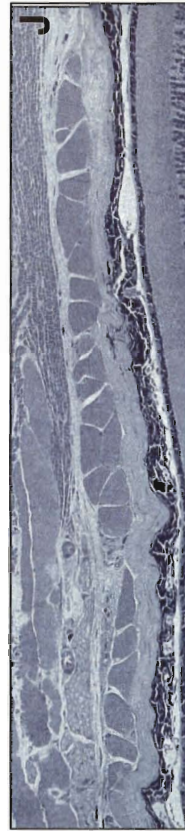
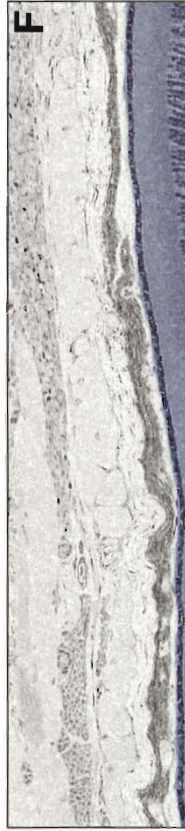
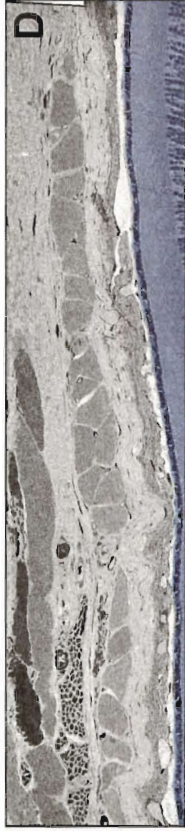
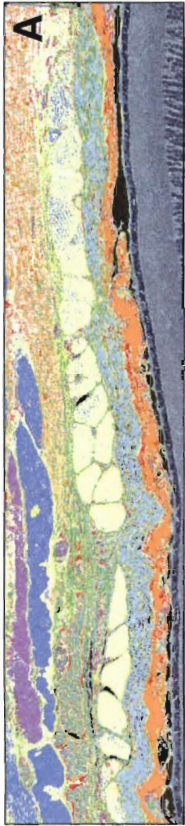
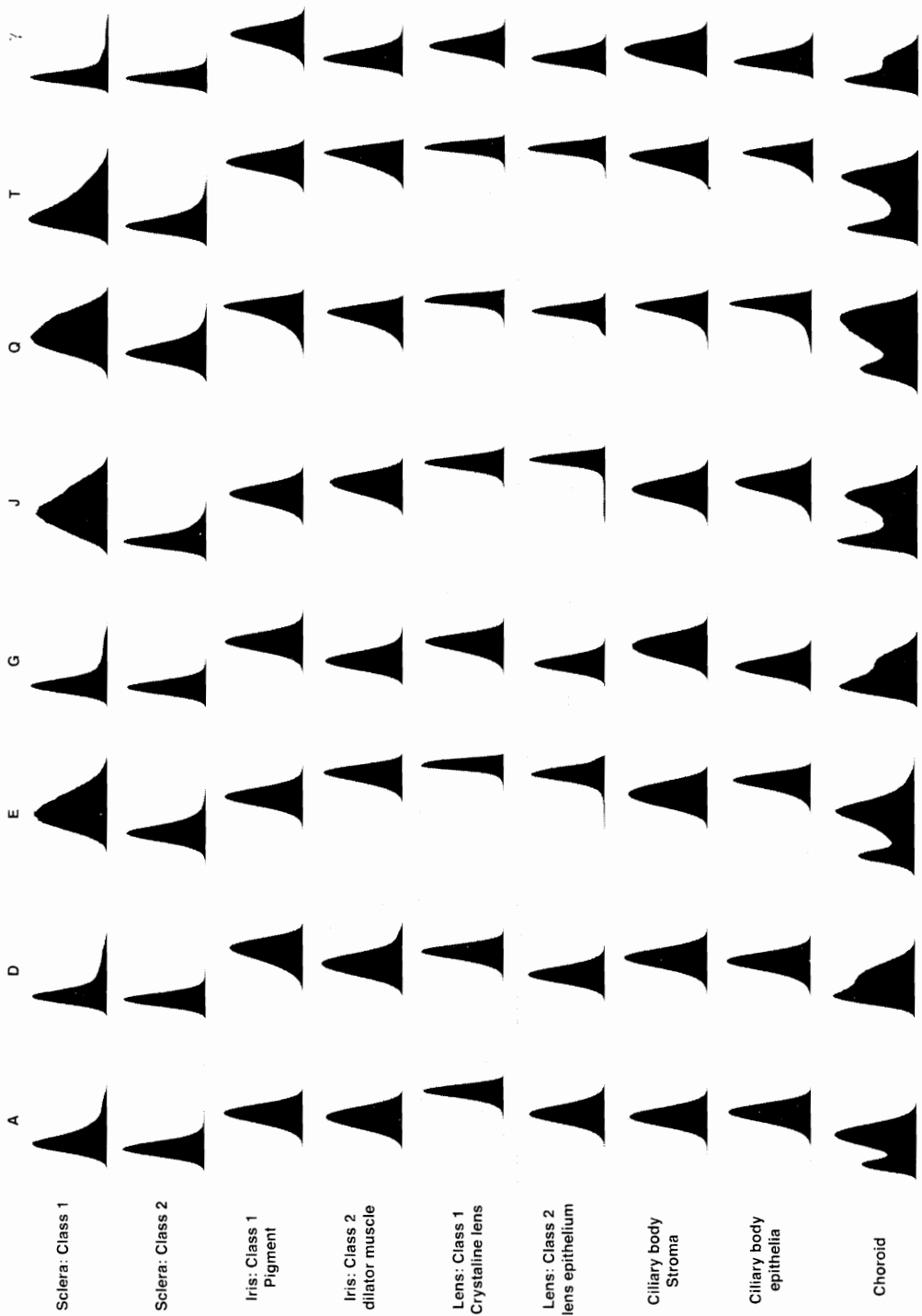


Figure 10. Univariate extra-retinal histogram matrix. A univariate signature matrix of the epi-retinal tissues of the murine eye. Horizontal columns identify the corresponding cell and theme classes. Vertical columns denote amino acid groupings. A, alanine; D, aspartate; E, glutamate; G, glycine; J, glutathione; Q, glutamine; T, taurine; γ , GABA. Each column demonstrates the distribution of a single amino acid across all theme classes and each row is the combined univariate amino acid signature for each class. Broadness of peaks in Sclera: Class 1 are due to small fibers not appearing in every section giving rise to kerf in the theme maps. Multiple peaks in the choroid distributions indicate multiple classes in the choroid which reflects its histologically complex nature. We did not attempt to completely characterize these classes as many of the cells were small and fusiform and many were not represented in all sections.



Iris

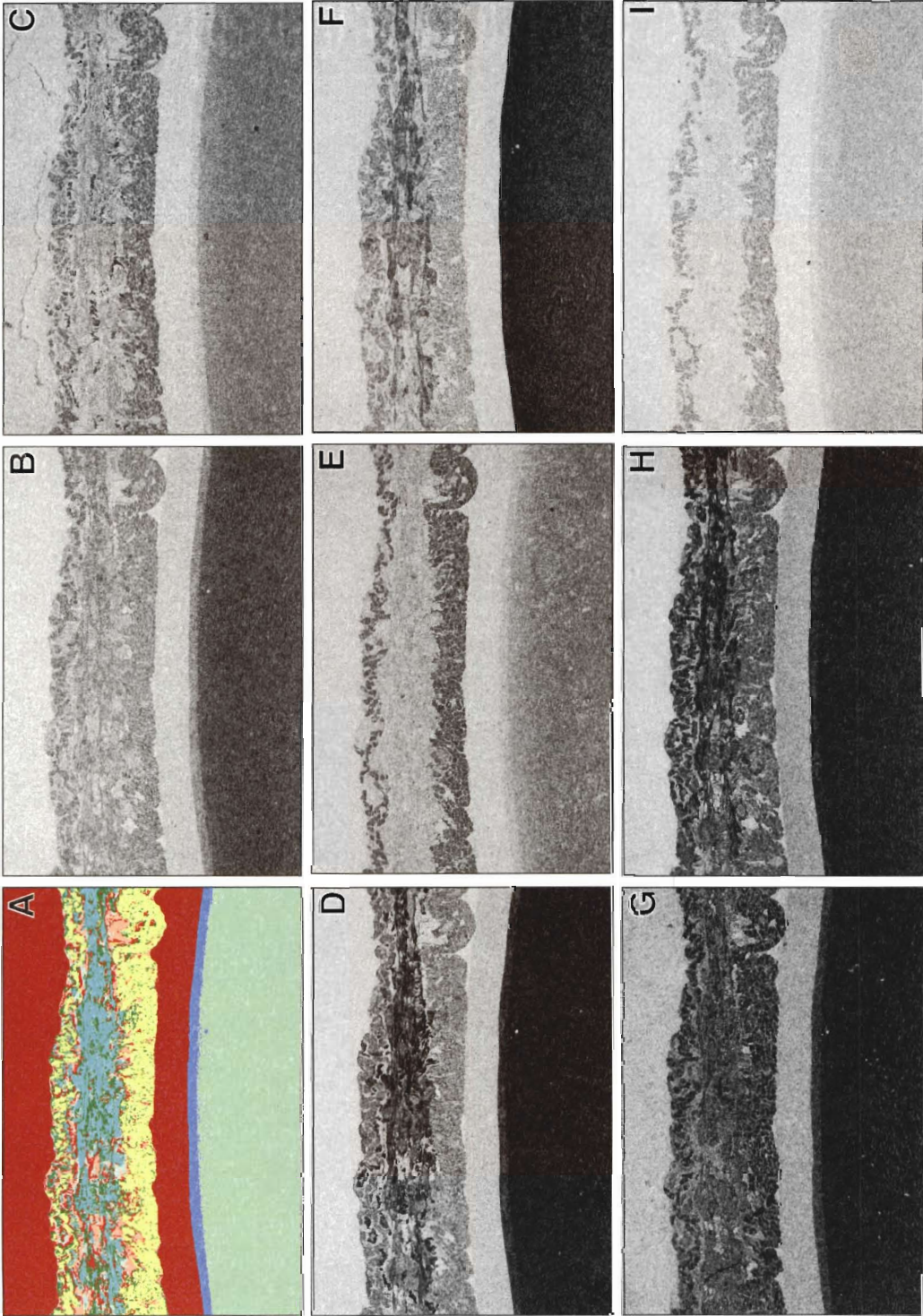
The iris divides the globe of the eye into anterior and posterior chambers and functions as an aperture stop controlling the amount of light that enters the eye via musculature that dilates or constricts it. Contraction of the iris depends upon a circular sphincter muscle that is present at the edge of the pupil, whereas the radial smooth dilator muscles of the iris cause the pupil to expand in diameter. The iris often contains melanin in pigment cells giving individuals a unique color, texture and pattern to the iris.

The molecular signatures of the iris are complex given its multicellular nature and we do not show the ciliary muscle of the iris in this dissertation. However, pigment containing cells of the iris contain all eight amino acids in at least moderate amounts with very high amounts of glutamine and taurine. The dilatory muscles segregate from the pigment or stromal layer primarily via the higher glutamate signal, a slightly higher glutathione signal, and a lower glycine signal (Figure 10, Figure 11).

Lens

The lens develops from ectodermal tissue and functions as a refractive lens to focus images onto the photoreceptor layer. The lens has two primary components including an outer epithelium and a central crystalline core, which are separable using CMP.

Figure 11. Iris and lens image matrix. A section through the iris and anterior portion of the lens showing eight amino acid labels: alanine (B), aspartate (C), glutamate (D), glycine (E), glutathione (F), glutamine (G), taurine (H) and GABA (I) and a classified theme mask (A). The musculature of the iris in these images show only the dilatory muscles of the iris (aqua color in the theme mask, A) and the stromal or pigment containing cells of the iris (yellow). The lens has two layers including the epithelial layer (blue color in A), and the crystalline lens (seafoam color in A).



Histologically, the lens epithelium is comprised mostly of proteins including laminin, entactin, heparin sulfate, proteoglycan and fibronectin as well as collagen types 1-4 (Schmut, 1978; Cammarata et al., 1986; Marshall et al., 1992), which describe the extracellular components and anterior acellular capsule of the lens. The lens epithelium is an avascular tissue that provides nutrients to the lens via diffusion from the aqueous and vitreous humor (Davson, 1990), and both the lens and lens epithelium contain significant concentrations of free amino acids in the databases tested for this study. The crystalline lens contains high concentrations of alanine, glutamate, glutathione, glutamine, and taurine with moderate concentrations of aspartate, glycine and GABA. The cellular components of the lens epithelium segregate most strongly from the crystalline lens along the alanine, aspartate, glycine and GABA axes by containing lower amounts of those four amino acids (Figure 10, Figure 11).

Ciliary body

The ciliary body of the retina lies just posterior to the iris and serves as an anchoring point for zonular attachments to the lens allowing for visual accommodation. Aside from an attachment point for the zonular fibers, functional importance of the ciliary body lies in the production of aqueous humor. Like other transport epithelia in mammals (Jean et al., 2002) and cyprinid species (Marc and Cameron, 2001), the basic signature appears similar with high basal

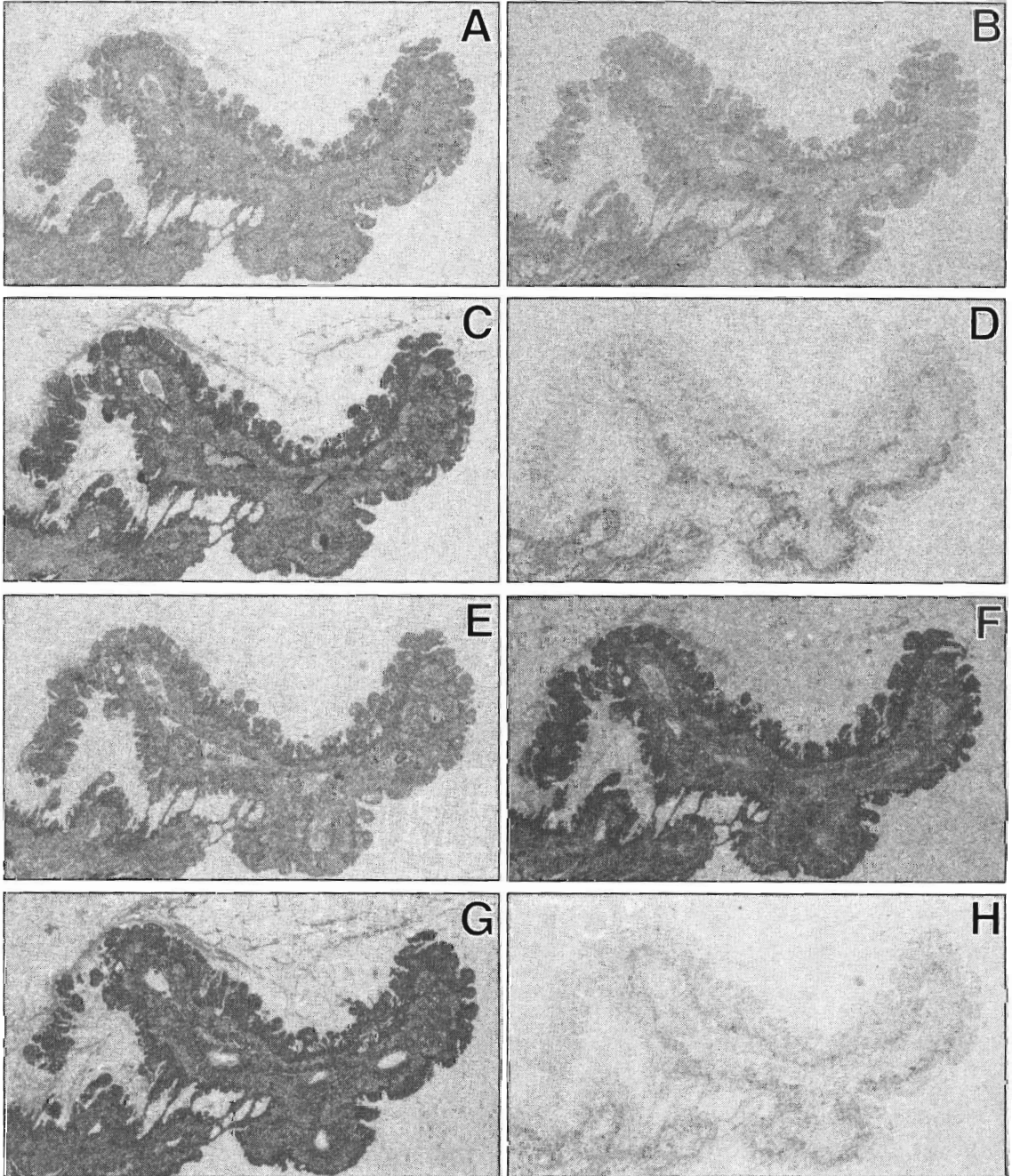
levels of glutamate, taurine and glutamine and moderately high levels of glutathione (Figure 10, Figure 12).

Choroid

The choroid, found between the sclera and retina, is a vascular layer that is also pigmented, preventing scatter of light to minimize glare and increase resolution. Most importantly, however, it functions as a vascular layer that provides nutrients to the distal retina and removes waste products. Given the highly vascular nature of the choroid, and the difficulty in isolating it from the rest of the eye structure, there is even less available literature on its small molecular biochemical composition than there is for the sclera. The advantage of immunocytochemical analysis with our approach is that we can quantify the amount of small molecules in tissues without need for dissociation or dissection of the choroid.

Our studies indicate the choroid in the murine retina contains high levels of glutathione, alanine, glutamine, glycine and moderate levels of glutamate and taurine, strongly separating on the biochemical vector axis from sclera by its glutathione and taurine vectors (Orange in theme map of Figure 9).

Figure 12. Image matrix of ciliary body. Located just behind the iris, the ciliary body is important for production of aqueous humor and serves as an attachment point for zonular fibers anchoring the lens. An image matrix of eight amino acid immunolabels of the ciliary body revealing alanine (A), aspartate (B), glutamate (C), glycine (D), glutathione (E), glutamine (F), taurine (G) and GABA (H). The signature of glutamate, taurine and glutamine appear to be common across species for transport epithelia indicating a possible common functional mechanism.



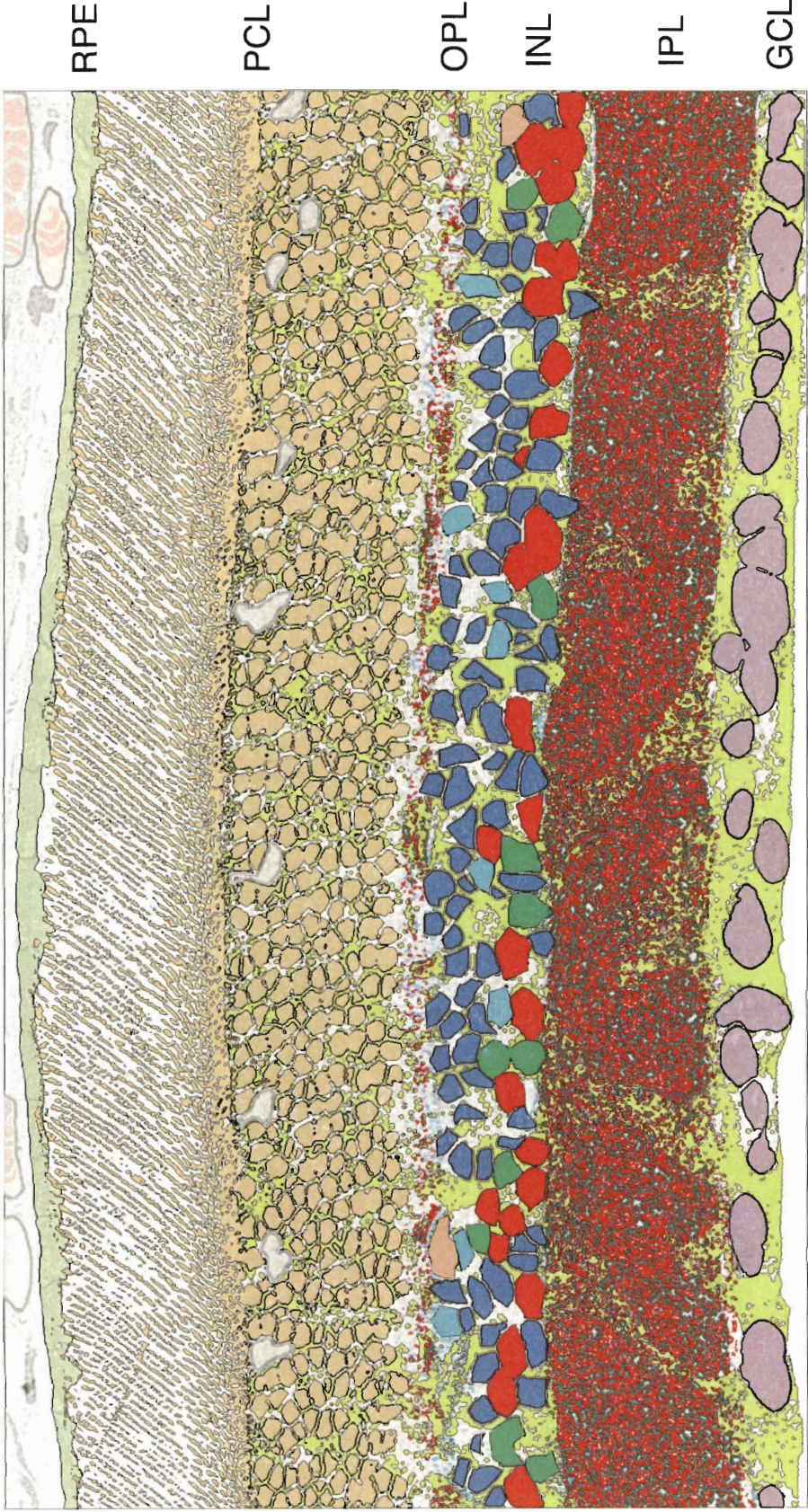
High glutamate and taurine contents in vascular tissues is a common feature observed in many vertebrate tissues (Marc and Cameron, 2001) with taurine perhaps being important for osmoregulation (Kalloniatis and Tomisich, 1999). Indeed, evidence from Jones et al. (2003b) indicates that in cases of light-induced retinal degeneration, atrophy of the choriocapillaris and the RPE impairs the ability of the retina to osmoregulate, triggering the formation of large intraretinal aqueous channels. The channels may form due to an osmotic pressure imbalance. The systemic retinal capillaries pressure likely remains normal while the residual Müller cells may not be able to transport water to the remnant choroidal stroma due to the collapse of their microvillar apical processes.

Retina proper and the retinal pigment epithelium

Normal retina has a multilaminar structure with six distinct layers as defined by traditional histologic techniques. These layers are: the retinal pigment epithelium layer (RPE), the photoreceptor layer (PCL), the outer plexiform layer (OPL), the inner nuclear layer (INL), the inner plexiform layer (IPL), and the ganglion cell layer (GCL) (Figure 13).

Data for this portion of the atlas are derived from large databases (~ 1 GB or larger) comprised of retinal tissue sections in both vertical and horizontal axes.

Figure 13. Theme map of rodent retina. A vertical section through a mouse retina illustrating the layers of the retina as retinal pigment epithelium (RPE), photoreceptor layer (PCL), outer plexiform layer (OPL), inner nuclear layer (INL), inner plexiform layer (IPL) and ganglion cell layer (GCL). This image is visualized as a theme map superimposed on a toluidine blue labeled section (grey) after classification. The map identifies rpe cells (light brown), two classes of photoreceptors (rods, brown; cones, tan), two classes of bipolar cells (light blue, ON cone bipolar cells; dark blue, rod and off cone bipolar cells), one class of horizontal cell (rust), two classes of amacrine cells (red, GABAergic; green glycinergic), Müller cells (yellow), and ganglion cells (purple).

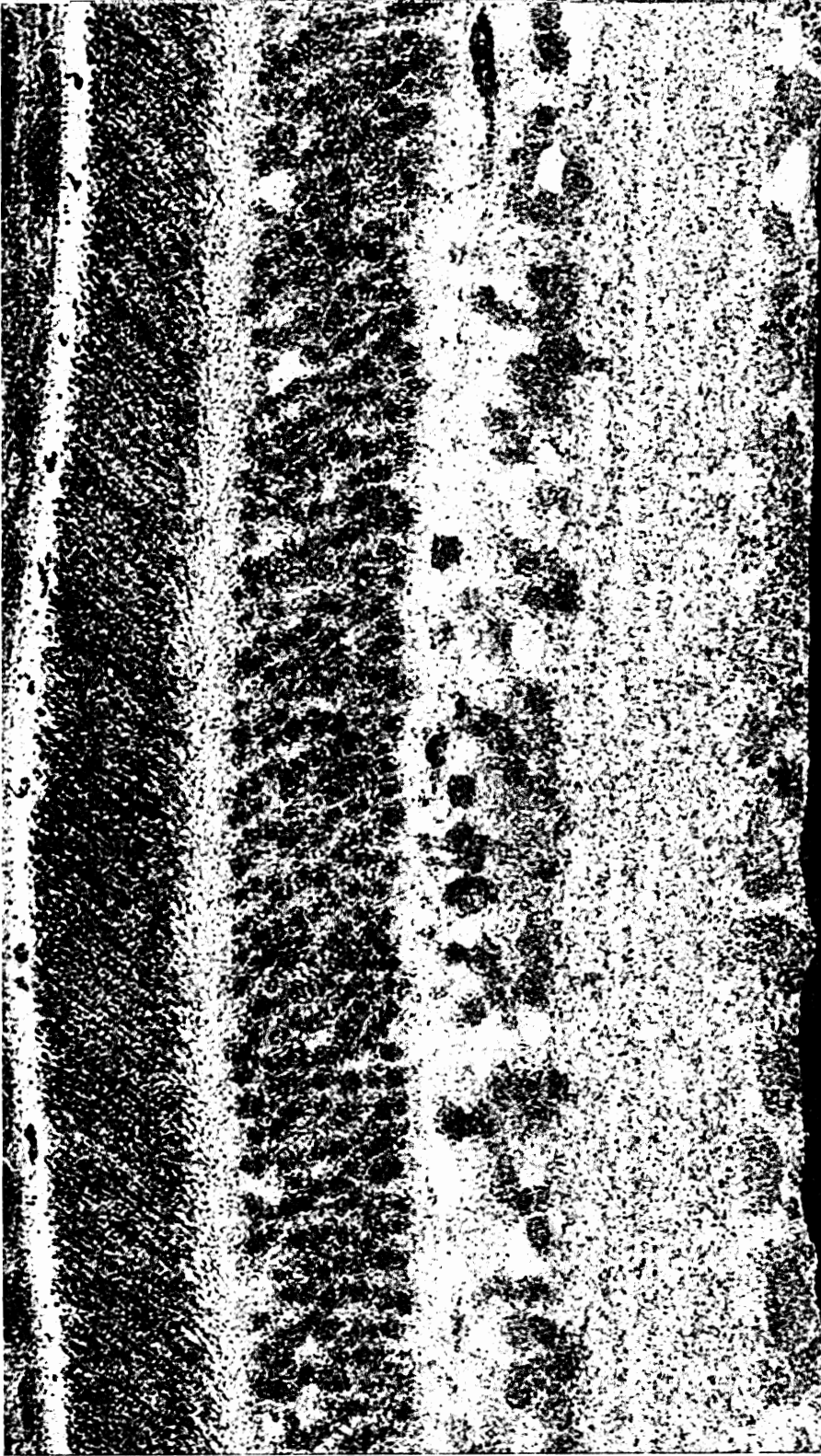


Vertical sectioning allows for comprehensive sampling of all retinal layers, while horizontal sectioning allows for examination of patternings of populations of neurons within each layer of the retina. (Figure 14, Figure 15).

Through the use of eight different amino acid probes we have partitioned the retina proper into spectral classes based upon each cell's individual amino acid concentration. Examining the overall retinal histogram matrix comprising all classes combined (Figure 16), we see multimodal histograms, which could be deconvolved using Gaussians into perhaps two or three additional individual classes.

However, there is no way to adequately classify the potentially 60 classes of cells in the mammalian retina from these comprehensive histograms based upon simple deconvolution of Gaussians, and establishing correlations between amino acids within each class would be impossible. There are simply too many classes and the relationships are too complex. Therefore multispectral unsupervised classifications were employed to classify each retina into its constituent classes, ultimately discriminating approximately half of the suspected retinal classes based upon intrinsic signals of alanine, aspartate, glutamate, glycine, glutathione, glutamine, taurine and GABA.

Figure 14. TQE→RGB vertical retinal section. A TQE to RGB coded vertical section through the retina. Three immunolabels including taurine, glutamine and glutamate are assigned to red, green and blue color channels respectively allowing for easy interpretation of cellular contents. RPE cells are at the top and colored light yellow. Photoreceptor outer segments are red with inner segments being pink. Cone photoreceptors contain higher amounts of glutamate coloring these cells blue in this assignment. Bipolar cells, amacrine cells and ganglion cells contain different amounts of these three amino acids resulting in combinations of colors whereas Müller cells in TQE to RGB constructions are seen as a yellow/gold color.



RPE

PCL

OPL

INL

IPL

GCL

Figure 15. TQE→RGB whole retina horizontal section. A glancing horizontal section through a complete mouse eye with taurine, glutamine and glutamate assigned to red, green and blue channels. In this image, the optic nerve head (ON) can be seen in the upper right portion of the image with the rectus muscles (RM, red/gold) attaching to the sclera (Sc, green) on the upper left portion of the image and one of the oblique muscles (OM) in the lower left of the image. Concentric rings of retinal layers are then represented from the sclera through to the vascular choroid, the RPE (light gold), photoreceptor outer segments (PRos, dark pink), photoreceptor inner segments (PRis, light pink), photoreceptor cell bodies (PR, dark centers surrounded by pink borders), bipolar cells (BC, shades of purple and pink), amacrine cells (AC, varying shades of blue to light green and red), inner plexiform layer (IPL, fine filigree of purple, blue and green), ganglion cell layer (GCL, varying shades of blue and green at center of image) and the optic fiber cell layer (fl, long blue structures at the center of the image).

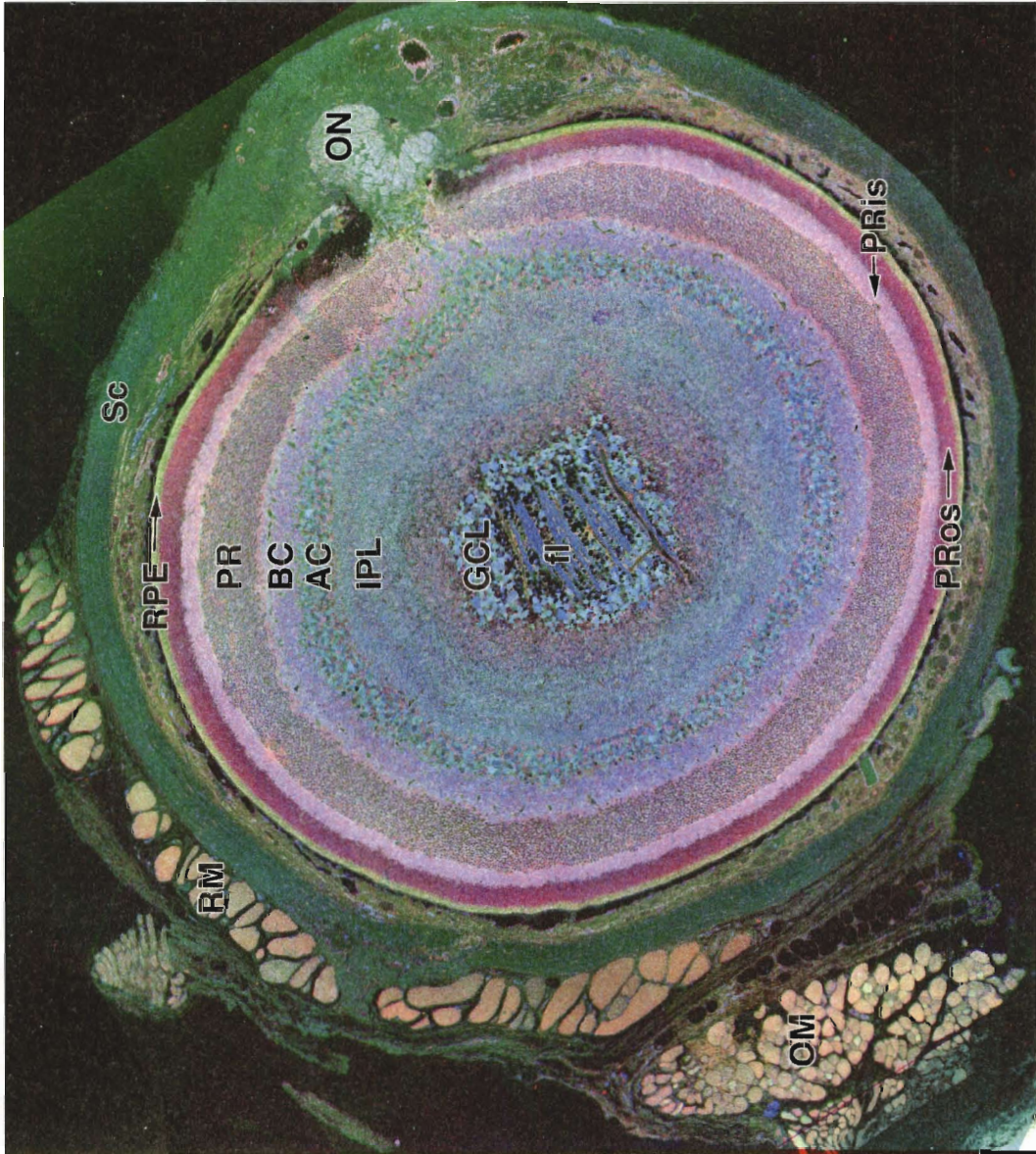
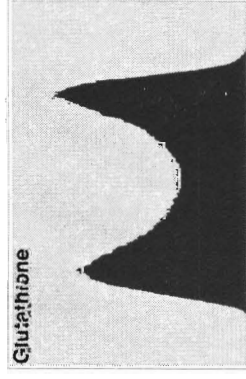
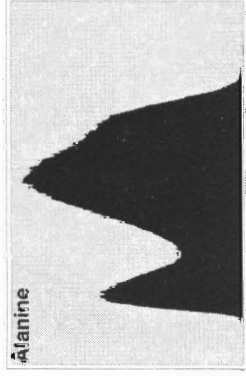
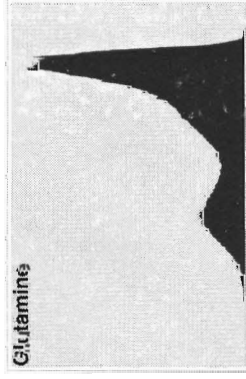
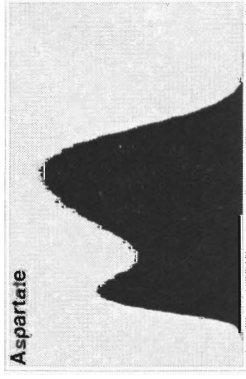
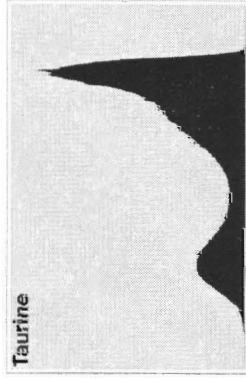
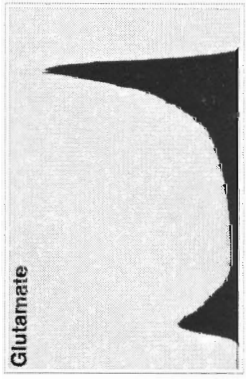
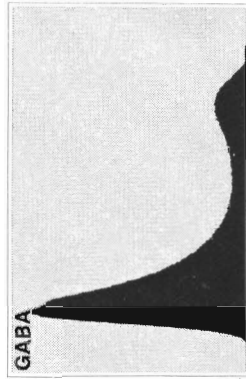
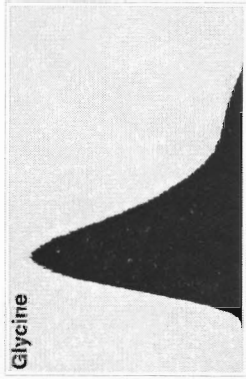


Figure 16. Whole retina histogram matrix. Univariate histograms taken from the entire murine eye with no classes subtracted from the total. Each individual label illustrates multiple peaks containing still more peaks hidden within. Simple Gaussian deconvolution of these histograms may reveal two, perhaps three peaks, but not the entire 30 classes that we were able to extract. Additionally, there is no way to adequately demonstrate any relationships between those peaks or classes in these whole retina histograms without a formal image classification. Furthermore, some of the rare classes of cells may approximate less than 1% of the total number of pixels within these histograms showing the power of image classification.



It is important to understand that the classification is comprehensive; no cells are excluded. Thus the cell coverage of the method is 100% even though the fraction of classes + superclasses resolved is only about 50%.

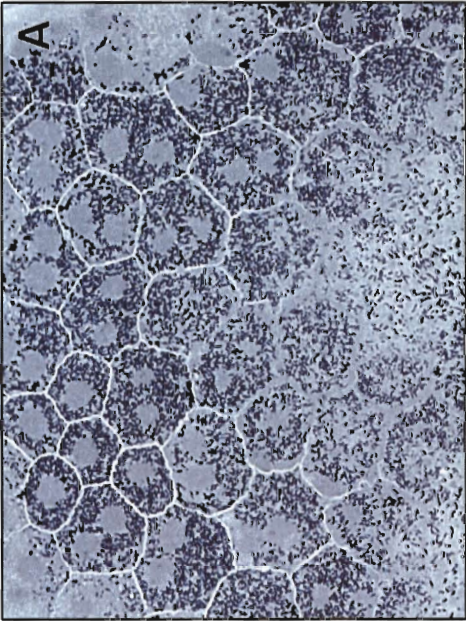
Retinal pigment epithelium

RPE cells are polygonally shaped multinucleate polarized epithelial cells (Figure 17) coupled via gap junctions (Gouras et al., 1976) that form the retinal-blood barrier in much the same manner as the capillary endothelial cells of the CNS: via basolateral tight junctions.

The RPE has numerous critical physiologic roles: (1) phagocytosis of shed outer segments of photoreceptors, (2) nutrient and oxygen transport from the blood into the retina, (3) directional transport of retinol and retinal, (4) conversion of all-trans retinol to 11-cis-retinol, (5) spatial buffering of extracellular potassium levels, (6) water transport from the retina to the choroids, (7) quenching of reactive oxygen species, (8) absorption of stray light via melanosomes (Bok, 1993).

Given their coupling, all RPE cells should express the same small molecular signature, which is the case in normal healthy retina. However, the RPE contains transporters for amino acids (Salceda and Saldana, 1993; Fletcher and Kalloniatis, 1996), and amino acid concentrations might be expected to change given appropriate conditions.

Figure 17. Horizontal section through RPE. An off-axis horizontal section through the retinal pigment epithelium (RPE) illustrating the multinucleate nature of these cells along with their cuboidal shape. RPE cells in the normal retina are connected via gap junctions and therefore maintain a confluent small molecular signature. In this figure, a toluidine blue labeled section (A) is illustrated along with the three principal molecular signals for this tissue including glutamate (B), glutamine (C) and taurine (D). The pigment granules can also be appreciated as the dark granular in the toluidine blue labeled section which correspond to the blank spots in B, C and D. Interestingly, there appears to be a slight gradient from apical to basal in the distribution of glutamine and taurine. This is also seen in high resolution vertical sections of the retina.



Indeed, in experimental retinal detachment (Marc et al., 1998a) and instances of genetic abnormalities (Fletcher and Kalloniatis, 1996), small-molecular biochemical alterations are observed in RCS rat revealing amino acid immunoreactivity for glutamate and aspartate changes, which can be seen to decrease while glutamine increases in the RPE (Fletcher and Kalloniatis, 1996) during degeneration. Additionally, in human retina, early in the degenerative process of retinal degenerative diseases, uncoupling of the retinal pigment epithelium has been inferred from heterogeneous RPE signatures (Marc et al., 2001), providing a possible early indicator of the RPE status (Figure 18). This supports earlier work revealing failure of the RPE in RCS rat (Caldwell et al., 1982; Caldwell et al., 1984) Ultimately it was discovered that the RPE defect in the RCS rat was triggered by a mutation in the *mertk* gene, coding for an epithelial transmembrane receptor tyrosine kinase (Gal et al., 2000).

The normal murine RPE is characterized by moderately high glutamate levels, high taurine and glutamine, light to moderate glutathione immunolabeling, and low levels of the other amino acids (Figure 17).

Müller cells

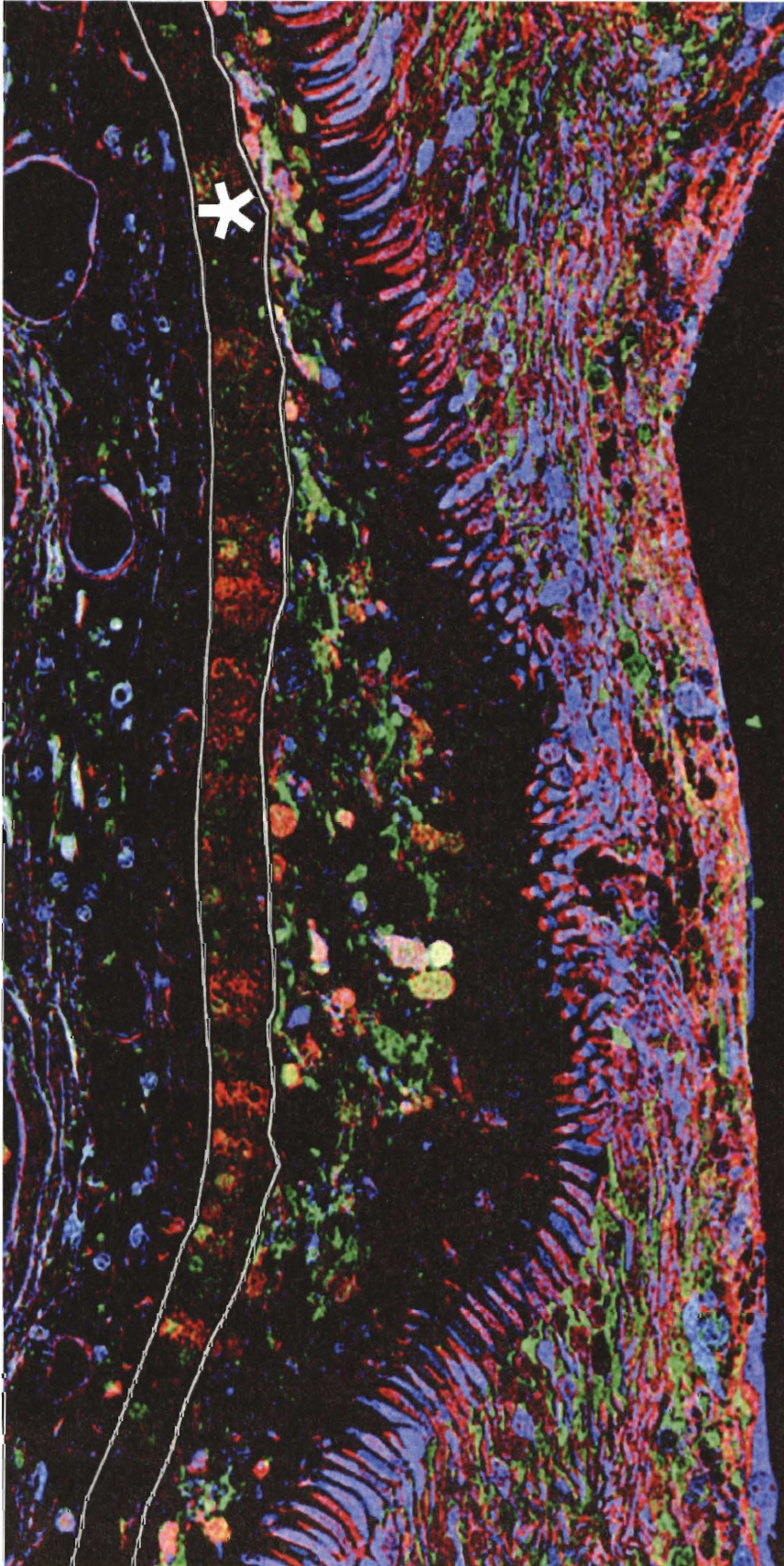
Müller cells are the retina's radial glial cells and occupy up to 50% of the total space of the peripheral retina in terms of volume (Kalloniatis et al., 1996). Most immunocytochemistry of Müller cells in the literature has focused on

proteins. The signature macromolecules of Müller cells are glutamine synthetase (Riepe and Norenburg, 1977), vimentin (Dahl and Bignami, 1982), and glial fibrillary acidic protein (Bignami, 1984). The latter protein is expressed at low levels in the end feet of Müller cells, and expression is upregulated in retinas that have undergone traumatic detachment (Erickson et al., 1987; Lewis et al., 1989), and display other pathologies such as retinal degeneration (Eisenfeld et al., 1984).

Müller cells serve a carbon skeleton recycling function (Kalloniatis et al., 1994) and as expected, immunolabeling of cells in the murine retina reflects this role with high levels of glutamine immunoreactivity seen throughout the extent of the cell. Other functions of Müller cells include transport of amino acids including glutamate (Brew and Attwell, 1987) and GABA (Malchow et al., 1989; Johnson et al., 1996) and ionic buffering (Newman and Reichenbach, 1996).

In normal murine retina, the Müller cell signature is distinguished by its unique mix of high taurine, high glutamine and low glutamate levels. No other retinal cell ever expresses this combination. Remarkably, all Müller cells contain low levels of glutamate in spite of the fact that they express the glutamate transporter EAAT1 (GLAST) (Otori et al., 1994; Derouiche and Rauen, 1995; Lehre et al., 1997). This is due to the fact that glial glutamine synthetase rapidly converts almost all transported glutamate to glutamine (Pow and Robinson, 1994; Marc et al., 1998a).

Figure 18. TQE→RGB of human RP fovea. A TQE to RGB reconstruction of the fovea in the human retina early in the degenerative process revealing multiple signatures within cells of the RPE. These differing signatures reveal evidence of uncoupling of cells within the retinal pigment epithelium (*) providing a possible early indicator of the RPE health or status of the degenerate retina. In normal, healthy tissue, the RPE signature should be confluent with no alteration or differentiation in the signatures, cell to cell. Also visible in this image is a buildup of detritus in the remnant subretinal space presumably from degenerate rod photoreceptors.



Blockade of glutamine synthetase, ischemic loss of ATP (glutamine synthetase is ATP-dependent), or down regulation of glutamine synthetase expression in retinal detachments all leads to increases in steady-state Müller cell glutamate signals. Similarly, a low GABA level is maintained in spite of the presence of GAT3, a GABA transporter (Malchow et al., 1989; Johnson et al., 1996), due to the high levels of GABA transaminase in Müller cells. The characteristic molecular phenotype of Müller cells is easily distinguished in RGB reconstructions using both TQE and YGE axes (gold color in Figure 14). These signatures hold in other vertebrate models as well (Marc et al., 1995; 1998b; Kalloniatis et al., 1996; Kalloniatis and Tomisich, 1999; Marc and Cameron, 2001; Marc and Jones, 2002a). In terms of cell classes dominated by amino acid immunolabels, Müller cells are the dominant glutamine labeled class in the murine retina. Functionally, the Müller cell signature reveals its role as that of a center for glutamine synthase conversion of glutamate to glutamine (Pow and Robinson, 1994; Derouiche and Rauen, 1995; Pow and Crook, 1996).

Photoreceptors

Photoreceptors function as the signal input layer of the retina. Structurally, they can be subdivided into outer segments (OS) and inner segments (IS). The OS of rods contains large numbers of membranous discs that contain high concentrations of the GPCR rhodopsin. The IS contains the

rest of the cell's cohort of organelles and is attached to the OS via a small stricture through which a cilium projects.

Evolutionarily, the rods are newer anatomical and functional transducers of light than are the cone photoreceptors (Okano et al., 1992; 1995) and, in mammals, appear to have co-opted much of the cone circuitry for signaling of scotopic light information, passing signals from rods to ganglion cells via an indirect pathway (Famiglietti and Kolb, 1975; Smith et al., 1986; Strettoi et al., 1990; 1992).

Although mice have cones containing S and M opsins indicating capacity for color vision (Applebury et al., 2000) and might contain the circuitry for color vision, they also contain novel circuitry providing a direct pathway from rods to OFF bipolar cells (Tsukamoto et al., 2001). However, that said, mice appear to have much the same organization as human retina, but without any foveal anatomy.

Rod cell bodies contain no alanine, very low levels of aspartate, high levels of glutamate, no glycine, no glutathione, high concentrations of glutamine, moderate levels of taurine and no GABA. Rod inner segments exhibit higher concentrations of glutamate than the outer segments with cones having lower glutamate concentration than the surrounding rods (Figure 19, Figure 20).

The decrease in small molecular signals in the outer segments most likely has to do with the high packing density of rhodopsin molecules (Zwas and

Alpern, 1976) and disks, with little cytosolic space. Other small molecular signals for inner segments reveal light immunolabeling, e.g., aspartate. Inner segments also label lightly for glutathione, very high glutamine levels, high taurine and low levels of GABA. Rod and cone cell bodies contain very similar amounts of small amino acids with cones exhibiting lower levels of glutamate, and slightly higher levels of glutathione and taurine.

The cone superclass contains no alanine, no aspartate, moderately high glutamate, no glycine, no to low levels of glutathione, high glutamine, high taurine, and no GABA (Figure 19, Figure 20). It is not surprising that most photoreceptors would have similar molecular signatures as they appear to be weakly coupled via gap junctions between cones and cones and rods (Wu and Yang, 1988; Tsukamoto et al., 1992). It is not certain that those junctions always remain open, however.

Horizontal cells

These cells comprise a small percentage of the total cohort of cells within the mammalian retina and approximate 5% of cells within the inner nuclear layer (Martin and Grunert, 1992; Strettoi and Masland, 1995; Jeon et al., 1998). Mice and rats express only one type of horizontal cell, whereas most other mammals express two morphologically distinct types (Masland, 2001b). Fish express yet a third and fourth type (Lasater, 1986; Marc and Cameron, 2001),

Figure 19. Univariate signature matrix of the inner nuclear layer. A univariate signature matrix of the inner nuclear layer tissues of the murine eye including the rod and cone photoreceptor cell bodies, the rod inner and outer segments, both principal classes of bipolar cells, Müller cells, and horizontal cells. Horizontal columns identify the corresponding cell and theme classes. Vertical columns denote amino acid groupings. A, alanine; D, aspartate; E, glutamate; G, glycine; J, glutathione; Q, glutamine; T, taurine; γ , GABA.

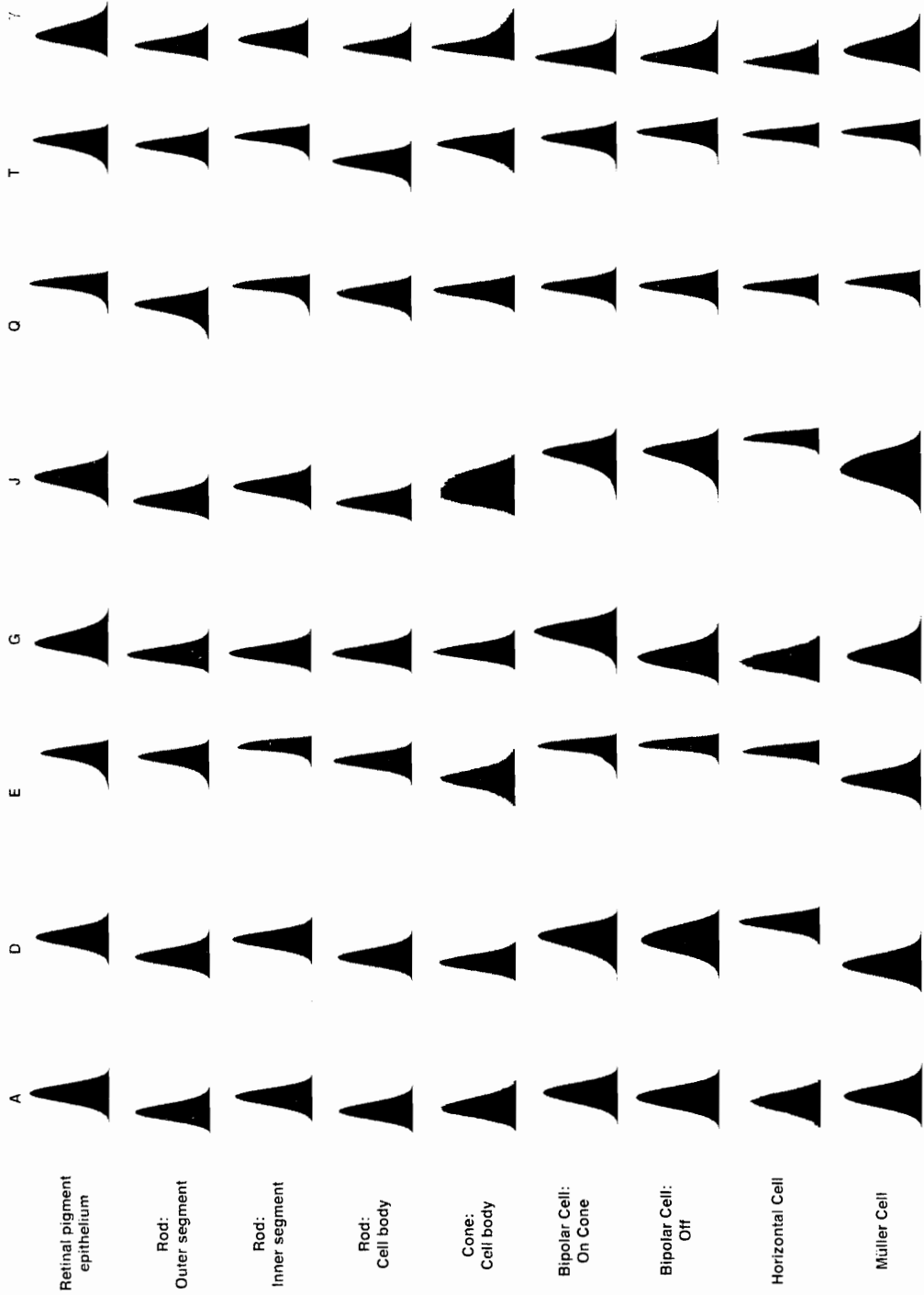
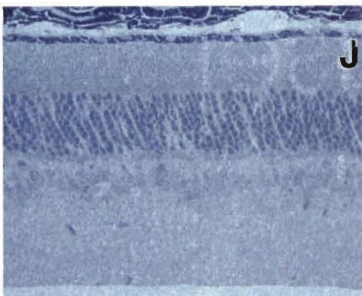
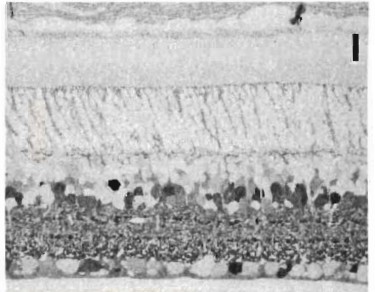
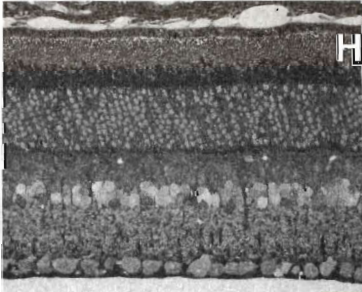
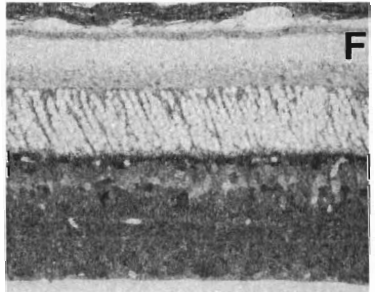
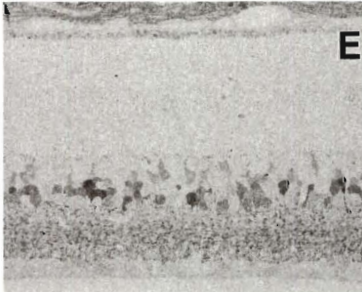
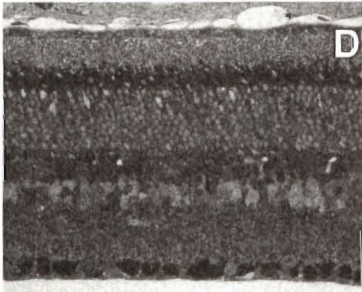
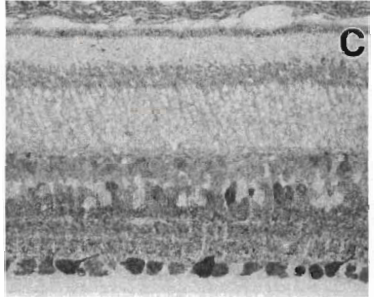
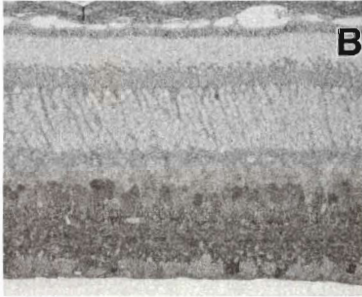


Figure 20. Image matrix of classified murine retina. A matrix of a classified normal murine retina showing (A) theme map of classes, (B) alanine, (C) aspartate, (D) glutamate, (E) glycine, (F) glutathione, (G) glutamine, (H) taurine, (I) GABA, and (J) tol blue. Each section is 200nm thick and immediately adjacent to the previous section and image classifications were constructed from images B-I creating the theme map shown in A.



and some evidence indicates a third type of horizontal cell may also be found in human retina (Kolb et al., 1994).

While horizontal cells express dendritic arbors and axons with teleodendritic arbors at the ends, the two ends are electrically isolated from one another leading to physiologically independent functions (Nelson et al., 1975). Given that there is only one horizontal cell population in murine retina, one would expect that lateral inhibition via the horizontal cells in the murine retina could take two forms: the teleodendritic arbors contacting rods and rod bipolar cells, and the dendrites from the cell body of the horizontal cell contacting the cones and the cone bipolar cells allowing for horizontally mediated local receptive fields. Horizontal cells are coupled to one another (Piccolino et al., 1984; Dacey et al., 2000; Packer and Dacey, 2002) and consequently would be expected to all have the same small molecular signature. All horizontal cells observed in the murine retina have the following signature: low alanine, moderately high aspartate, very high glutamate, no glycine, very high glutathione, very high glutamine, very high taurine, and no GABA. (Figure 19, Figure 21).

Horizontal cells separate from other ONL classes primarily on the aspartate and glutathione axes with horizontal cells containing the highest concentration of aspartate and glutathione of the neurons in the INL (Figure 19, Figure 21). In fact, differentiating the horizontal cells from the other classes in

the INL can be accomplished with aspartate or glutathione immunolabeling alone in the murine retina (Figure 21).

Bipolar cells

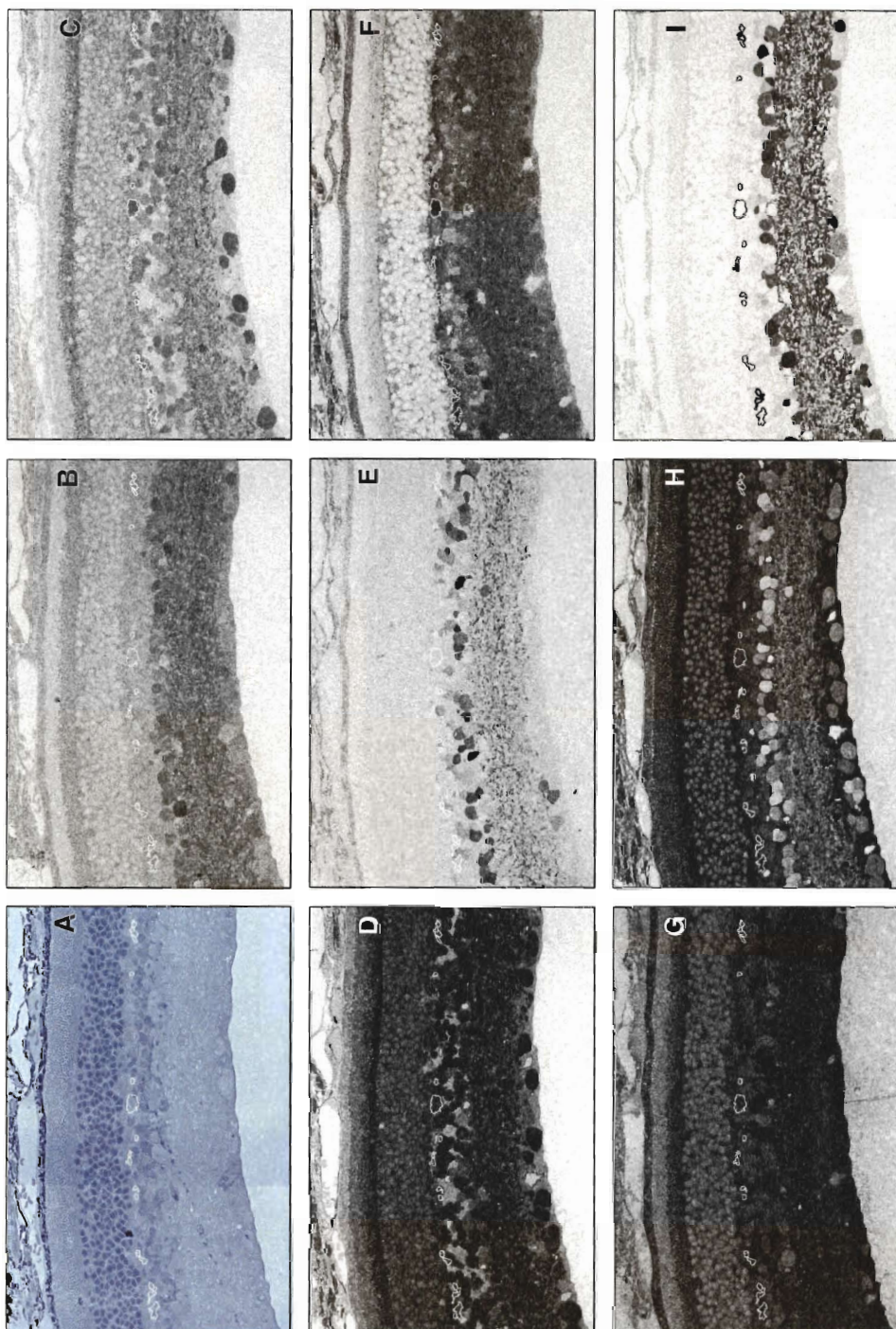
There are 10 classes of cone bipolar cells in the mammalian retina. Rod bipolar cells (Ishida et al., 1980), blue cone bipolar cells (Kolb et al., 1992), 4 ON cone bipolar cell varieties, and 4 OFF cone bipolar cell varieties. The 4 types of ON and 4 types of OFF might be distinguished by sustained versus transient light response properties (Awatramani and Slaughter, 2000; DeVries, 2000).

Bipolar cells may be classified according to their small molecular content, calcium binding proteins, receptors or synapse number, distribution and stratification (McGuire et al., 1984; Grunert et al., 1994; Hartveit et al., 1994; Marc et al., 1995; 1998b; Marc, 1999a; Haverkamp and Wässle, 2000) and reflect each cell type's individual function within the retinal circuitry.

Physiologically, cone bipolar cells may be subdivided into sustained and transient varieties in both the ON and OFF pathways mediated by differential expression of glutamate receptors (Awatramani and Slaughter, 2000; DeVries, 2000).

Our current methods do not resolve all bipolar cell classes. The immunocytochemistry of the eight intrinsic small amino acids in our IgG library reveals two classes of bipolar cells, the OFF center cone and ON center rod

Figure 21. Image matrix with horizontal cell. A matrix of peripheral normal murine retina with the horizontal cell class and horizontal cell processes outlined against the amino acid labeling. The image labels are (A) tol blue, (B) alanine, (C) aspartate, (D) glutamate, (E) glycine, (F) glutathione, (G) glutamine, (H) taurine, (I) GABA. Each section is 200nm thick and immediately adjacent to the previous section. From this image the relative invisibility of the horizontal cell can be appreciated in the tol blue, alanine, glutamate, glycine, glutamine, taurine and GABA labels. The small molecular amino acid signature for the horizontal cells in murine retina is as follows: low alanine, moderately high aspartate, very high glutamate, no glycine, very high glutathione, very high glutamine, very high taurine, and no GABA. Image classification reveals their separation along the aspartate and glutathione axes with horizontal cells containing the highest concentration of aspartate and glutathione of the neurons in the INL.



class containing low alanine, moderate aspartate, high glutamate, no glycine, moderate glutathione, high glutamine, high taurine, and no GABA. The ON center cone class contains low alanine, moderate aspartate, high glutamate, low, but significant and unique levels of glycine indicating their coupling with All amacrine cells (Famiglietti and Kolb, 1975; Mills and Massey, 1995; Trexler et al., 2001), moderate glutathione, high glutamine, high taurine, and no GABA. The signatures of all bipolar cells are almost identical but for the glycine signal of ON center cone bipolar cells (Figure 19, Figure 20, Figure 21).

Bipolar cell populations can often obscure horizontal cells if one were to examine single glutamate, glutamine or taurine alone or in combination. Aspartate and glutathione are the principal amino acids that separate the horizontal and OFF center rod bipolar cell classes. Horizontal cells also exhibit slightly lower concentrations of glutamate than do bipolar cells, illustrating the quantitative benefits of a multispectral analysis in partitioning cells (Figure 21).

Inner plexiform layer

The inner plexiform layer is roughly 30 μm thick in the mouse retina, containing massive numbers of synapses among the terminals of the bipolar, amacrine and ganglion cells. A dense meshwork of GABA, glutamate and glycine signals is observed in the inner plexiform layer, and these conform to the signals found in their somas.

Amacrine cells

Amacrine cells outnumber other types of retinal neurons (Martin and Grunert, 1992; Strettoi and Masland, 1995; Jeon et al., 1998) with the exception of photoreceptors and bipolar cells, and tend to have much more narrowly specified, diverse roles than do the other lateral channel elements, the horizontal cells.

On the whole, amacrine cells in the mouse retina contain similar levels of glutamate to bipolar cells and are grouped into three principal categories based upon the levels of GABA and/or glycine with almost all amacrine cells exhibiting either GABA or glycine (Marc et al., 1995; Kalloniatis et al., 1996). One class of amacrine cell expresses neither GABA nor glycine in significant levels, and we believe this class to be the dopaminergic cell class, which we discuss below.

The GABA dominated superclass comprises 8 classes of cells differentiated primarily on the bases of GABA levels, taurine levels and aspartate levels with weakly differential glycine levels. Five of the 8 amino acid levels examined in the GABA dominated superclass contain no significant correlations with GABA content, but there does appear to be a weak correlation between GABA levels and alanine levels. The mean level of GABA measured by immunocytochemistry decreases with the mean level of alanine. With the exception of one class ($\gamma 5$) there also appears to be a weak trend towards lower

glycine levels in GABAergic amacrine cells that express the lowest levels of GABA. These relationships do not hold true for the glycine superclass of amacrine cells. Additionally, most of the GABAergic amacrine cells appear to be responsive toward kainic acid in previous studies of rabbit retina (Marc, 1999a) with a kainic acid response trend that appears to reflect the amount of GABA contained in them, and all glycinergic amacrine cells tested in the rabbit were kainic acid responsive (Marc, 1999a). Perhaps these trends hold here, but elucidation will depend upon AGB testing. Finally, with the exception of 2 amacrine cell classes ($\gamma 3$, $\gamma 4$) taurine appears to also have an inverse relationship with taurine levels increasing while GABA levels decrease (Figure 22).

Five glycinergic amacrine cell classes were identified and were separable primarily on the basis of glycine, GABA, taurine and aspartate levels. Two of the glycine classes also had low levels of GABA in them with the other three classes exhibiting no measurable GABA. Taurine levels varied widely with a trend towards higher taurine levels in those glycinergic amacrine cells with lower levels of glycine (Figure 23).

The murine retina contains glycinergic A11 and GABAergic A17 amacrine cells that play crucial roles in the circuitry of scotopic vision in mammals by bridging the rod pathway into the cone pathway (Bloomfield and Dacheux, 2001).

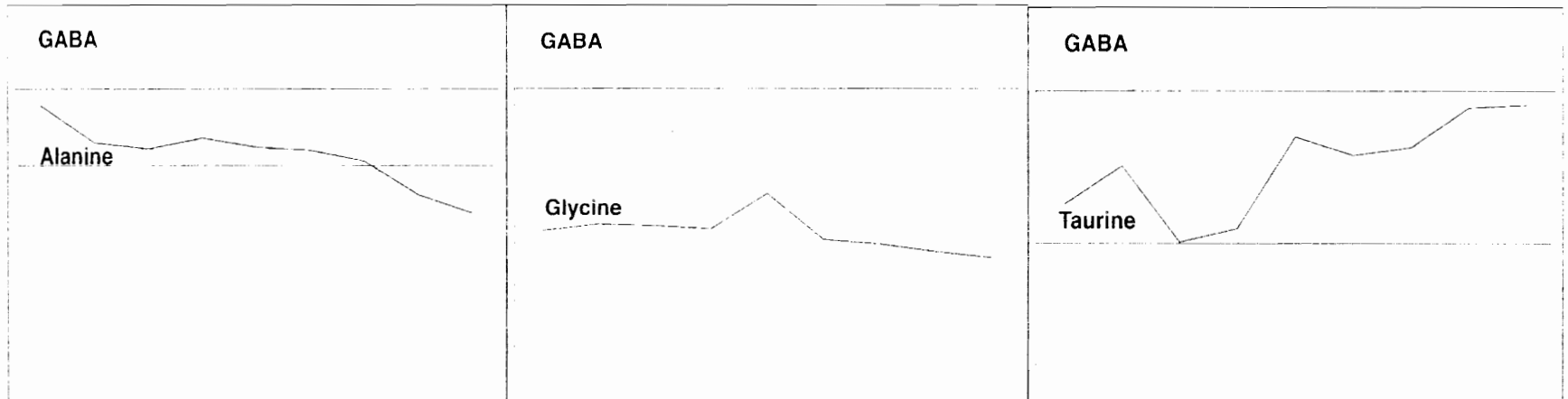


Figure 22. Immunoreactivity of GABAergic amacrine cells. Graphs of the levels of immunoreactivity in the GABAergic amacrine cells for alanine, glycine and taurine versus GABA. The y-axis represents concentration of amino acids with the x-axis demonstrating different classes of GABAergic amacrine cell classes. The trend for alanine versus GABA shows alanine levels dropping along with GABA levels in all GABAergic amacrine cell classes. The trend for glycine versus GABA reflects this same trend with the exception of one class, ($\gamma 5$) representing the peak in the glycine signals in the second graph. Taurine with the exception of amacrine cell classes ($\gamma 3$ and $\gamma 4$) has an inverse relationship with GABA levels.

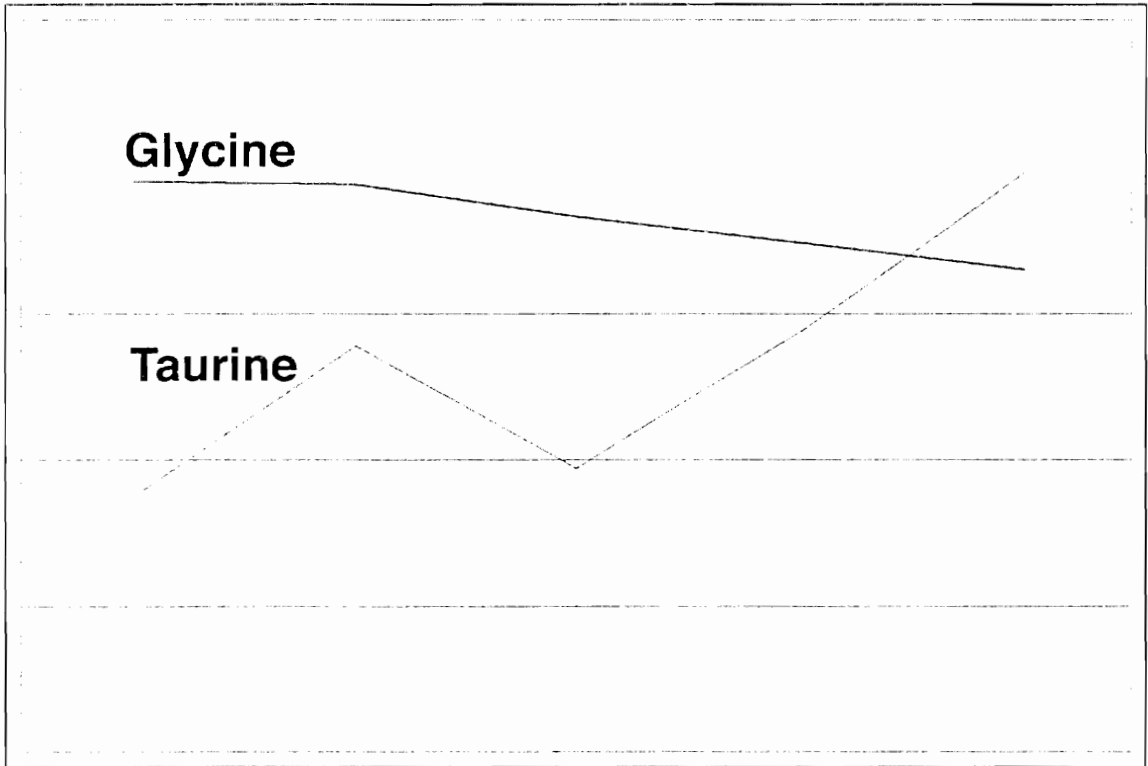
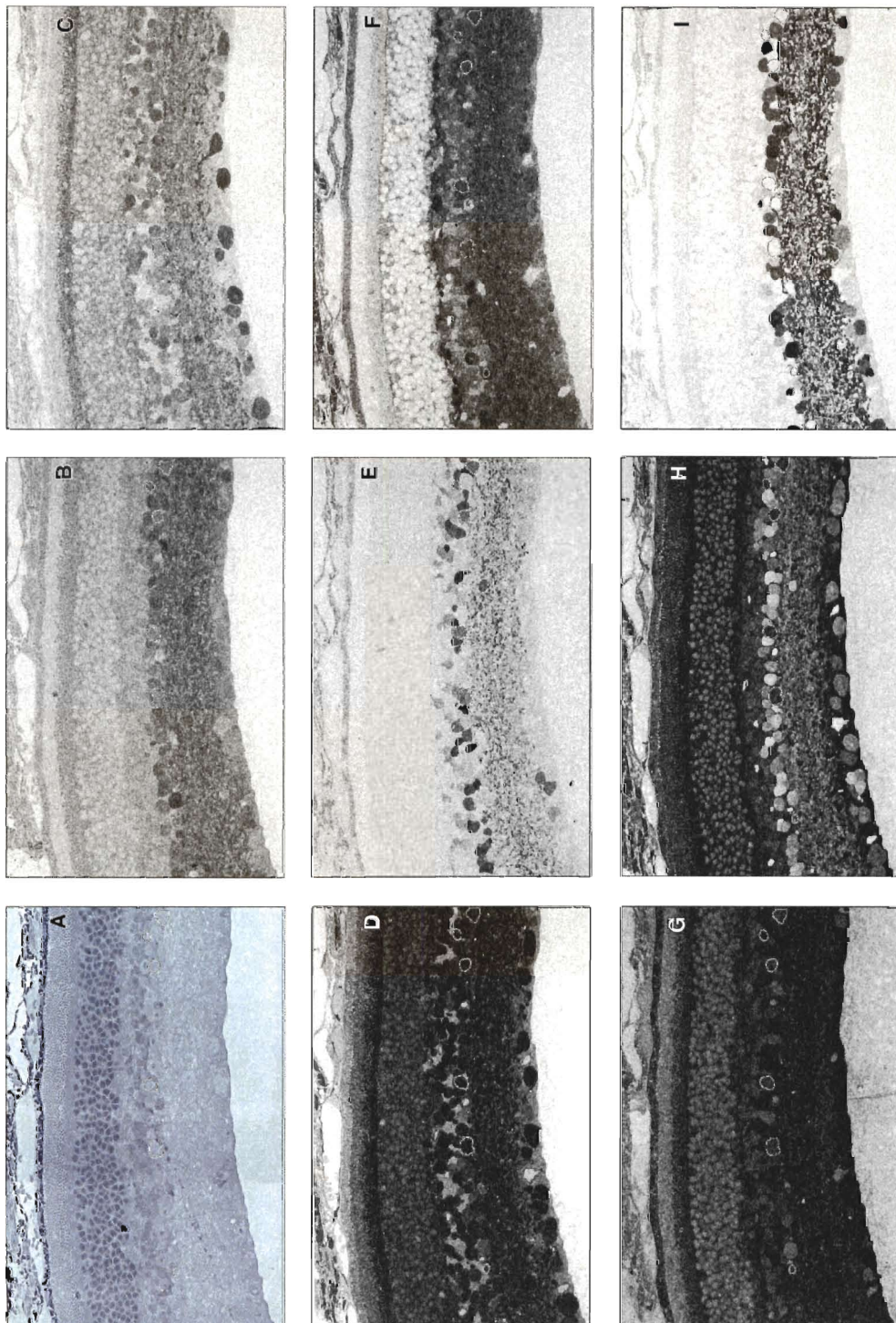


Figure 23. Glycine and taurine in the glycinergic amacrine cells. This graph shows the relationship of glycine to taurine in the glycinergic amacrine cells. All glycinergic amacrine cells with the exception of class G3 have increasing amounts of taurine in them as glycine levels decrease. The y-axis represents concentration of amino acids with the x-axis demonstrating different classes of glycinergic amacrine cell classes.

The All amacrine cell along with the A17 play roles as intermediates allowing the evolutionarily newer scotopic visual system to piggyback upon the cone based or photopic visual system. The All amacrine cells comprise approximately 13% of the amacrine cell population (MacNeil et al., 1999) and collect information from bipolar cells receiving information from rods and then delivers a depolarizing potential to ON cone bipolar cells via gap junctions and a hyperpolarizing signal to OFF cone bipolar cells via a strychnine-sensitive glycine receptor (Strettoi et al., 1992).

Our data indicate that the G5 amacrine cell class is likely the All amacrine cell class as they share a common signature. In the periphery of the retina, this cell class is found primarily at the margin or border of the IPL (Figure 24), and the molecular fingerprint reveals a strong taurine signal coupled with the weakest glycine signal of the glycinergic amacrine cells which corresponds to previous data on the All amacrine cell in the literature (Kolb and Nelson, 1983; Hendrickson et al., 1988; Wassle et al., 1995; Marc, 1999a). However, unlike primate retina (Kalloniatis et al., 1996), molecular signals for glutamate and glutamine are higher in this class, reflecting the murine retina's higher overall concentration of glutamate and glutathione across cell classes.

Figure 24. Image matrix with All amacrine cell. A matrix of peripheral normal murine retina with the All amacrine cell class highlighted against the amino acid immunolabeling. The image labels are (A) tol blue, (B) alanine, (C) aspartate, (D) glutamate, (E) glycine, (F) glutathione, (G) glutamine, (H) taurine, (I) GABA. Each section is 200nm thick and immediately adjacent to the previous section. No assessment other than the typical All amacrine cell location and cell % could be ascribed to a tol blue image to guess at the possible identity of these cells. However, their location combined with a strong taurine signal and a weak glycine signal suggest that this cell class is the All amacrine cell.

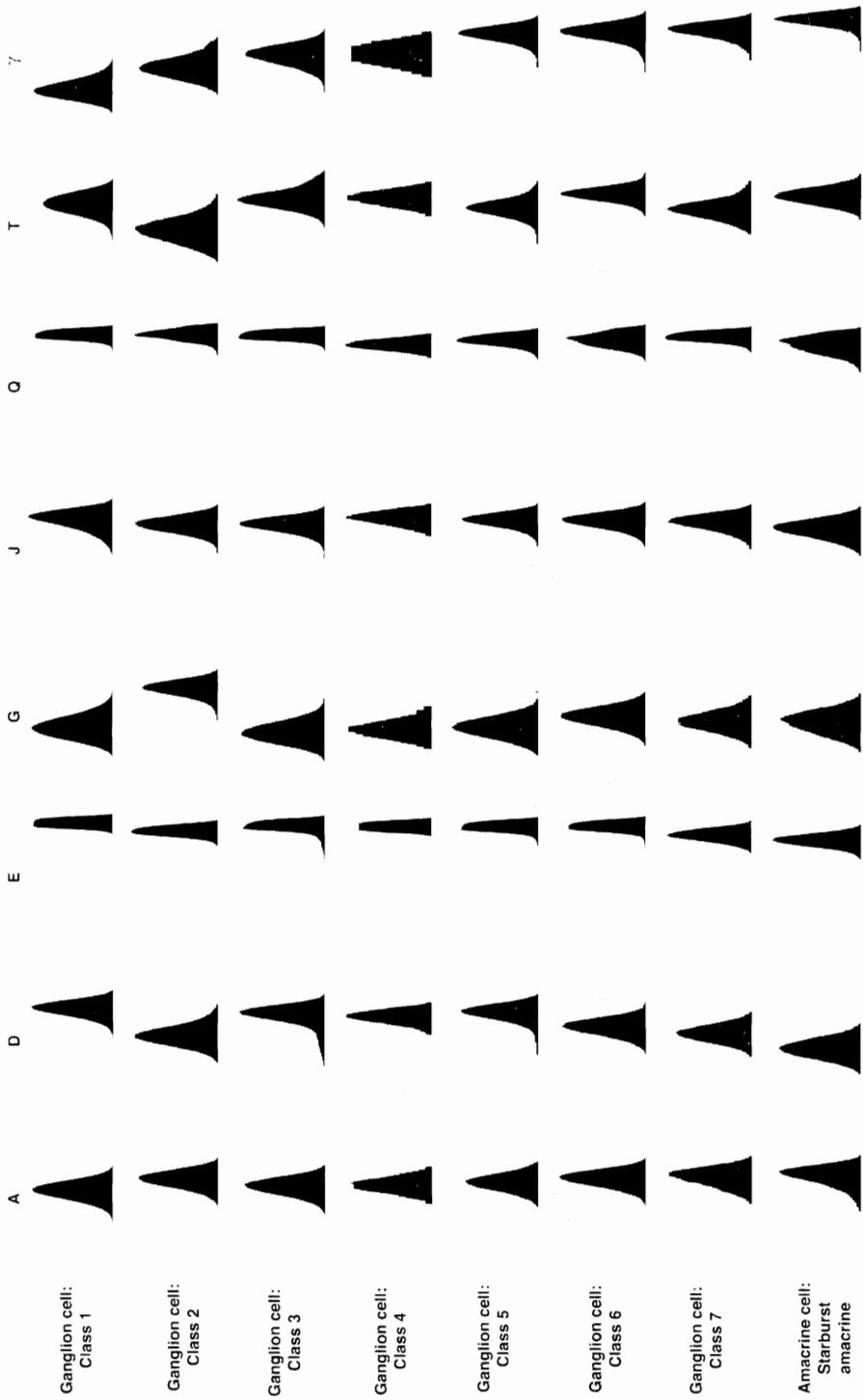


The A17 amacrine cell circuitry is less well understood. However, it appears that A17 amacrine cells accumulate signals from rod-bipolar cells and amplifies them prior to delivering feedback to the rod BC (Kolb, 2003). Additionally the A17 has been demonstrated to be GABAergic but not glycinergic (Pourcho and Goebel, 1983; Massey et al., 1992). This evidence of immunoreactivity combined with the anatomical evidence indicating its sparse, wide field diffuse nature suggests that class $\gamma 7$ may be the A17 amacrine cell population.

Displaced amacrine cells (including starburst amacrine cells) found in the ganglion cell layer (Figure 25) are one of potentially three classes of amacrine cells found in the ganglion cell layer.

Using intrinsic amino acids as probes, we were unable to fully distinguish these three potential classes in the murine retina without excitation mapping (Marc and Jones, 2002a). However, starburst amacrine cells must dominate this class as they are the largest GABAergic population in the ganglion cell layer (Vaney and Young, 1988) and the most numerous cells in the ganglion cell layer in all species (Marc and Jones, 2002a), and are characterized by small cell bodies, with the following small molecular signature: strong GABA signals (starburst amacrine cells contain intrinsic GAD65; (Brandon and Criswell, 1995)), moderate taurine signals, high glutamine signals, moderately low glutathione signals, no glycine signal, moderate glutamate signals,

Figure 25. Univariate histogram matrix of GCL. A univariate signature matrix of the matrix of cells within the ganglion cell layer in the murine eye illustrating seven superclasses of ganglion cells and one amacrine cell class. The N-dimensional separability of ganglion cells versus the amacrine cells is based upon glutamate, aspartate and glutamine concentrations. Superclass 1 represents large, very common cells that likely correlate with rabbit superclass 1abc (Marc and Jones, 2002a) due to their size and high aspartate and glutamine signals while containing no GABA. Superclass 2 cells are fairly common and perhaps contain cells similar to rabbit classes 2, 3 and 4 due to high glutamine but low aspartate signals and size correlates. Superclass 6 may represent a unitary class of large cells correlating with rabbit class 7 due to the presence of dual GABA and glycine signals. Horizontal columns identify the corresponding cell and theme classes. Vertical columns denote amino acid groupings. A, alanine; D, aspartate; E, glutamate; G, glycine; J, glutathione; Q, glutamine; T, taurine; γ , GABA.



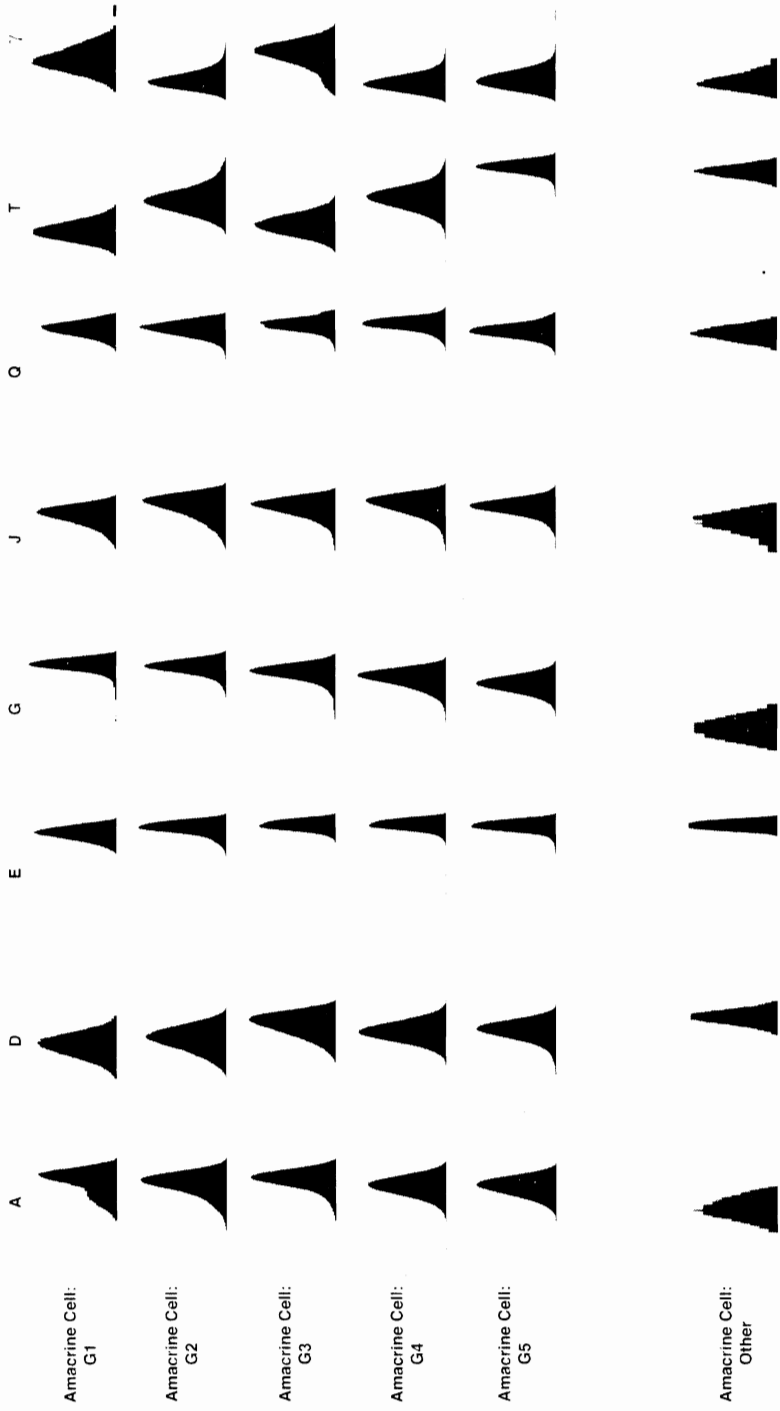
no aspartate and a moderately high alanine signal (Figure 25). These amacrine cells in the ganglion cell layer also differ from the ganglion cells by containing less glutamate, glutamine and aspartate.

One other class of cells observed in the amacrine cell layer contains no glycine and almost no GABA, but is distinguished by a high glutamate signal. While displaced ganglion cells are well known in many retinas (Marc et al., 1990), it is also clear that they express low or moderate taurine levels. This cell expresses a high taurine and glutamate signature resembling bipolar cells. It is presumed that all vertebrate amacrine cells are either GABAergic or glycinergic (Marc et al., 1995; Kalloniatis et al., 1996). It does not resemble a bipolar cell in morphology, and its signature is similar but not identical (Figure 26).

Based upon observations in rabbit tissues, we believe these cells are, in fact, tyrosine hydroxylase positive (TH+) and are thus the dopaminergic amacrine cells of the mammalian retina. Since the dopaminergic amacrine cell clearly shares a signature with glutamatergic neurons such as BCs, it is possible that they are glutamatergic.

This cell may have critical significance for retinal function, as it would represent the only known form of stimulus-independent excitatory drive for the retina in retinal degenerations where the photoreceptor layer is absent. TH+ cells are spiking neurons with incomplete Na⁺ inactivation and spike continuously in the absence of any inputs (Feigenspan et al., 1998).

Figure 26. Univariate histogram matrix of glycinergic amacrine cells. A univariate signature matrix of the glycinergic amacrine cell matrix and amacrine cell "other" matrix of the murine eye illustrating five classes of glycinergic amacrine cells and one class of amacrine cell whose small molecular fingerprint does not match that of the glycinergic or GABAergic amacrine cells. The glycinergic amacrine cells N-dimensional separability is, like the GABAergic amacrine cells, based primarily upon GABA and taurine concentration. Again, aspartate levels also vary, but to a lesser degree. The other amacrine cell class identified has a much higher aspartate signature than the other classes, and it also contains a higher glutamate concentration, yet has to GABA or glycine. We hypothesize based on recent (unpublished) evidence that this cell may be a dopaminergic amacrine cell. Horizontal columns identify the corresponding cell and theme classes. Vertical columns denote amino acid groupings. A, alanine; D, aspartate; E, glutamate; G, glycine; J, glutathione; Q, glutamine; T, taurine; γ , GABA.



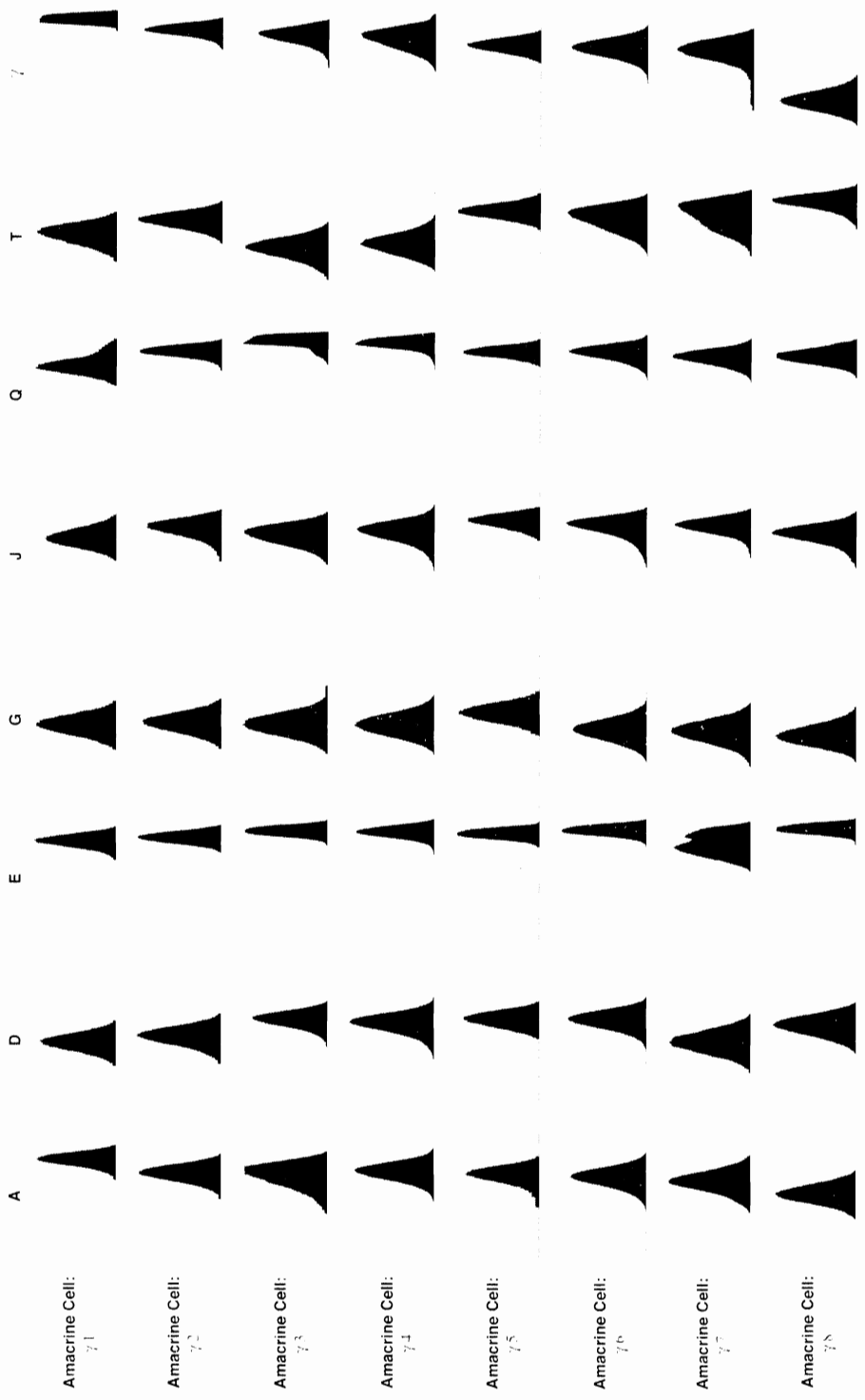
Whether or not this cell actually expresses vGlut 1, 2 or 3 to load synaptic vesicles with glutamate remains unknown (Figure 26).

Ganglion cells

As in rabbit (Marc and Jones, 2002a), we were able to segregate the ganglion cell layer of the mouse retina into seven superclasses of ganglion cells and one superclass of amacrine cells based upon the eight intrinsic amino acid signatures in vertical and horizontal sections. Broadly, the ganglion cells may be grouped into those cells that are uncoupled from amacrine cells, those ganglion cells that are coupled to glycinergic amacrine cells and those cells that are coupled to GABAergic amacrine cells. Ganglion cells can be further divisible by cell size analysis and glutamate mediated excitation histories (Marc and Jones, 2002a). However those procedures were not completed for this dissertation.

Ganglion cell and amacrine cell superclasses are separated from each other primarily along glutamate, aspartate and glutamine immunolabeling illustrating the levels of small molecular metabolic signatures they contain and their various degrees of coupling to amacrine cells (Xin and Bloomfield, 1997), including ganglion cells that are coupled to GABAergic amacrine cells and ganglion cells that are coupled to glycinergic amacrine cells.

Figure 27. Univariate histogram matrix of GABAergic amacrine cells. A univariate signature matrix of the GABAergic amacrine cell matrix of the murine eye illustrating eight classes of GABAergic amacrine cells whose N-dimensional separability is based primarily upon GABA and taurine concentration. Aspartate levels also vary, but to a lesser degree. One class, class 5 also is immunoreactive for glycine. Horizontal columns identify the corresponding cell and theme classes. Vertical columns denote amino acid groupings. A, alanine; D, aspartate; E, glutamate; G, glycine; J, glutathione; Q, glutamine; T, taurine; γ , GABA.



Murine ganglion cells also contain higher levels of glutathione, glutamine and taurine than other vertebrates such as rabbit (Marc and Jones, 2002a) making classification more difficult in these animals. That said, previously the ganglion cell layer was thought to be difficult to classify based upon intrinsic signals (Marc et al., 1995; Kalloniatis et al., 1996), but better classification algorithms and datasets proved successful in separating these cells into their constituent superclasses and classes (Marc, 1999a; 1999b; Marc and Jones, 2002a).

Though true GABAergic amacrine cells separate via strong GABA signals, a number of ganglion cells have high GABA levels, perhaps signifying greater degrees of amacrine cell coupling in the mouse versus rabbit. All ganglion cell classes with the exception of GC1 appear to be coupled to GABAergic amacrine cells due to the amount of GABA contained within them indicating greater degrees of coupling in the mouse versus rabbit (Figure 25). GC7 appears to have very high levels of GABA, approaching but not equal to GABA levels observed in starburst amacrine cells that contain GAD65. Additionally, ganglion cell class (GC1) in this atlas contains almost indistinguishable GABA levels from Müller cells rendering them invisible against a background of GABA immunolabeling, illustrating the advantage of using multiple immunocytochemical probes combined with CMP.

Ganglion cell class, GC2 also contains moderate glycine signals possibly indicating glycinergic amacrine cell coupling. Ganglion cell classes GC6 and GC7 have very low levels of glycine possibly indicative of low levels of glycine synthesis for basic metabolic needs or low degrees of glycinergic amacrine cell coupling. Glycine signals in the retinal ganglion cell layer are very weak with three ganglion cell classes exhibiting low levels of glycinergic immunoreactivity, much lower than that observed in amacrine cell populations. Of the glycine positive ganglion cell classes, class GC2 contains the highest concentration of glycine, with roughly equivalent levels of GABA, and may correspond to superclass 7 in the rabbit.

Most ganglion cell classes contain the highest glutamate levels observed in murine retina. Classes GC2 and GC7 contain statistically lower glutamate levels than other cell classes and even slightly lower glutamate levels than amacrine cell classes G6, G8 and G5 (Figure 26). Aspartate levels differ significantly across ganglion cell classes, varying more than other retinal cells displaying similar intrinsic glutamate concentrations (Figure 25). Interestingly, similar to rabbit, aspartate concentration correlates positively with ganglion cell size in that larger ganglion cells contain higher concentrations of aspartate (Figure 20, Figure 21).

All ganglion cell classes exhibited at least low levels of taurine (GC2), with all other ganglion cell classes exhibiting moderate to moderately high levels of

taurine, in marked contrast to ganglion cells observed in other mammals.

Taurine in the ganglion cell layer is exclusively observed in Müller cells in rabbits, cats, primates and all non-mammalian vertebrates observed to date. Another apparent difference between larger vertebrates is the level of glutamine. In rabbit, for instance, some ganglion cells have high glutamine signals, but there is considerable variation with some populations expressing no signal. However, the murine retinal ganglion cells immunolabel glutamine at high levels, much more than reported in the rat (Fletcher and Kalloniatis, 1996) and resemble cyprinids in this regard. While most retinal neurons express glutamine levels at least at moderate levels, the ganglion cells exhibit the highest levels of glutamine immunoreactivity and like goldfish, chicken and primate retinas provides a good univariate label for ganglion cells (Marc et al., 1990; 1995; Kalloniatis et al., 1994; 1996) and serve as a univariate separator from the bipolar cell population.

In the ganglion cell layer, cell populations of ganglion cells and amacrine cells exhibit a correlation between aspartate and GABA revealing a small but statistically significant inverse relationship with aspartate levels decreasing as GABA levels increase (Figure 28).

Based upon GABA content and their larger size, mouse GC1 correlates with superclass 1 in rabbit. In the rabbit, this superclass is further subdivisible into three natural classes based deconvolution of cell-size histograms and having strong AGB response profiles indicating robust AMPA responses. Mouse GC6

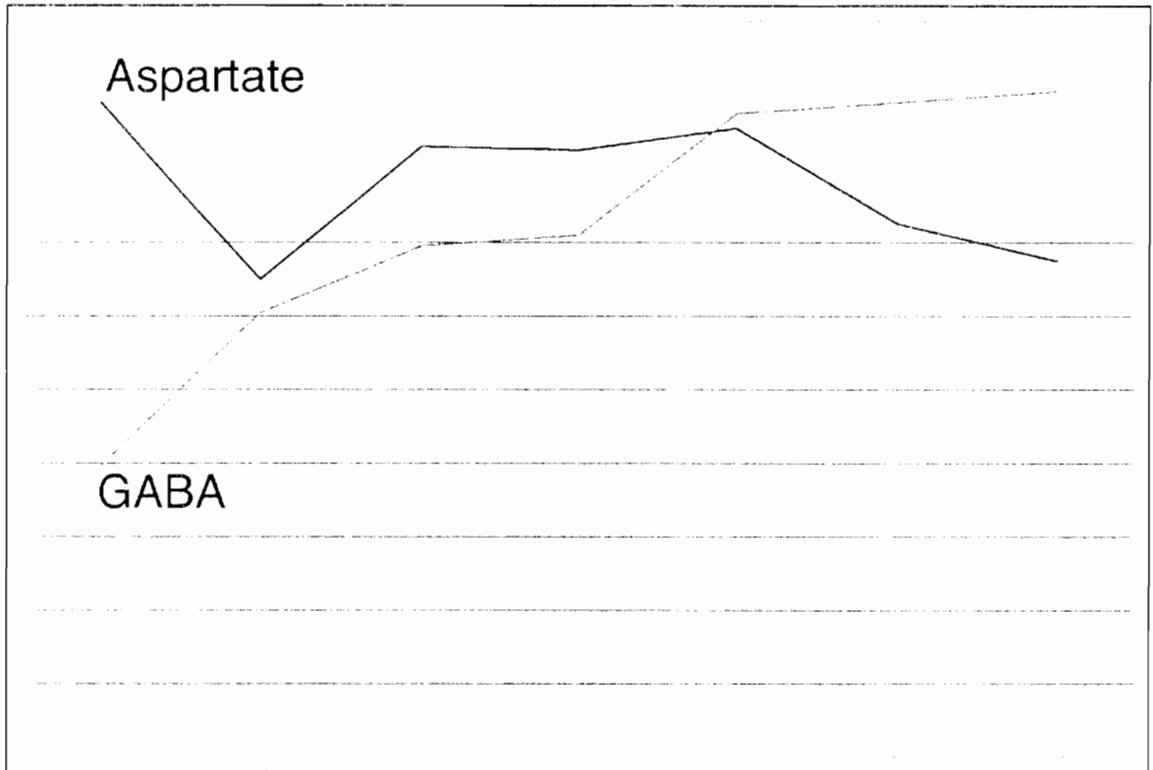


Figure 28. Aspartate and GABA in the ganglion cell layer. This figure represents the inverse correlative relationship between aspartate and GABA in the ganglion cell layer. The y-axis represents concentration of amino acids with the x-axis demonstrating different classes of cells within the ganglion cell layer.

might correlate with ganglion cell superclass 9 in the rabbit based upon these cells GABA content, lower aspartate content and large size. In the rabbit, superclass 9 contains moderately strong AMPA response profiles. If these relationships were to hold true after testing with AGB in the mouse, these cells would be the α -ganglion cells with class GC1 representing the ON-center ganglion cells and GC6 representing the OFF-center ganglion cells (Marc and Jones, 2002a).

Mouse GC2 correlates with classes 2 and 4 in the rabbit based upon cell size, high glutamine content and lower aspartate content. In the rabbit, these classes are divisible based upon their AMPA response profiles with rabbit class 2 possessing low AMPA responsivity and rabbit class 4 possessing high AMPA responsivity. Mouse GC2 cells may represent the concentric sluggish cells and/or the ON DS cells of the rabbit retina (Marc and Jones, 2002a).

Mouse GC7 might correlate with classes 5, 8, 10 and 11 in the rabbit based upon these cells GABA content at the high end of the spectrum in mouse and rabbit and based on cell size. Classes 5, 8, 10 and 11 in rabbit are separable from this superclass based upon AMPA responsivity and size deconvolution.

It is possible that some classes of ganglion cells were not separated from superclasses due to their statistical rarity. This possibility of failure to separate is

not uncommon in clustering methodologies when the unidentified class is of low encounter frequency or comprises few pixels. Not all ganglion cells are associated with visual perception and many appear to project to structures that mediate nonvisual functions such as setting the circadian rhythm (Morin et al., 2003), control of pupil size and optokinetic responses (Oyster et al., 1980; Buhl and Peichl, 1986). The nature of these functions does not require input from large populations of ganglion cells and therefore the cells could be reasoned to be rare and finding them might prove difficult. It is also possible that these cells were indeed found within the seven ganglion cell classes observed, but their molecular signature does not uniquely identify them from the other classes.

Summary

Amacrine cells use both GABA and glycine, whereas glutamate is used as a neurotransmitter in photoreceptors, bipolar cells and ganglion cells. Amino acids have many other roles and are involved in a variety of biochemical functions with their individual structures and function being found to be intimately related (Michal, 1999). Glutamate, glutamine, alanine and aspartate are termed glucogenic amino acids because they can be used for gluconeogenesis. Glutamine synthase is found in all organs of the body including the retina, where its primary function is binding free ammonia liberated by metabolic processes.

However, glutamine synthetase is restricted to glia in the nervous system as is not expressed by neurons. Glutamine thus becomes the principal form of amino group transfer and its formation via glutamine synthase functions to bind toxic free ammonia species, thus the likely high levels found in the Müller cells. Glutamine also is commonly utilized for protein synthesis and in neurons is likely the immediate precursor to glutamate synthesis, which is the primary fast excitatory neurotransmitter in the retina (Michal, 1999). The amino acids GABA and glycine appear to be the primary fast inhibitory neurotransmitters of retinal communication (Marc et al., 1990; 1995; Davanger et al., 1991; Crooks and Kolb, 1992; Kalloniatis and Fletcher, 1993; Kalloniatis, 1995). Amino acids that function as precursors to glutamate, such as aspartate and glutamine, are commonly seen in glutamatergic neurons while taurine is seen as an osmolyte (Marc et al., 1990; 1995; Kalloniatis and Fletcher, 1993; Kalloniatis and Napper, 1996). Glutamate also functions as the immediate precursor to GABA prior to its decarboxylation and is a key intermediate in other biosynthetic pathways such as formation of ornithine, arginine and proline. All neuronal cells in the murine retina label for glutamate to at least some degree. However, glutamate concentrations vary widely with some neurons in the vertical pathways having concentrations consistent with what would be required for vesicular loading, while others appear to have concentrations that would be expected for metabolic needs. For

instance, some horizontal and amacrine cells label for glutamate but at lower concentrations than that seen in neurons that support glutamatergic signaling such as bipolar cells, ganglion cells or photoreceptors possibly indicating that the glutamate utilized in these populations is for cellular metabolic requirements including the synthesis of other neurotransmitters such as GABA. Aspartate is a contributor to the synthesis of glutamate by participating with α -ketoglutarate via aspartate amino transferase. Aspartate is present in the murine retina and is most likely important for cellular metabolism and maintenance of other neurotransmitter pools, as there is no evidence in the literature that aspartate serves as a neurotransmitter in retina. Alanine functions as an alternative to glutamine for amino group transfer while the tri-peptide glutathione functions as a cytoprotective molecule quenching reactive oxygen species and detoxifying compounds through conjugation reactions (Michal, 1999). It is not known why mouse retina contains higher quantities of glutamine, glutamate and taurine than does rabbit retina, but the difference in vascularity between the retinas of the two animals could partially explain the difference. The rabbit has a completely avascular retina that relies upon the Müller cells for transport of oxygen and metabolic products to deeper layers of retina, whereas the mouse retina is much more vascular on both the RPE and vitreal sides of the retina. Therefore, the flux of amino acids could be much greater in the mouse retina than it is in rabbit.

All neural retinal space can be accounted for by immunolabeling for three amino acids, glutamate, GABA and glycine, but they are just three of many small molecular metabolic components of cellular function and the relationships between amino acids in the retina are complex. Despite this complexity, the use of CMP can, in addition to identifying cell classes, reveal hidden patterns within each class that may ultimately give some insight into metabolic relationships (Figure 29, Figure 30).

Classification does not prove that separable signatures indicate and reveal physiologically disparate functions. However, from mapping of all classes in the eye including retinal and extra retinal tissues, we have found individual 40 small molecular phenotypes. The retinal phenotypes are significantly different from the extra-retinal phenotypes that have differing physiologic functions. Of the retinal phenotypes, the RPE has a well-defined physiologic function, and its small molecular phenotype is statistically separable from all others (Figure 29). Müller cells have a distinctly separate physiologic function, and they too have small molecular phenotypes that are statistically separable from all other signatures (Figure 29). This same argument can be applied to the two classes of photoreceptors, rods and cones, the two classes of bipolar cells, ON cone and OFF, the horizontal cell class, certainly the three superclasses of amacrine cells and the ganglion cell superclass. Each superclass has a distinct small molecular

phenotype that can be subdivided into classes, which have distinct roles. This argument is bolstered by the findings that classifications do not take anatomy into consideration, and furthermore, these signatures can reliably be found across samples within the same species indicating stability of classes, and in some cases, can be found across species indicating common function is reflected in common metabolic fingerprints. Therefore, it is thought that given enough probes, we can identify all traditionally defined cell types in the retina with small molecular phenotypes that reflect their physiologic role, and that uniquely identifies them as an absolute measure of identity.

Small molecular phenotypes can, under some circumstances be altered or changed. This, however, would be expected given that small molecular fluxes are fundamental to cellular viability. Therefore, circumstances such as ischemia, traumatic detachment (Marc et al., 1998a), genetically mediated disease (Fletcher and Kalloniatis, 1996; 1997), reflect altered small molecular phenotypes and given that cells are not born with their final adult phenotype, development (Fletcher and Kalloniatis, 1997) also reflects alterations in small molecular phenotype.

Aside from the identification of cellular populations in ways not possible with any other technique, other benefits of small molecule signature extraction

with CMP may be the revelation of occult biochemical pathways involved in cellular metabolism allowing for the development of molecular or biochemical models of cellular function. Correlations in the levels of alanine, glycine, GABA and inverse correlations with taurine suggest some degree of interrelatedness of these metabolic pathways. Alanine is a fundamental transport molecule for amino group metabolism and in muscle serves as an acceptor of amino groups from glutamate. However, for CNS metabolism a more important role for alanine may be its conversion to pyruvate to play a role in gluconeogenesis. Glycine, of course, is an inhibitory neurotransmitter, but its retinal biosynthetic pathways are unknown. Other systems reveal that glycine-hydroxymethyl-transferase mediates transfer of a methylene group from serine to tetrahydrofolate thus releasing glycine. However Marc et al. (1995) report that there is very little of the necessary precursor serine in glycinergic amacrine cells. So, how might these amino acid biosynthetic pathways be related and how do retinal neurons make glycine? It is possible that alanine-glyoxylate transaminase mediates the conversion of alanine to glycine in retinal neurons. This would be potentially dangerous as glyoxylate could function as a fixative, but high levels of alanine might mediate the rapid depletion of the glyoxylate pool, yielding sufficient glycine for neurotransmission and metabolically useful pyruvate. Taurine has

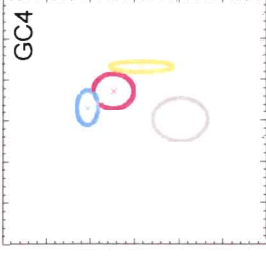
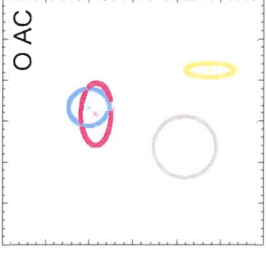
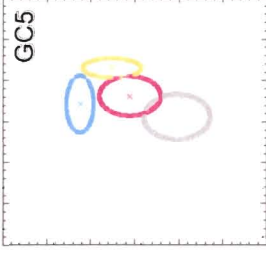
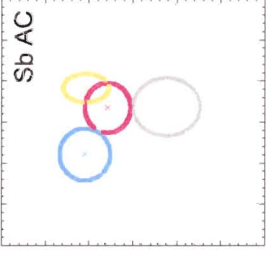
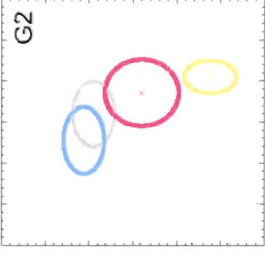
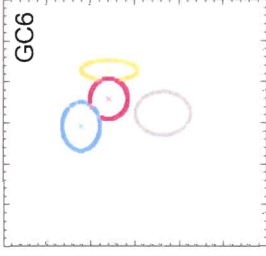
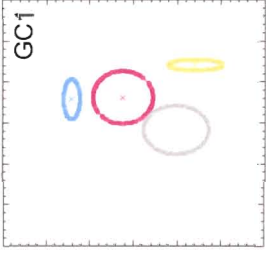
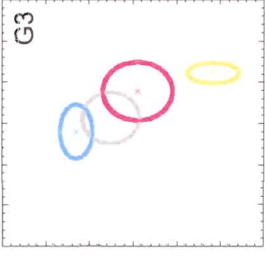
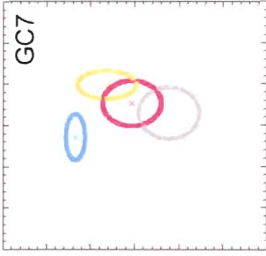
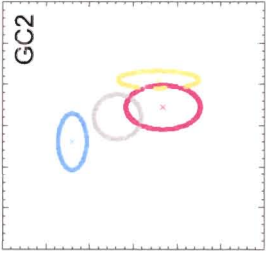
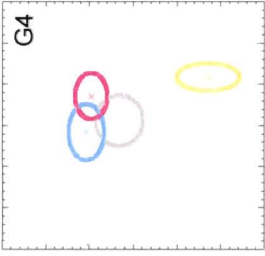
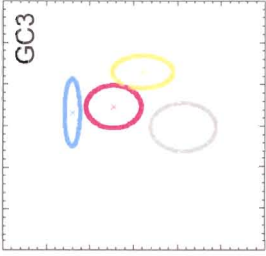
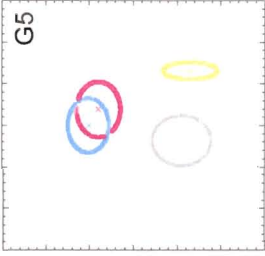
been hypothesized to function as possessing a detoxifying and membrane protective effect (Michal, 1999) and as previously noted, in cells that contain decreasing levels of alanine, glycine and GABA contain increasing levels of taurine. Perhaps the taurine flux and utilization is greater in those cells with higher levels of glycine.

Among ganglion cells, increases in GABA levels are matched with a weak inverse correlation of aspartate levels (Figure 28) possibly indicating pathway shuttling from GABA through succinate to aspartate for induction into either the urea cycle or the synthesis of alanine and subsequent deamination to pyruvate.

The development of biochemical models of small molecular fluxes will depend upon databases populated with data such as these to either validate models or inform models of cell function, and interaction and may eventually be required if efforts at building biological computation methods are to succeed.

Figure 29. Bivariate plots cell classes 1. Bivariate signal plots representing each signature cell class of the RPE, rod and cone photoreceptors, both bipolar cell classes, the horizontal cell class, the Muller cell class and all GABAergic amacrine cells. The plots are made on bivariate log millimolar scales that map proportionally to pixel intensity. Each colored "X" is the centroid of a bivariate class statistical mean for a particular pair of pixel values and the surrounding circle demarcates the 2 SD boundary for that class. The X, Y axes are defined by their color and are represented by the following notation: Grey, 03=alanine, glycine; cyan, 15=aspartate, glutamine; magenta, 46=glutathione, taurine; gold. 27=glutamate, GABA.

Figure 30. Bivariate plots cell classes 2. Bivariate signal plots representing each signature cell class of the glycinergic amacrine cells, one other amacrine cell class, the starburst amacrine cells and ganglion cells. The plots are made on bivariate log millimolar scales that map proportionally to pixel intensity. Each colored "X" is the centroid of a bivariate class mean for a particular pair of pixel values and the surrounding circle demarcates the 2 SD boundary for that class. The X, Y axes are defined by their color and are represented by the following notation: Grey, 03=alanine, glycine; cyan, 15=aspartate, glutamine; magenta, 46=glutathione, taurine; gold. 27=glutamate, GABA.



CHAPTER 5

DEGENERATE RETINA

Abstract

Many photoreceptor degenerations initially affect rods, secondarily leading to cone death. It has long been assumed that the surviving neural retina is largely resistant to this sensory deafferentation. New evidence from fast retinal degenerations reveals that subtle plasticities in neuronal form and connectivity emerge early in disease. By screening mature natural, transgenic and knockout retinal degeneration models with computational molecular phenotyping, we have found an extended late phase of negative remodeling that radically changes retinal structure. Three major transformations emerge: (1) Müller cell hypertrophy and elaboration of a distal glial seal between retina and the choroid/retinal pigmented epithelium; (2) apparent neuronal migration along glial surfaces to ectopic sites; (3) rewiring through evolution of complex neurite fascicles, new synaptic foci in the remnant inner nuclear layer, and new connections throughout the retina. Though some neurons die, survivors express molecular signatures characteristic of normal bipolar, amacrine and ganglion cells. Remodeling in human and rodent retinas is independent of the initial molecular targets of retinal degenerations, including defects in the retinal pigmented epithelium, rhodopsin or downstream phototransduction elements. Though remodeling may constrain therapeutic intervals for molecular, cellular or bionic rescue, it suggests that the neural retina may be more plastic than previously believed.

Introduction

Rod and cone photoreceptors of the sensory retina drive signal-processing circuitries of the neural retina. Most retinal degenerations such as retinitis pigmentosa (RP) affect the sensory retina, and the resultant loss of photoreceptor input constitutes deafferentation of the neural retina. RP is a family of inherited retinal degenerations involving >40 known genes, with many mutations in the rhodopsin gene (<http://www.sph.uth.tmc.edu/RetNet/>). These disorders progress through night blindness and photopic vision impairment at different rates, advancing to severe and sometimes total vision loss. Primary rod cell death is often followed by secondary loss of cones, effecting a substantial and sometimes complete destruction of the sensory retina, and a complete deafferentation of the neural retina. As clinical rescue of rods or cones is not yet feasible, cell-based (Young et al., 2000; Coffey et al., 2002) and bionic (Humayun et al., 1996; Chow and Chow, 1997; Zrenner et al., 1998) therapies have been explored as methods to provide surrogate inputs to the surviving neural retina.

The presumed preservation of the neural retina in advanced RP and allied diseases is central to cellular and bionic rescue, and is often asserted or assumed (Scarlatis, 2000; Zrenner, 2002), though based on limited evidence from early stages in rodent models of retinal degeneration. However, the neural

retina in human RP is highly remodeled (Li et al., 1995; Fariss et al., 2000) and severely depleted of neurons in areas devoid of cones. Anatomical surveys of the macula in human RP (Stone et al., 1992; Santos et al., 1997; Humayun et al., 1999) document variable ganglion cell loss, from mild to severe, but well-preserved regions of the neural retina invariably possess surviving sensory retina harboring cones. Conversely, regions of high cone loss express both neuronal loss and remodeling (Marc et al., 2001), suggesting that cone loss and subsequent neuronal loss are related.

Analyses of acquired (de Raad et al., 1996) and inherited (Fletcher and Kalloniatis, 1996) rodent degeneration models reveal subtle changes in cellular molecular phenotypes in the neural retina, some even preceding rod degeneration. Subtle remodeling of rod pathways emerges rapidly in the *rd1* mouse (Strettoi and Pignatelli, 2000; Strettoi et al., 2002), where a phototransduction defect evokes death of rods by postnatal day (pnd) 21. Rod-driven bipolar cells and horizontal cell axon terminals retract their fine dendrites and rod bipolar cell axon terminals assume immature synaptic structures. Defects extend to cone circuits: both cones (Fei, 2002) and cone horizontal cells (Strettoi et al., 2002) in the young *rd1* mouse sprout new neurites, while cone bipolar cells retract dendrites (Strettoi et al., 2003). During human rod degeneration, surviving rods, horizontal and amacrine cells similarly extend anomalous neurites throughout the retina (Li et al., 1995; Fariss et al., 2000).

But many human and rodent retinal degenerations progress slowly, and no consensus on the fate of the inner retina has emerged as aged rodent retinal degeneration specimens are rare and studies rarely extend beyond pnd 90. Furthermore, standard histology and *ad hoc* immunocytochemistry, where small sets of probes are employed, are ineffective tools for tracking the fates of the 55-60 classes of cells (Masland, 2001b) in the mammalian retina.

To explore the impact of advanced stages of deafferentation on the neural retina, we screened all retinal cells in a library of 20 human and 67 aged natural, transgenic, and knockout rodent retinal degenerations using computational molecular phenotyping (Marc et al., 1995; Marc and Cameron, 2001; Marc and Jones, 2002a) and overlay electron microscopy (Marc and Liu, 2000). Most animal sample ages were in the pnd 150-900 interval. While samples of retinas from advanced rodent ages are rare, our findings are consistent across many different forms of retinal degeneration: massive neural and glial remodeling follows loss of the sensory retina in rodents, mimicking the progression of human RP. Sensory deafferentation consequent to photoreceptor degeneration can thus activate neuronal and glial plasticity in the mature mammalian retina, perhaps through activation of the same plasticity mechanisms underlying sensory experience-induced rewiring in young mouse retina (Tian and Copenhagen, 2001).

Results

Computational molecular phenotyping of retinal degenerations. The objective of this work was to track the fates of all the major groups of retinal cells. Serial monochrome images of normal rat retina probed for different small molecules display patterns of immunolabeling similar to those of other mammals (Figure 31).

No single probe captures all cells, but taken together, virtually all cellular elements can be grouped into well-known classes or superclasses. Mapping signals as γ GE \rightarrow rgb triplets permits visualization of large cohorts, such as GABA⁺ and glycine⁺ amacrine cells, photoreceptors, bipolar cells and ganglion cells (Figure 32A), while τ QE \rightarrow rgb mapping sets Müller cells, the retinal pigmented epithelium and other elements apart from all other cells (Figure 32B).

The rat shows essentially the same composite patterns of small molecule signatures as primate, cat and rabbit retinas (Fletcher and Kalloniatis, 1996; Kalloniatis et al., 1996; Marc et al., 1998b; Marc, 1999a). Classifying all the data with isodata clustering produces raw theme maps, which are then converted to refined theme maps (see Methods) superimposed on a single reference channel (Figure 32C, D).

Figure 31. Normal rat immunohistochemistry matrix. Normal rat retina. Ten monochrome images from a series of twelve 250 nm sections. Each section was also double-labeled with DAPI. (A) alanine, section 1; (B) aspartate, section 2; (C) glutamate, section 9; (D) glycine, section 10; (E) glutathione, section 5; (F) glutamine, section 6; (G) taurine, section 7; (H) GABA, section 11; (I) toluidine blue, section 12, (J) DAPI, section 11. Layers indicated on panel I: gcl, ganglion cell layer; inl, inner nuclear layer; ipl, inner plexiform layer; isl, inner segment layer; opl, outer plexiform layer; osl, outer segment layer. Scale, 20 μ m.

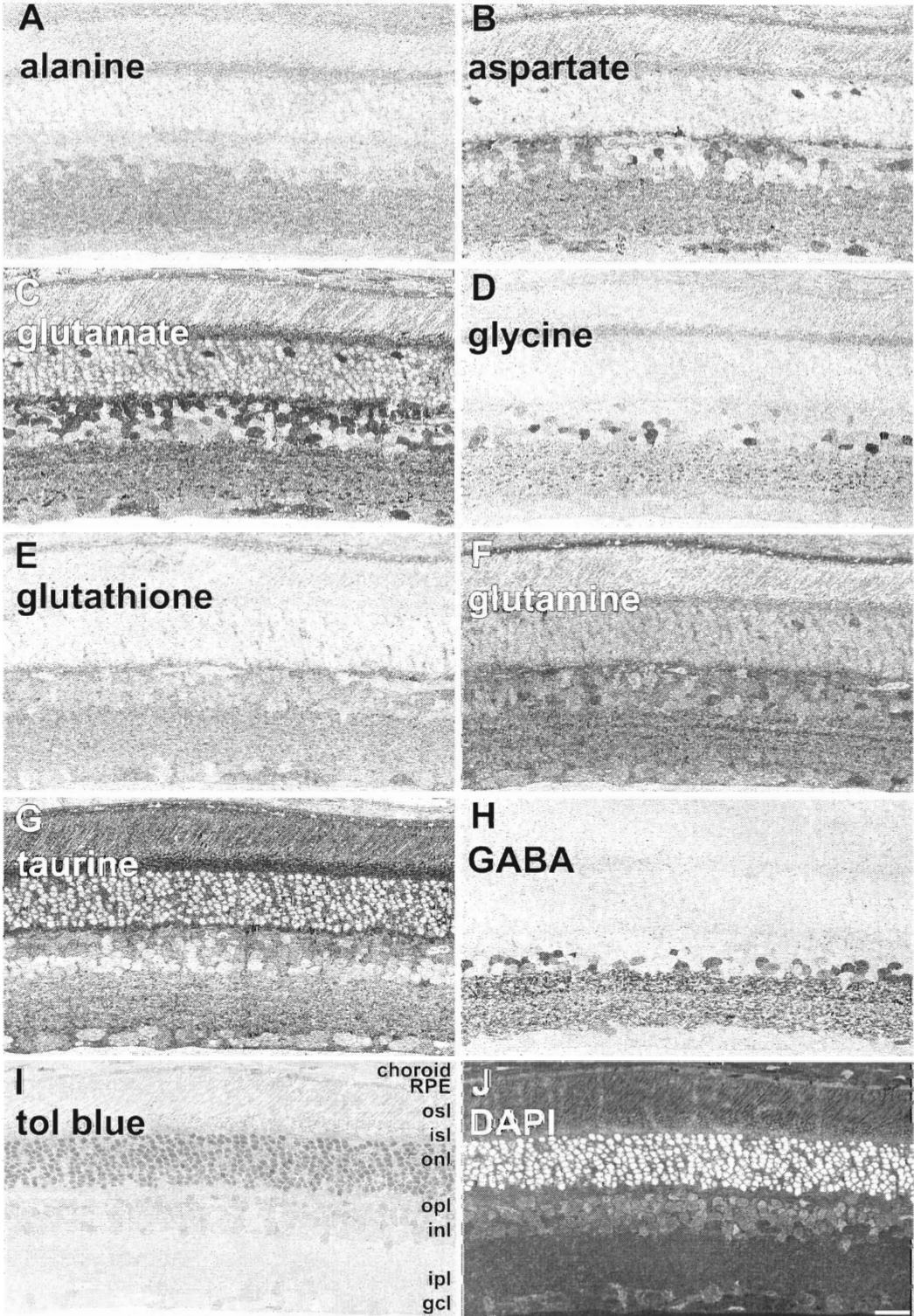
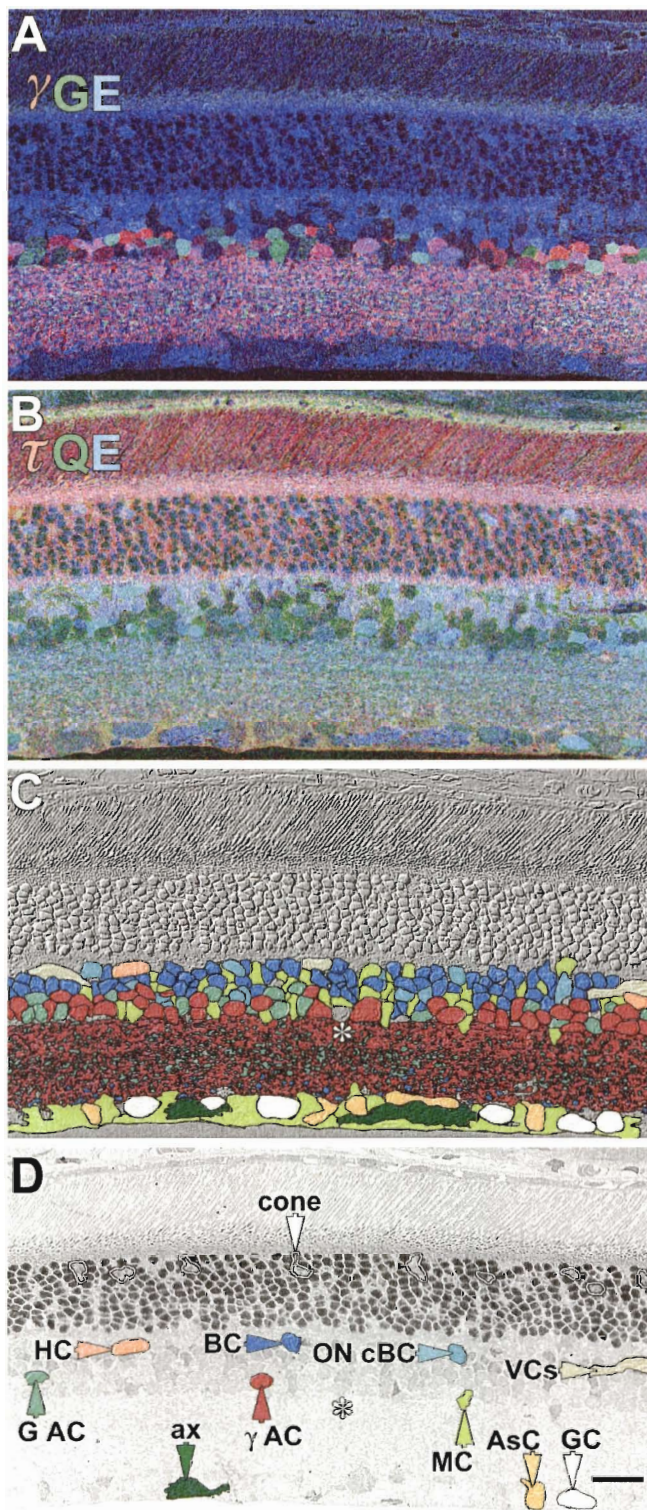


Figure 32. RGB and theme map of normal rat retina. Multichannel rgb mappings and theme maps from normal rat retina. (A) GE rgb mapping. (B) QE rgb mapping. (C) Refined theme map superimposed on a monochrome digital phase version of the toluidine blue channel. (D) The theme map key superimposed on raw toluidine blue monochrome channel. Abbreviations: AsC, astrocyte; ax, axon bundle; BC, OFF-center cone and ON-center rod bipolar cell superclass; ON cBC, ON center cone bipolar cell; G AC, glycine+ amacrine cell; AC, GABA+ amacrine cell; GC, ganglion cell; HC, horizontal cell; MC, Müller cell; VC, vascular cells (endothelia + pericytes). Outlines, cone nuclei. Asterisk, unclassified cell. Scale, 20 μ m.



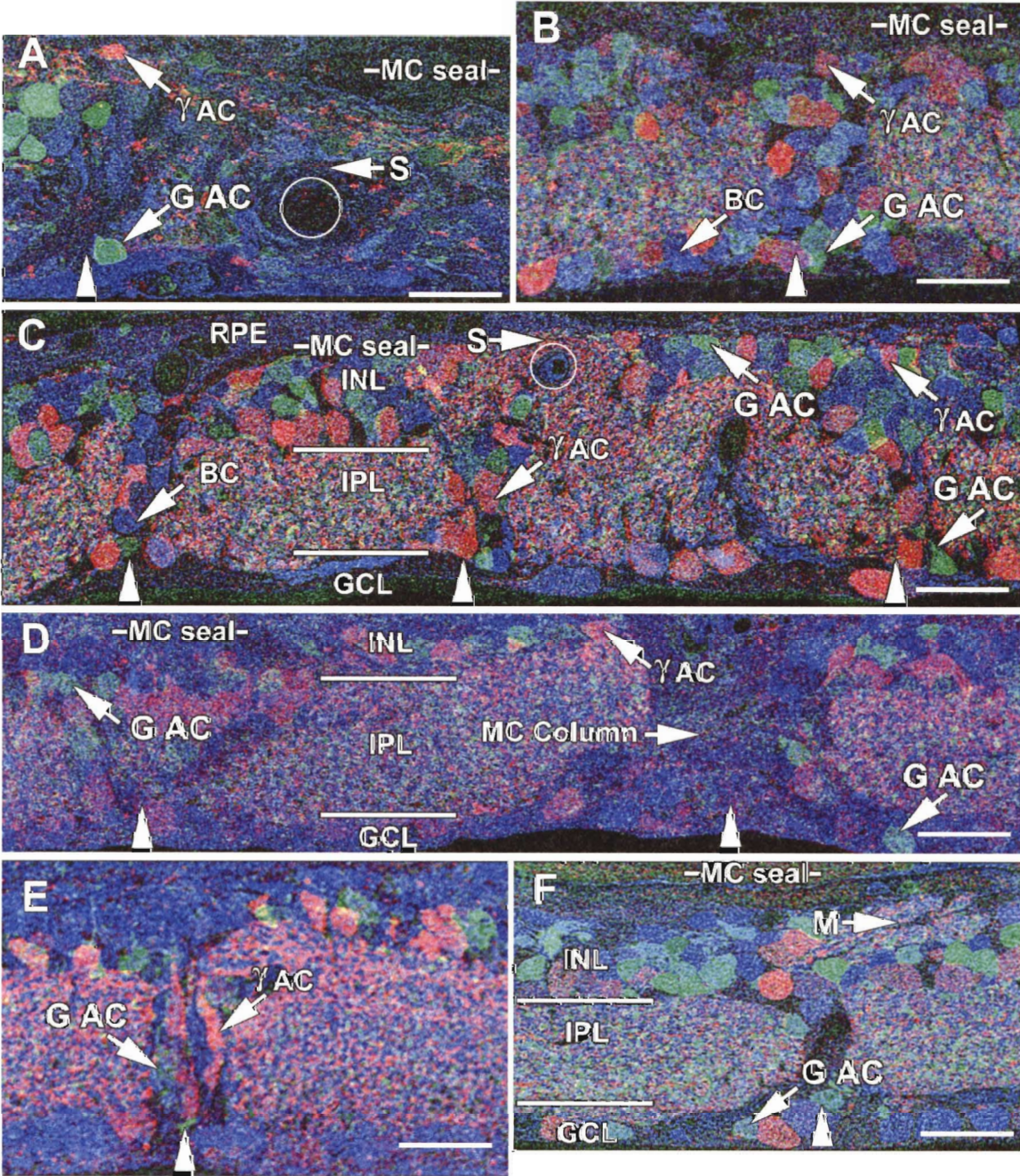
Theme maps and rgb displays simplify tracking of 10 major cell phenotypes in retinal degeneration material: photoreceptors, horizontal cells, ON-center cone bipolar cells identified as glycine+ bipolar cells (Kalloniatis et al., 1996), all remaining bipolar cells as a mixed group of rod and OFF-center cone bipolar cells, glycine+ amacrine cells, GABA+ amacrine cells, ganglion cells, Müller cells, vascular elements, and the retinal pigmented epithelium. These 10 phenotypes account for virtually all retinal space.

Analysis of theme and rgb maps of 13 retinal degeneration models reveals that late remodeling does not appear until the outer nuclear layer is depleted of rods and cones and a seal of Müller cell processes is formed between the remnant retina and the choroid or any surviving retinal pigmented epithelium (Figure 33, Figure 34).

Different initial defects in the various rodent models influence the timing and coherence of cell death in the sensory retina, resulting in different earliest onset times for remodeling of the neural retina (Table 1), spanning rapid (TG9N, P160) to slow onsets (RCS, P270) for models where we have sufficient numbers of samples.

Figure 33. Degenerate rat RGB matrix. Representative GE rgb mappings of retinal degeneration models. Downward arrows indicate inversions from the inner nuclear layer to the ganglion cell layer; upward arrows indicate eversions from the inner nuclear layer to the distal margin of the remnant retina; vertical arrowheads indicate glial columns; circles denote blood vessels. Abbreviations: M, inner nuclear layer microneuroma; S, stricture; P, neuropil patch. All other abbreviations are as shown in Figures 1 and 2. Scales, 20 μ m. (A) Human RP retina, FFB accession #378, 76-year-old female, 2 hours post-mortem, RP diagnosed at age 33, no vision at death. This vertical image demonstrates massive cell loss typical of late stage RP, with complete loss of the inner nuclear and ganglion cell layers at the right margin. A column of apparent neuronal migration is bordered by glycinergic amacrine cells in the ganglion cell layer and GABAergic amacrine cells at the distal margin of the remnant. Strictures distort the remaining inner plexiform layer and a Müller cell fibrotic seal separates the retina from the choroid/retinal pigmented epithelium. (B) *rd1* mouse, pnd 630. A large column of neurons bridges the depleted inner nuclear layer, displaying inverted amacrine and bipolar cells and everted amacrine cells. (C) RCS rat retina, pnd 900. This image shows three columns of neuronal migration (vertical arrowheads) where bipolar and amacrine cells are displaced from their proper locations. Distorted regions of the inner plexiform layer often pass through strictures as small as 5 μ m. (D) S334ter rat, pnd 363. This image shows two glial columns (vertical arrowheads), with right column exhibiting Müller cell hypertrophy breaking up the normal tiling of the retina. Everted and inverted glycinergic amacrine cells are abundant. (E) P23H rat, pnd 372. A glial column (vertical arrowhead) traverses the inner plexiform layer accompanied by migrating glycinergic and GABAergic amacrine cells. (F) GHL mouse, pnd 746. A broad glial column (vertical arrowhead) serves as a pathway for migration for amacrine and bipolar cells into the ganglion cell layer. A microneuroma has formed distal to the heavily depleted inner nuclear layer. (G) TG9N mouse, pnd 160. An oblique column forms a neuron migration path with both inverted and everted cells. Strictures deform the inner plexiform layer and microneuromas form in the midst of the inner nuclear layer, but a mere 5 μ m from the distal glial seal. (H) *nr* mouse, pnd 720. Two columns of neuronal migration are indicated, with inversion and eversion of amacrine cells. The inner nuclear layer is thinned to less than half its normal thickness. (I) *chx10* mouse, pnd 365. Few neurons survive in this defect, and only in small clusters with tiny patches of apparent neuropil surrounded by massive fields of apparent Müller cells. (J) *Chx10/P27^{Kip1}-/-* hypocellularity rescue mouse, pnd 60. This model initially displays roughly normal lamination, but with few bipolar cells and severely reduced photoreceptor numbers. However, even in the absence of clear glial columns or seals, microneuromas emerge and columns of neurons strung

through the inner plexiform layer are common, as are misplaced amacrine cells in the ganglion cell layer. (K) RKO mouse, pnd 365. No neuron migration has emerged, and positions of amacrine cells, including presumed starburst amacrine cells (S AC), are normal. However, microneuromas are forming next to the glial seal. (L) RhoCTA mouse, pnd 541. Migration across the inner plexiform layer has not begun, but microneuromas are emerging, and the entire inner nuclear layer displays disordering of neurons, with everted amacrine cells and bipolar cells moving into the former amacrine cell layer. (M) *pcd* mouse, pnd 321. At this age, retinal lamination appears normal and no microneuromas have emerged. ? (N) *rd2* mouse, pnd 151. At this age, retinal lamination appears normal and no microneuromas have emerged. These image data will be available for public access at <http://prometheus.med.utah.edu/~marclab/>.



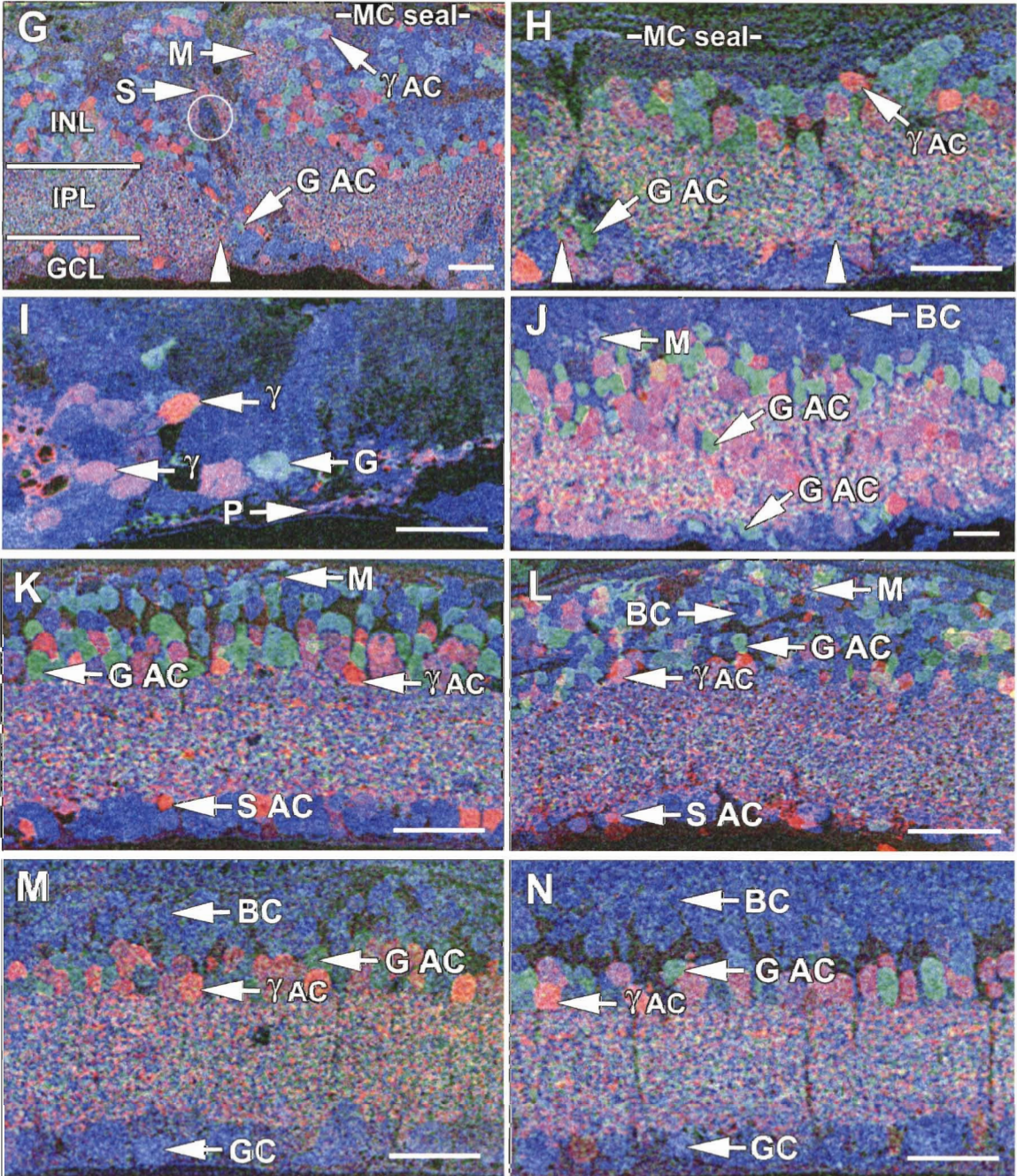


Figure 34. Theme maps of normal and degenerate retina. Theme maps of (A) normal pnd 700 Sprague-Dawley (SD) rat, (B) pnd 900 RCS rat, (c) P372 P23H line 1 transgenic rat, and (d) human RP (Foundation Fighting Blindness accession #133-OD, 67-year-old female, advanced RP, simplex, fixed 2.5 hours postmortem). In normal retina, cell layers are precisely defined. Remodeling clearly disrupts lamination via migration on Müller glia columns (C), yielding eversion (E) of GABAergic and glycinergic amacrine cells to the distal Müller glial seal (M) and inversion of amacrine and bipolar cells (I) to the ganglion cell layer. Glial hypertrophy and neuronal movement can be so extensive that the inner plexiform layer is segmented, distorted and forced through strictures (S) as small as 10 m.

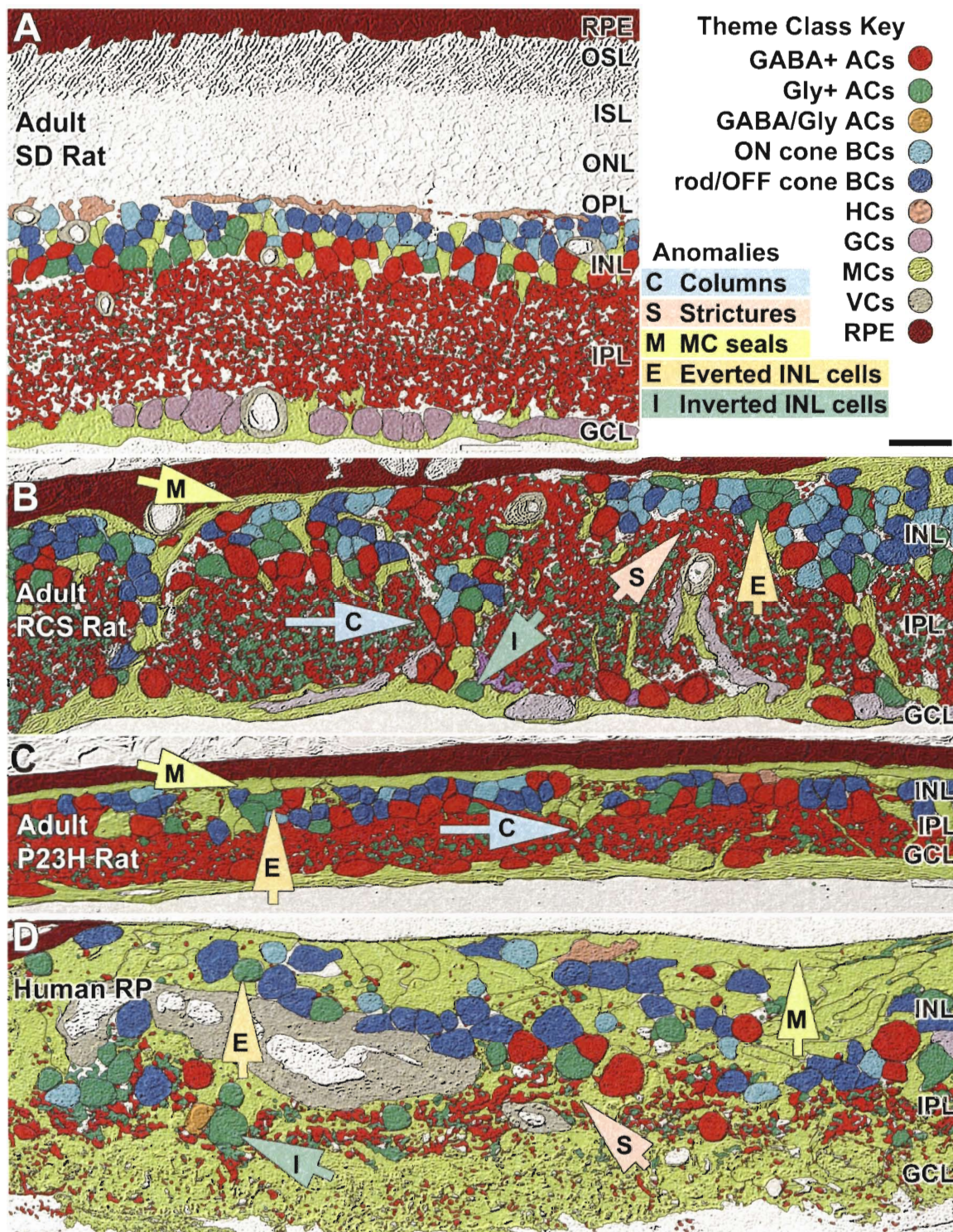


Table 1 Remodeling in retinal degenerations. Abbreviations: + present, o absent, ? undetermined, IPL = inner plexiform layer, dGly ACs = displaced glycinergic amacrine cells, MP = macrophages, mG = microglia, t = transgenic, ko = knockout, HS = *Homo sapiens*, RN *Rattus norvegicus*, MM *Mus musculus*. (a) Only isolated retinal patches survive in *chx10*. (b) The *p27^{Kip1}* ko rescues hypocellularity in *chx10* but also exhibits neuronal remodeling.

| Species | HS | tRN | tRN | RN | MM | tMM | tMM | MM | MM | koMM | MM | MM | tMM | tMM |
|----------------|-------|------------|------------|--------------|--------------|------------|-------------|-----------|--------------|---------------------------|----------------|-------------|---------------|----------------|
| Gene defect | mixed | <i>rho</i> | <i>rho</i> | <i>merlk</i> | <i>pde6β</i> | <i>rho</i> | <i>rgs9</i> | ? | <i>chx10</i> | <i>p27^{Kip1}</i> | <i>Agtppb1</i> | <i>prp2</i> | <i>rho</i> | <i>rho</i> |
| Model | RP | S334ter | P23H | RCS | <i>rd1</i> | GHL | TG9N | <i>nr</i> | <i>or</i> | <i>chx10(b)</i> | <i>pcd</i> | <i>rd2</i> | <i>rho-/-</i> | <i>rhoΔCTA</i> |
| Specimens | 20 | 9 | 12 | 7 | 9 | 8 | 19 | 3 | 3 | 1 | 2 | 1 | 4 | 8 |
| Onset | ? | P340 | P372 | P270 | P610 | P555 | P160 | P300 | <P0 | <P63 | P321 | >P151 | >P365 | >P541 |
| Neurons | | | | | | | | | | | | | | |
| Cell Death | + | + | + | + | + | + | + | o | + | + | o | o | o | o |
| Strictures | + | + | + | + | + | + | + | + | + | + | o | o | o | o |
| dGlyACs/mm | 2 | 4 | 6 | 12 | 2 | 6 | 35 | 2 | (a) | 5 | o | o | o | o |
| Fascicles | + | + | + | + | + | + | + | + | + | + | o | o | o | o |
| Microneuromas | + | + | + | + | + | + | + | + | + | + | o | o | + | + |
| Glia | | | | | | | | | | | | | | |
| Migration | + | + | + | + | + | + | + | + | + | + | o | o | o | o |
| Columns | + | + | + | + | + | + | + | + | + | + | + | o | o | o |
| Seals | + | + | + | + | + | + | + | + | o | o | + | + | + | + |
| Other | | | | | | | | | | | | | | |
| VC invasion | ? | + | + | + | + | + | + | + | + | o | o | o | o | o |
| RPE invasion | + | + | + | + | + | + | + | + | + | o | o | o | o | o |

Later onset times in Table 1 (e.g., *rd1*) reflect large gaps in our age samples between very young and old animals. As the study progressed, it became clear that it would be desirable to screen intermediate times, but that would require breeding new animals, requiring many years to produce complete chronologies. Despite uncertainty regarding precise onset times, two things are clear: as long as identifiable photoreceptors exist in the residual outer nuclear layer, remodeling is absent or cryptic; when remodeling is present, it exists in stereotyped form in most of retinal degenerations. Remodeling involves 10 major types of restructuring of the retina: (1) neuronal death as evidenced by focal or global cell depletion, including instances of massive ganglion cell loss; (2) relocation of all types of surviving neurons, including eversions of amacrine cell somata to the distal surface of the remnant retina and inversion of amacrine and bipolar cell somata to the ganglion cell layer; (3) fragmentation of the inner plexiform layer lamination into frequent, small tracts of processes we term strictures; (4) evolution of new neurites in complex fascicles surrounded by Müller cell processes; (5) evolution of new foci of synaptic neuropil (microneuromas) in the remnant inner nuclear layer and formation of new synapses throughout the retina; (6) migration of Müller cell somata to both distal and proximal borders of the retina; (7) formation of hypertrophic columns of Müller cells; (8) formation of a thick seal of Müller cell processes at the distal margin of the retina; (9) invasion of blood vessels from both the vitreal and choroidal margins of the

retina; (10) invasion of retinal pigmented epithelium cells or apical processes deep into the retina. Each of these events is a complex process, and this paper will be restricted to analysis of the neuronal and glial events in remodeling.

Figure 33 and Figure 34 survey instances of remodeling in human and rodent retinal degenerations as γ GE \rightarrow rgb maps and theme maps. Taken together, most retinal degenerations display extensive remodeling, and the examples shown are unexceptional, culled from thousands of examples and over 100 Gb of optical and electron microscopic image data. Due to space considerations, the companion τ QE maps identifying Müller cells are not shown, but Müller cells and their processes are indicated on the rgb images of Figure 33 and theme maps of Figure 34.

In advanced human RP, regions devoid of cones display massive remodeling, and the remnant tissue bears no resemblance to a normal retina. Evidence of neuronal migration is supported by the presence of glycinergic amacrine cells at the proximal margin of the retina, nominally the remnant ganglion cell layer, and by GABAergic amacrine cells at the distal margin of the retina (Figure 33A). Using the inversion of glycinergic amacrine cell somata to the ganglion cell layer as a semiquantitative index of remodeling, we determined the incidence of misplaced glycinergic amacrine cells in the normal mammalian retina (human, monkey, cat, rabbit, rat, mouse) in a linear aggregate of mammalian samples totaling over 1 m (> 500 individual glycine probed sections ranging from 0.5-2

mm long). The probability of encountering a misplaced glycinergic amacrine cell in a vertical section is $p < 0.001/\text{mm}$. The incidence of misplaced glycinergic amacrine cells in human, rat and mouse retinal degeneration tissue ranges from 2-35/mm (Table 1) representing a 10^3 - 10^4 -fold increase over misplaced glycinergic amacrine cells in the normal retina. In human and many rodent models, patches of retina completely devoid of neuronal somata in the inner nuclear or ganglion cell layers, or both, can also be located. These are so frequent that they cannot be due simply to depopulation by migration, and we interpret them as evidence of focal neuronal death. For example, a case of advanced human RP viewed as a theme map of all cellular space displays a complete absence of ganglion cells, virtually complete scrambling of the inner nuclear layer and depletion of inner plexiform layer processes, accompanied by extensive Müller cell hypertrophy (e.g., Figure 34D).

Of the rodent models examined, the natural *pde6 β* nonsense mutation in the *rd1* model is an aggressive defect that rapidly kills rods, with eventual degeneration of the entire outer nuclear layer. By pnd 630 large columns of cells traverse the inner plexiform layer, with inversions of all types of amacrine and bipolar cells into the ganglion cell layer (Figure 33B). We do not know the precise onset of remodeling in the *rd1* model.

Another transduction pathway defect model, the TG9N mouse, is a very aggressive degeneration that starts neural remodeling by pnd 160, with large

tracts of neurons traversing the inner plexiform layer, numerous inversions of amacrine cells and bipolar cells to the ganglion cell layer, and eversions of amacrine cells to the distal seal (Figure 33G). Disruptions of the inner plexiform layer lead to numerous neuropil strictures.

Defects in RPE function and rhodopsin expression generally lead to slower rod degenerations and later onsets of remodeling, but the outcomes are the same as the faster models. The RCS rat begins remodeling by pnd 270 and eventually displays massive reorganization of the inner nuclear and ganglion cell layers, with numerous hypertrophic columns of Müller cells surrounded by displaced neurons and disrupted inner plexiform layer segments (Figure 33C, Figure 34B). Very few identifiable normal ganglion cells remain in these regions, and most of the ganglion cell layer appears repopulated by new cells. Axon tracts become captured by the inward movement of vitreal vessels (Villegas-Perez et al., 1998), which also leads to the compression or displacement of neuropil, forming strictures (Figure 34B). The theme map of glial processes in the RCS rat also shows the characteristic thick fibrotic layer that seals the neural retina from the choroid or any remaining retinal pigmented epithelium. This seal is often incomplete in advanced remodeling, and the remnant inner plexiform layer often approaches the distal limit of the retina at these breaks (Figure 34B). This highly disordered neural retina can clearly be seen to bear little resemblance to a theme map of the normal rat retina.

In a transgenic model of rhodopsin truncation, we have examined advanced age samples (pnd 340-418) of four lines of the S334ter rat, which display different rates of rod degeneration, likely due to different transgene integration sites or integration of different transgene copy number. All lines show remodeling ranging from inner plexiform layer thinning and mild cell loss to severe restructuring as shown in Figure 33D (pnd 363). As is common in almost all remodeling retinas, the inner nuclear layer is often reduced to a single layer of amacrine cells at the distal margin of the retina, while columns of amacrine cell and bipolar cells reposition into the ganglion cell layer. The depletion of the ganglion cell layer is difficult to gauge in the absence of whole mounts, for which aged animals would have to be raised, especially in the presence of amacrine cell migration from the inner nuclear layer, but long tracts of the ganglion cell layer spanning several hundred microns are depleted of cells.

We examined three lines of the P23H transgenic rat, a model for the most common form of human adRP. All show some remodeling, but again the severity varies. Over the pnd 372-410 interval, glial columns emerge, and with them the migration of inner nuclear layer neurons into the ganglion cell layer begins (Figure 33E). Line 1 of the P23H transgenic rat is particularly aggressive, and displays extensive neuronal cell death throughout the retina, depleting in excess of 90% of the retinal ganglion cells, thinning the amacrine cell layer to $<10\ \mu\text{m}$ in

many regions, and often reducing the inner nuclear layer to a single layer of amacrine and bipolar cells (Figure 34C).

The GHL transgenic model is the murine homologue of human adRP, the first system in which late remodeling was found (Jones et al., 2001), and the original impetus for this survey. The GHL mouse displays slow rod and cone loss the first year of life (Frederick et al., 2001), but no major remodeling occurs in this phase, though rod circuitry may be altered in early degeneration stages as in the *rd1* mouse (Strettoi and Pignatelli, 2000; Strettoi et al., 2002). An unknown mechanism eventually leads to cone death in this and other models (Mohand-Said et al., 1998; Fintz et al., 2003), and remodeling of the neural retina begins prior to pnd 555-746, by which time the GHL mouse retina displays many migrating neuronal columns, hypertrophic Müller cells, microneuromas and glial seals (Figure 33F). We do not have a precise onset chronology for this model.

The $\rho\Delta\text{CTA}$ model is the murine homologue of the S334ter rat and, though it displays rapid loss of rod photoreceptors, it does not remodel as quickly as the rat systems. By pnd 541, major glial columns have yet to emerge, but the distal seal is complete and microneuromas are forming in the distal retina (Figure 33L). Despite lack of migration through the inner plexiform layer, the inner nuclear layer is clearly disordered in the aged $\rho\Delta\text{CTA}$ mouse, with Müller and amacrine cell somata repositioned at the distal margin of the retina and many bipolar cells in the amacrine cell layer.

The rhodopsin gene knockout mouse (RKO) is also a fairly gentle remodeling retina as the initial waves of cell death seem highly rod-restricted. But eventually the entire outer nuclear layer appears ablated and, similar to the $\rho\Delta\text{CTA}$ model, microneuromas and inner nuclear layer cell migration occur (Figure 33K). But by pnd 365, at least, no migration into the ganglion cell layer has emerged. Given the slowness of the remodeling in the GHL model we might expect the RKO to show more complete remodeling by pnd 500.

Two Purkinje cell degeneration mutants are well-known for inducing slow photoreceptor degenerations, though the mechanisms remain unclear. The *nervous* (*nr*) mutant expresses Müller cell seals and columns, neuronal inversion and eversion events, microneuromas and significant neuron depletion in the inner nuclear layer (Figure 33H). Remodeling is absent at 1 year, is well underway by pnd 450 and is extensive by pnd 730. Our oldest *pcd* sample (pnd 321) shows no evidence of remodeling, although the Müller cell seal is complete. If it progresses at the same rate as the *nr* mouse, we would not expect to see remodeling at this stage.

As in our *pcd* murine model, our oldest sample of the *rd2* mouse (formerly the *rds*, *rd slow* model) is still rather young by remodeling standards (pnd 151) and still possesses remnant cones and some rod nuclei. It displays no remodeling in the neural retina, and we would expect that given the availability of older models,

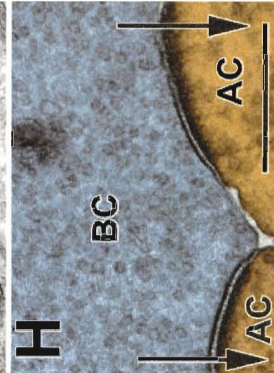
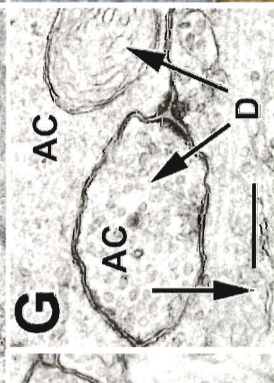
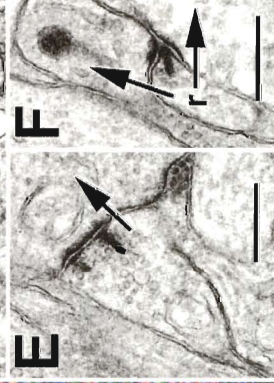
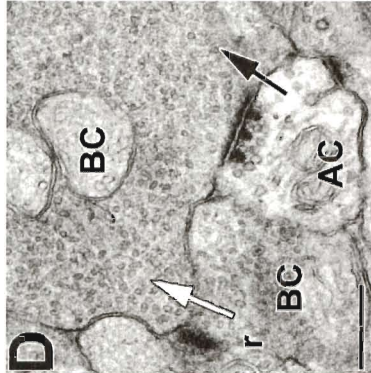
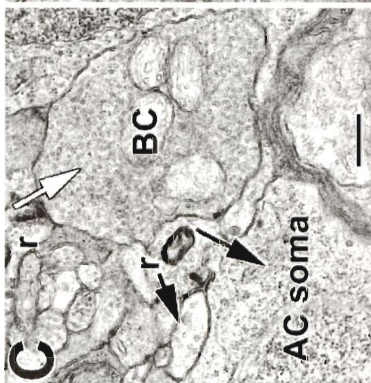
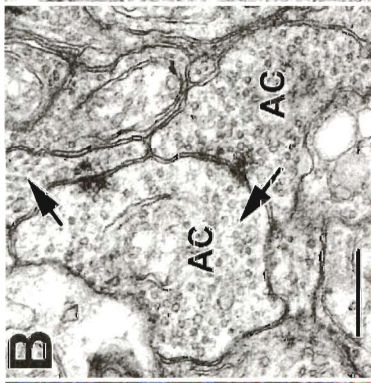
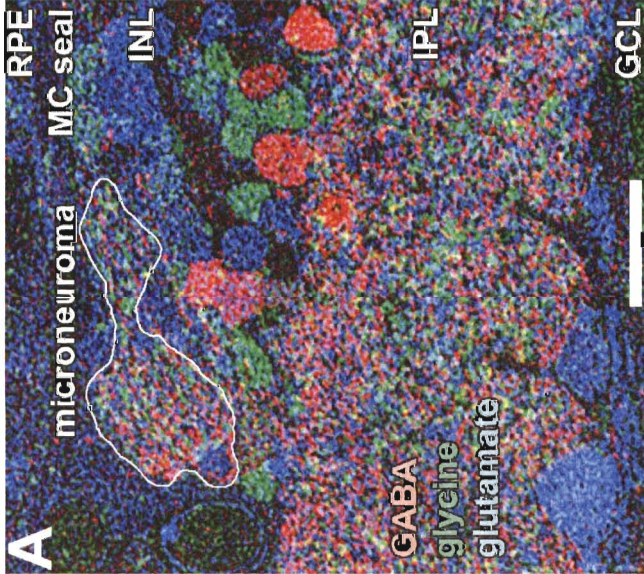
we would begin to see the same sequelae of retinal degeneration observed in other models.

The *or* hypocellularity mutant is a developmental defect caused by a natural *chx10* transcription factor gene null mutation. Though it is not a true post-maturation photoreceptor degeneration model and is a defect caused by impaired production of inner nuclear layer neurons, especially bipolar cells (Liu et al., 1994), the sequelae of the *or* defect far exceed simple loss of inner nuclear layer neurons. By pnd 365 there are no photoreceptors and no identifiable lamination, and virtually all of the retina is absent, but for tiny patches of roughly a dozen neurons accompanied by tiny foci of apparent neuropil (Figure 33I). While this may not represent the same kind of remodeling observed in retinal degenerations, it suggests that maintenance of a normal retinal structure may require a nearly complete cohort of neurons. The *chx10/p27^{Kip1}* double null mutation represents a quantitative but not qualitative proliferation rescue from hypocellularity, resulting in an abundance of amacrine cells, a reduced number of photoreceptors, and partially normal retinal lamination (Green et al., 2003). GABAergic and glycinergic amacrine cells are found in bands throughout the inner plexiform layer, misplaced to the ganglion cell layer, adjacent to the thinned outer nuclear layer, and engaged in microneuroma formation (Figure 33J). However, the *chx10/p27^{Kip1}* double null mouse expresses neither a distal glial seal nor hypertrophic Müller cell columns.

Rewiring, microneuromas and neurite fascicles. Remodeling neurons make new connections. Ectopic fascicles of hundreds of small neurites traverse the disordered inner nuclear layer along glial surfaces, elaborating 20-100 μm diameter microneuromas at densities exceeding $\approx 30,000/\text{retina}$ in some models (GHL, TG9N, RCS). Microneuromas are tangles of GABAergic and glycinergic amacrine cell and glutamate+ cell processes (Figure 35A), some extending additional tracts of neurites along glial seals while others merge with the remaining inner plexiform layer.

New synapses are formed within these new sites in the remnant inner nuclear layer and around the somata of survivor neurons. Microneuromas contain both conventional and ribbon synapses and display abundant common synaptic arrangements: amacrine \rightarrow amacrine (Figure 35B), bipolar \rightarrow amacrine (Figure 35C), and amacrine \rightarrow bipolar (Figure 35D). The amacrine bipolar contact of figure 5D also bears a resemblance to multiprojection synapses of cortex. Unusual bipolar \rightarrow bipolar contacts are present in both microneuromas and the remnant inner plexiform layer (e.g., Figure 35C, Figure 35D), and various synapses are made by and onto neuronal somata in the fragmented inner nuclear layer (e.g., Figure 35C).

Figure 35. EM synaptic images. Microneuromas and apparent retinal rewiring. (A) GE rgb mapping of RCS rat retina showing the emergence of new neuropil beneath the distal Müller cell (MC) seal. Microneuromas are tangles of GABAergic (red), glycinergic (green) and glutamate+ (blue) neurites. Scale, 20 μ m. (B) Microneuroma amacrine-amacrine target synapse chains. (C) Anomalous bipolar-amacrine cell soma and bipolar-bipolar synapses. (D) Presynaptic multiprojection amacrine-bipolar and bipolar-bipolar cell contacts. (E) Multi-ribbon synapses. (F) Classic bipolar cell presynaptic dyad element in a process 100 nm diameter, with few vesicles. (G) Anomalous dyad-like synapse (D) with amacrine cell feedback. The presynaptic element contains few vesicles and resembles an amacrine cell dendrite. (H) Theme map of a large bipolar cell terminal lacking ribbons but making large conventional contacts onto amacrine cell dendrites. The blue overlay denotes the signature of an ON-center cone bipolar cell; orange denotes GABAergic amacrine cells. Synaptic directions are indicated by arrows; white arrows, bipolar-bipolar cell contacts; scale for electron micrographs, 200 nm.



Multiribbon and extremely small ribbon contacts are abundant (Figure 35E,F), but we have also found these to be common in the normal rat retina. Complex contacts, such as amacrine cell feedback arrangements (Figure 35G), are common but not detectably more so than in normal retina. Finally, we have used multichannel overlay microscopy (Marc and Liu, 2000) to identify characteristic synaptic profiles as definitively bipolar or GABAergic amacrine cell elements (Figure 35H). Unlike normal bipolar cells, this process in the remnant inner plexiform layer appeared to make large ribbon-free conventional, flat contacts onto target GABAergic amacrine cells. While many forms of contacts in the inner plexiform layer proper appeared quite normal, including gap junctions between ON-center cone bipolar cells and glycinergic amacrine cells, we cannot determine whether most synaptic contacts in microneuromas represent proper or improper assemblies. The exceptions are bipolar → bipolar contacts, which do not occur in normal retina, new contacts associated with migrating neurons, ribbon contacts made by bipolar cell somata, and ribbon synapses onto the distal or lateral aspects of amacrine cells.

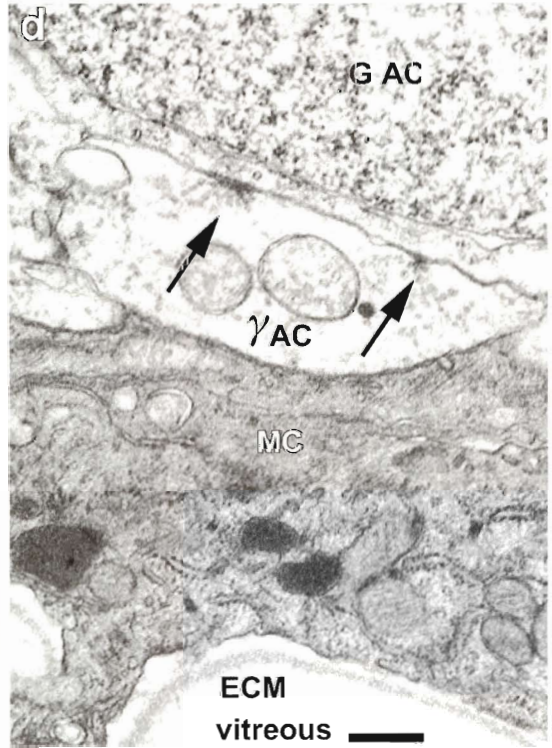
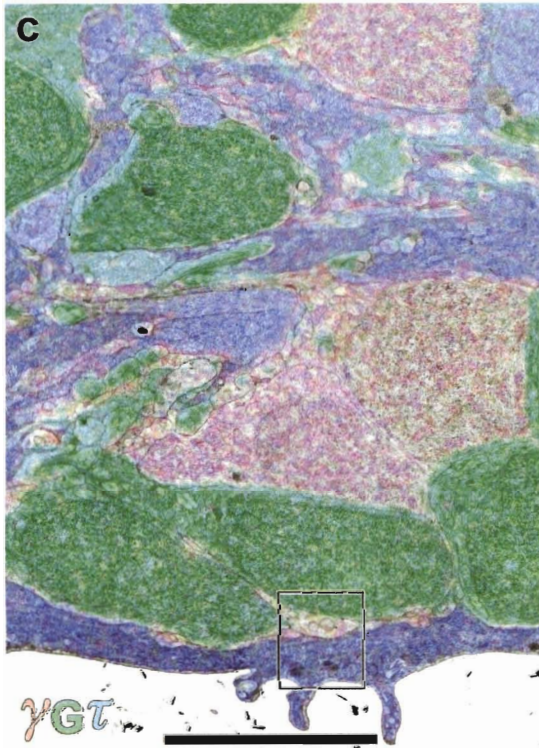
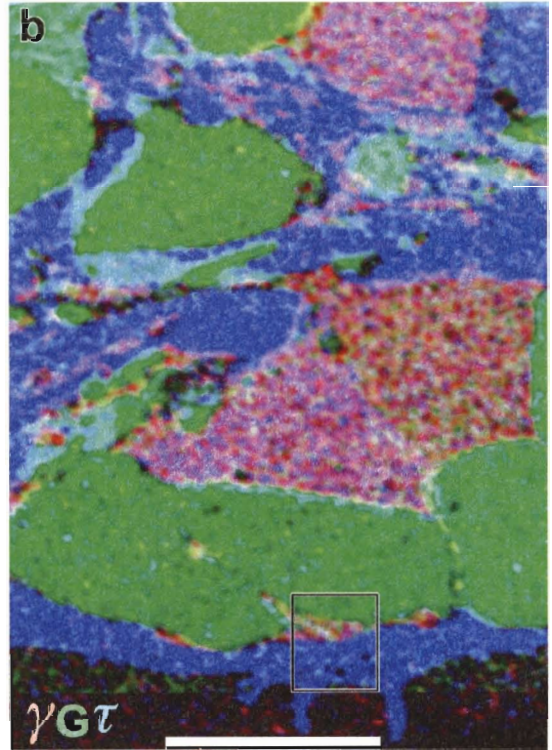
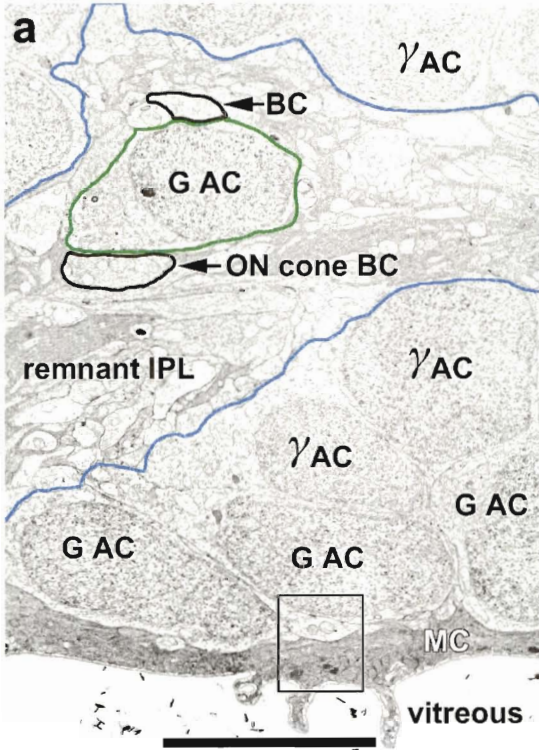
Overlay microscopy permitted us to determine the nature of some of the connections made by migrating neurons in remodeling retinas. Figure 36A is the ultrastructural channel (a montage) from a 6-channel registered dataset (GABA, glycine, glutamate, glutamine, taurine, ultrastructure) and shows a cluster of

neuronal somata separated from the vitreous by a thin border of Müller cell processes and overlaid by an irregular strip of remnant inner plexiform layer.

The $\gamma G\tau \rightarrow \text{rgb}$ mapping (Figure 36B) reveals that most of the cells are glycinergic amacrine cells that have migrated into the former ganglion cell layer. By using the rgb image as a transparent overlay, a complete map of cell identities is realized (Figure 36D), including a glycinergic cell in the midst of the remnant inner plexiform layer and two classes of bipolar cell terminals: glycine+ (ON-center cone bipolar cells) and glycine- (either rod or OFF-center cone bipolar cells). At higher resolution, a small GABAergic terminal can be seen to make focal presynaptic specializations on the proximal aspect of the repositioned glycinergic amacrine cell. This likely represents formation of a new contact by GABAergic amacrine cell processes invading the ganglion cell layer.

Neurite fascicles are common within and distal to the remnant inner nuclear layer in remodeling retinas, and are often visualized as bands of parallel processes or small punctae bearing characteristic inner plexiform layer signatures. At the optical level it is difficult to distinguish cross-sectioned neurite fascicles from small microneuromas, but overlay electron microscopy clearly reveals their nature and composition.

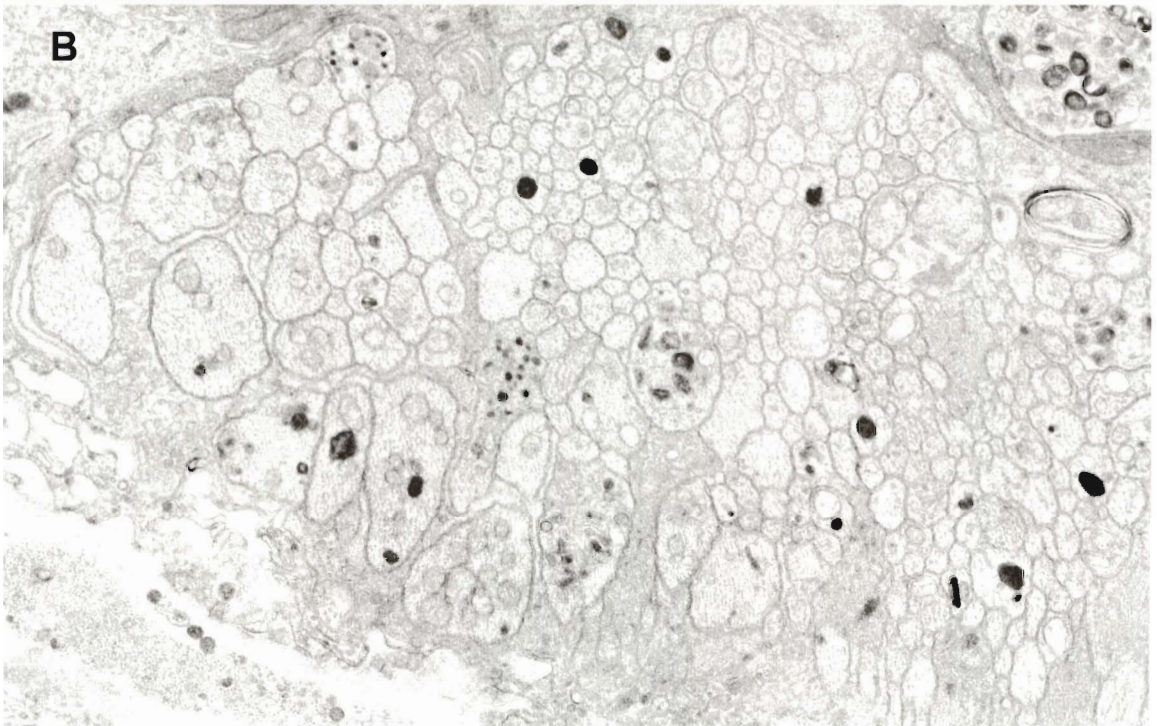
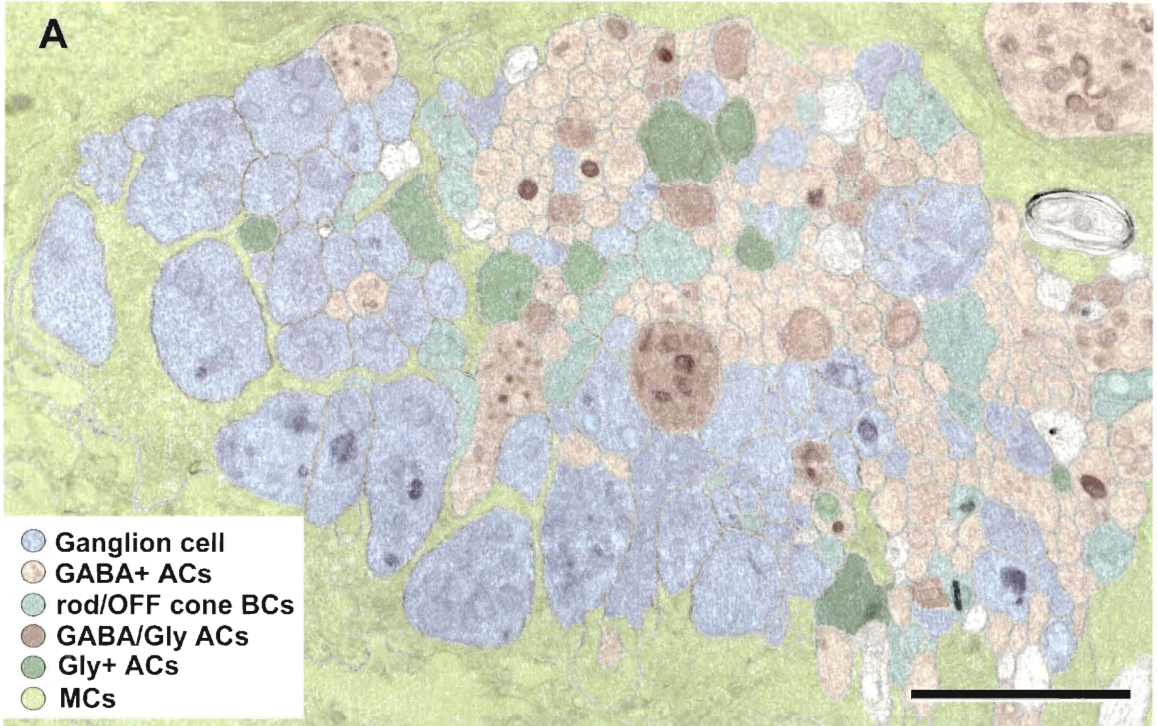
Figure 36. EM overlay displaced amacrine cells. Repositioned glycine+ and GABA+ amacrine cells in the former ganglion cell layer. (A) Monochrome digital montage of glycine+ and GABA+ amacrine cells after migration into the ganglion cell layer, bordered proximally by Müller cell processes and the vitreous and distally by a strip of remnant inner plexiform layer, outlined in blue. A single glycine+ amacrine cell (outlined in green) within the remnant inner plexiform layer is completely surrounded by neuropil. (B) Registered G rgb mapping of the same field. (C) Overlay of the G image on the ultrastructural channel. (D) Enlarged inset (box) of two GABA+ amacrine cell presynaptic sites (arrows) on the soma of a repositioned glycine+ amacrine cell. Abbreviations as in Figure 2. ECM, extracellular matrix. Scales: a-c, 10 μ m; d, 500 nm.



Serial section channels of the distal RCS rat retina were probed for GABA, glycine, glutamine, taurine and glutamate in addition to ultrastructure. The five-dimensional signatures from this signature data-set can uniquely be used to classify structures into ganglion, GABAergic amacrine, glycinergic amacrine, bipolar and Müller cell profiles in all species (Marc et al., 1995; Kalloniatis et al., 1996). The aligned channels and theme maps may then be used to classify ultrastructural data at resolutions often exceeding the Rayleigh limit and with far superior signal-to-noise ratios to immunogold methods (Marc and Liu, 2000). Figure 37A displays an ultrastructural theme map of a neurite positioned $\approx 10 \mu\text{m}$ proximal to the remnant retinal pigmented epithelium and Figure 37B is the underlying monochrome image.

The fascicle contains clear accumulations of ganglion, GABAergic amacrine, glycinergic amacrine and bipolar cell-like processes, apparently segmented into preferential groups. The large ganglion cell dendrites (blue) tend to run together, as do the smaller GABAergic amacrine cell processes (red). The entire fascicle is encased and partially invaded by Müller cell processes. Similar structures were observed by ultrastructural analysis in GHL mouse retinas, and by optical microscopy in S334ter rat, P23H rat, TG9N mouse, and *rd1* mouse retinas.

Figure 37. EM overlay microneuroma fascicle. Neurite fascicle 2 m away from distal margin of the retina and the Müller cell seal. (A) Ultrastructural theme map. Six classes of elements are color coded according to characteristic signatures: ganglion cells (blue; high glutamate, low taurine); GABAergic amacrine cells (light red; high GABA), glycinergic amacrine cells (olive; high glycine), a mixed glycine+ and GABA+ class (dark red); bipolar cells (cyan, high glutamate, high taurine); Müller cells (yellow, high taurine, high glutamine). Unclassified elements are not colored. Scale, 250nm. (B) The corresponding monochrome ultrastructural channel.



Discussion

After loss of the outer nuclear layer, retinal remodeling ensues, leading to substantial topological, cell population and connectivity changes. These include the emergence of a distal glial seal, inversions of amacrine and bipolar cell somata to the ganglion cell layer and eversions of amacrine cells to the distal margin of the retina, neuronal death, and extensive rewiring. The rodent neural retina clearly remodels in the same manner as human RP retinas. No normal vertebrate retina in our archive of over 6000 specimens and 40 species, including human retinas of >65 years and rodent retinas of pnd 700 and greater ever display any of these features of remodeling. Remodeling is not associated with senescence and is uniquely the sequelae of disease. Remarkably, however, the basic signatures of retinal cells in advanced retinal degenerations are essentially indistinguishable from those of normal retinas. In some instances, glutamate levels are slightly elevated in Müller cells. In no cases do intermediate signatures emerge, and this suggests that remodeling phenomena do not trigger significant changes in the gene expression profiles that create the molecular phenotypes of the retina. This then allows us to track anatomical changes underlying remodeling with good cellular precision. Virtually all retinal degenerations display remodeling regardless of whether they are triggered by RPE failure, defects in rhodopsin expression, defects in transduction pathway elements, alterations in retinal progenitor cell proliferation patterns, or other

mechanisms. Some genetic defects elicit little or no late remodeling (*rd2*, *rho*^{-/-}, *pcd*, or *Rho* Δ CTA), as remnant cones persist for hundreds of days beneath the glial seal, albeit transformed in structure. However, given enough time, remodeling may emerge, as patches of cone loss in the *pcd* mouse retina are associated with deformations in the borders of the inner plexiform layer, and the *nr* Purkinje cell degeneration model eventually progresses to severe remodeling with time.

Cone loss in most retinal degenerations appears to activate formation of glial columns and seals, cell migration, neuronal loss, and rewiring. This large-scale glial remodeling is similar to that triggered in retinal detachment, including the migration of glial somata to the distal margin (Lewis et al., 2002). The repositioning of neurons is dramatic, and the presence of entire columns of neurons spanning the inner plexiform layer suggests that a nonselective migratory process is triggered. We have observed few instances of ganglion cell eversion to the inner nuclear layer, but this rarity is complicated by sampling, as inner nuclear layer inversion is roughly five times more probable just because of the number of cells involved. On balance, it appears that all cells can migrate once hypertrophied glial tracts have developed.

We cannot discount the effects of glial hypertrophy in reshaping the retina, but this hypothesis does not easily account for phenomena such as bidirectional displacement of cells. We believe that these data, while composed of static

images, do reflect dynamic activity and cellular migration similar to a developmental time series. For instance, relocated amacrine cells from the inner nuclear layer have distinctive signatures and are not present in the ganglion cell layer of younger animals within models that, at later time points, exhibit bona fide glycinergic amacrine cells in the ganglion cell layer, leading us to conclude that these cells are either migrating (Sullivan et al., 2003) or are being forced by glial elements into the ganglion cell layer. Conversely, other neuronal classes do not migrate, but are in abnormal locations due to massive loss of photoreceptor and bipolar cell populations.

We have not used cell counts to document cell death for three reasons. First, many retinal degeneration models display obvious depletion of the ganglion cell and inner nuclear layers, with regions devoid of ganglion or amacrine cell and bipolar cells (Figure 34D) or with reduction of the inner nuclear layer to a thickness of but two cells at points (Figure 34C). Second, nearly all of the samples we have employed were archival, osmicated resin embedded tissues acquired over a span of 30 years and could not be used for conventional whole mount methods. Third, cell loss is clearly focal in many cases, and patches of depleted retina are adjacent to those containing nearly normal numbers (Figure 34B). Global cell counts would not capture this spatial inhomogeneity. We have not observed compensatory thickening of any cell layers that would reasonably account for depletion in others. It is also unlikely that neurons could be caught in

apoptotic states (if generic apoptosis is the mechanism) during remodeling. If the inner nuclear layer is reduced in thickness by 50% over a period of 150 days, a uniform rate of cell death would mean that only 3 in 1000 cells would actually be in the process of dying at any sample point. This number would be smaller for slower remodeling systems and undetectable in most cell death visualization protocols.

Rewiring accompanying new neurite extension, microneuromas formation, evolution of new synaptic contacts in the ganglion cell and remnant inner nuclear layers, loss of retinal neurons, and globally disturbed retinal topology implies that remodeled retinas are unlikely to process visual signals properly. Further, if the apparent bipolar \rightarrow bipolar cell contacts we have observed are functional, they represent re-entrant circuits that can display resonance and instability, providing network-driven excitation in the absence of photoreceptor inputs. The triggers for this profusion of new synapses and the mechanisms by which partners are found are clearly important issues. However, remodeling appears to be a classical CNS deafferentation response in many respects and we expect that similar molecular mechanisms are likely involved. Physical or environmental deafferentation of sensory pathways evokes atrophy of targeted neurons (Von Noorden and Crawford, 1978; Levitt et al., 2001) and remodeling in corticothalamic circuits in adult mammals (Buonomano and Merzenich, 1998; Jones and Pons, 1998). Degeneration of the sensory retina clearly triggers

similar effects in the surviving neural retina. Defects in cone-driven OFF channel circuits occur long before photoreceptor degeneration is complete in transgenic pigs with rhodopsin gene defects (Banin et al., 1999), suggesting that subtle rewiring (Peng et al., 2000) may be a persistent process that erupts into full-scale late remodeling upon loss of all afferent signaling. We hypothesize that global neural remodeling in degenerating retinas is, in part, an active process that restores essential trophic signals to neurons, perhaps through re-entrant signals that set up oscillatory excitations. Indeed, RP patients often report photopsias (scintillating photic illusions) consistent with erratic, nonspecific signaling in the surviving neural retina (Weleber and Gregory-Evans, 2001). More importantly, recent physiological data suggest that retinal connectivity, or at least synaptic efficacy, is shaped by postnatal visual experience (Tian and Copenhagen, 2001), and considering the extent of plasticity in adult neural retinas long after the degeneration of the sensory retina, it is plausible to hypothesize incipient plasticity as an attribute of the normal adult retina.

Retinal rescue strategies will have to confront remodeling and circuit corruption in addition to overcoming simple neuronal loss. The distal glial seal must be breached to add new progenitor/stem cells and, even then, cell-based therapies may not reverse degeneration, as new cells may be co-opted to produce aberrant wiring by the remodeling retina (Li et al., 1995). The possibility of stem cell fusion (Terada et al., 2002) with host neurons is also a serious

impediment to rescue and analysis. There is yet no evidence that transplantation can stop or delay remodeling, and transplanting cells into the retina without triggering further remodeling seems doubtful. Bionic implants are similarly impacted. The subretinal chip strategy also requires traumatic breach of the glial seal and depends on normal retinal topology (Zrenner et al., 1998; Zrenner, 2002) which remodeling abrogates. Epiretinal implants are compromised by rewiring, probable re-entrant excitation of retina through ganglion cell-amacrine cell coupling (Xin and Bloomfield, 1997; Marc and Jones, 2002a), ganglion cell death and migration-induced disorder in the ganglion cell layer.

The initiators of remodeling are unknown and may constrain therapeutic windows for genetic and molecular rescues, such as survival factor delivery (Faktorovich et al., 1990). If rescues are to proceed, prevention of remodeling may have to precede intervention. On the other hand, the exuberance of synaptic remodeling is provocative, for if neurons in the retina can make novel synapses and circuits, might they not be retrained with patterned competitive inputs?

The overall small molecular phenotypes of cells ultimately depend upon biosynthetic pathways for the creation of molecules, metabolic pathways they become involved in, transport mechanisms and biological sinks from protein synthesis and cellular signaling to energy maintenance and elimination of waste

products and toxic compounds. Of course it can be expected that these presumably balanced pathways can go awry in instances of physical or genetic trauma, and it is reasonable to assume that these perturbations would be reflected in a cell's small molecular phenotype. Indeed, this is the case in instances of retinal degeneration and retinal detachment (Fletcher and Kalloniatis, 1996; 1997; Marc et al., 1998a; 2001; Jones et al., 2003a; 2003b).

CHAPTER 6

DISCUSSION/FUTURE DIRECTIONS

We sought to test the hypothesis that the neural retina is largely preserved in photoreceptor based retinal degenerations, and by extension, in human RP. In brief, we rejected the hypothesis. The retina can be categorized by CMP and using intrinsic signals of 8 amino acids including alanine, aspartate, glutamate, glycine, glutathione, glutamine, taurine and GABA we were able to extract and define 28 retinal cell classes. The same techniques can be used to quantify and define the course and scope of retinal pathologies including retinal degenerations.

Through the use of CMP we have been able to describe a number of retinal degenerative models and conclude that many photoreceptor degenerations initially affect rods, leading to secondary cone death and sensory deafferentation of the surviving neural retina. In the mature central nervous system, deafferentation evokes atrophy and connective repatterning, and it has been assumed that the neural retina is an exception: a passive survivor. New evidence from fast retinal degenerations reveals subtle plasticities in neuronal form and connectivity early in disease. By screening mature natural, transgenic and knockout retinal degeneration models with computational molecular phenotyping, enabling quantitative tracking of all retinal cell types, we have described aggressive remodeling in which neurons migrate along aberrant glial columns and seals, restructuring the adult neural retina. Many neurons die, but surviving classes of neurons display unexpected plasticity, rewiring the remnant

inner plexiform layer and forming thousands of novel ectopic microneuromas in the remnant inner nuclear layer. Bipolar and amacrine cells engage in new circuit topologies, assemble novel presynaptic architectures and form abundant small synapses with immature structure. Modeling reveals that these new circuitries are most likely corruptive. Remodeling in human and rodent retinas is independent of the initial molecular targets of retinal degenerations, including defects in the retinal pigmented epithelium, rhodopsin or downstream phototransduction elements. Though remodeling may constrain therapeutic intervals for molecular, cellular or bionic rescue, the exposure of intrinsic retinal remodeling by the removal of sensory control in retinal degenerations suggests that neuronal organization in the normal retina may be more plastic than previously believed.

There are several proposed approaches to rescuing the retina and thus vision. The bionic retinal implants proposed take the direct implantation approach of placing photosensitive chips onto the retina with the goal of activating ganglion cells directly. There are a number of problems to this approach including the engineering limitations of the chip itself in terms of light sensitivity. However, even overcoming technical silicon sensitivity issues, cone and neuronal loss is mosaicked in degenerate retina, not uniform. Neuronal loss or remodeling occurs after cone degeneration with many surviving neurons migrating and projecting dendrites. Ganglion cell loss is massive in the periphery

in some models and significant in the macula, and in particularly large numbers in areas where there are no cones, rods or bipolar cells. If there is significant ganglion cell loss in the retina of those patients with advanced retinal degeneration, the effectiveness of silicon-based implants will be dramatically lessened. Other approaches to retinal rescue include biological methods to either attempt to restore the retinal pigment epithelium by transplantation of sheets of RPE in-between the systemic circulation and the photoreceptors or transplantation of the photoreceptors themselves. Transplantation of RPE is conceptually an easier approach and may hold promise as long as the intervention takes place before retinal degeneration occurs. Photoreceptor transplantation is significantly more difficult technically (Gouras et al., 1994) and biologically difficult in terms of getting the photoreceptors to wire correctly. This approach too assumes that the inner neural retina is intact. Therefore any intervention late in the degenerative phase will fail. Transplantation may have to also deal with glial reactivity. In many genetically inherited retinal degenerations, the primary genetic lesion is in one cell type such as the photoreceptors or the bipolar cells causing these cells to degenerate. Secondary insults may be from the retinal glial cells becoming reactive causing further degeneration or even the retinal remodeling that we are seeing. Indeed there appears to be no evidence that answers whether or not transplantation can stop or even delay loss of visual

function in humans, and the technical considerations for transplanting cells into the macula without further trauma are not yet resolved.

The most promising approaches may be developmental or regenerative strategies, soluble factor delivery (Reh and Levine, 1998; Horner and Gage, 2000; Levine et al., 2000), gene therapy targeted towards the primary degenerative cells (Kumar-Singh and Farber, 1998) or the secondary reactive Müller cell populations to maintain the retina until transplantation or other means may be employed. But cellular rescues must cope with an active aberrant, remodeled retina that may integrate new cells and corrupt them. However, the finding that the retina is dynamic in its degeneration may indicate that regenerative or regrowth strategies may be possible. All available evidence appears to indicate that the human retina does not undergo any cell divisions after development. However cyprinids and other fish have a proliferative zone in their retinas that can generate all of the cell types of the retina in adult fish throughout their adult life.

Remodeled retinas clearly contain wiring errors and synaptic forms unlike those of mature mammalian retina. If we imagine the successful restoration of light-driven input to the neural retina by cellular or bionic means, ultimately, these bionic or tissue based rescues must accommodate persistent ganglion cells loss, remodeling, and generation of non-neural seals in addition to the technical considerations that will have to be overcome.

BIBLIOGRAPHY

- Anderson B, Jr. 1968. Ocular effects of changes in oxygen and carbon dioxide tension. *Trans Am Ophthalmol Soc* 66:423-474.
- Applebury ML, Antoch MP, Baxter LC, Chun LL, Falk JD, Farhangfar F, Kage K, Krzystolik MG, Lyass LA, Robbins JT. 2000. The murine cone photoreceptor: a single cone type expresses both S and M opsins with retinal spatial patterning. *Neuron* 27:513-523.
- Awatramani GB, Slaughter MM. 2000. Origin of transient and sustained responses in ganglion cells of the retina. *J Neurosci* 20:7087-7095.
- Banin E, Cideciyan AV, Alemán TS, Petters RM, Wong F, Milam AH, Jacobson SG. 1999. Retinal rod photoreceptor-specific gene mutation perturbs cone pathway development. *Neuron* 23:549-557.
- Barnett NL, Osborne NN. 1995. Redistribution of GABA immunoreactivity following central retinal artery occlusion. *Brain Res* 677:337-340.
- Benca RM, Gilliland MA, Obermeyer WH. 1998. Effects of lighting conditions on sleep and wakefulness in albino Lewis and pigmented Brown Norway rats. *Sleep* 21:451-460.
- Bennett J, Tanabe T, Sun D, Zeng Y, Kjeldbye H, Gouras P, Maguire AM. 1996. Photoreceptor cell rescue in retinal degeneration (rd) mice by in vivo gene therapy. *Nat Med* 2:649-654.
- Bignami A. 1984. Glial fibrillary acidic (GFA) protein in Muller glia. Immunofluorescence study of the goldfish retina. *Brain Res* 300:175-178.
- Bird AC. 1995. Retinal photoreceptor dystrophies. *Am J Ophthalmol* 119:543-562.
- Blanks JC, Mullen RJ, LaVail MM. 1982. Retinal degeneration in the pcd cerebellar mutant mouse. II. Electron microscopic analysis. *J Comp Neurol* 212:231-246.

- Bloomfield SA, Dacheux RF. 2001. Rod vision: pathways and processing in the mammalian retina. *Prog Retin Eye Res* 20:351-384.
- Bok D. 1993. The retinal pigment epithelium: a versatile partner in vision. *J Cell Sci Suppl* 17:189-195.
- Bonfanti L, Strettoi E, Chierzi S, Cenni MC, Liu XH, Martinou JC, Maffei L, Rabacchi SA. 1996. Protection of retinal ganglion cells from natural and axotomy-induced cell death in neonatal transgenic mice overexpressing bcl-2. *J Neurosci* 16:4186-4194.
- Brandon C, Criswell MH. 1995. Displaced starburst amacrine cells of the rabbit retina contain the 67-kDa isoform, but not the 65-kDa isoform, of glutamate decarboxylase. *Vis Neurosci* 12:1053-1061.
- Brew H, Attwell D. 1987. Electrogenic glutamate uptake is a major current carrier in the membrane of axolotl retinal glial cells. *Nature* 327:707-709.
- Brindley GS, Lewin WS. 1968a. The sensations produced by electrical stimulation of the visual cortex. *J Physiol* 196:479-493.
- Brindley GS, Lewin WS. 1968b. The visual sensations produced by electrical stimulation of the medial occipital cortex. *J Physiol* 194:54-55P.
- Buhl EH, Peichl L. 1986. Morphology of rabbit retinal ganglion cells projecting to the medial terminal nucleus of the accessory optic system. *J Comp Neurol* 253:163-174.
- Bunker CH, Berson EL, Bromley WC, Hayes RP, Roderick TH. 1984. Prevalence of retinitis pigmentosa in Maine. *Am J Ophthalmol* 97:357-365.
- Buonomano DV, Merzenich MM. 1998. Cortical plasticity: from synapses to maps. *Annu Rev of Neurosci.* 21:149-186.
- Burgess DW. 1993. Automatic Ship Detection in Satellite Multispectral Imagery. *Photogrammetric Engineering and Remote Sensing* 59:245-254.
- Burmeister M, Novak J, Liang MY, Basu S, Ploder L, Hawes NL, Vidgen D, Hoover F, Goldman D, Kalnins VI, Roderick TH, Taylor BA, Hankin MH,

- McInnes RR. 1996. Ocular retardation mouse caused by Chx10 homeobox null allele: impaired retinal progenitor proliferation and bipolar cell differentiation. *Nat Genet* 12:376-384.
- Caldwell RB, McLaughlin RJ, Boykins LG. 1982. Intramembrane changes in retinal pigment epithelial cell junctions of the dystrophic rat retina. *Invest Ophthalmol Vis Sci* 23:305-318.
- Caldwell RB, Wade LA, McLaughlin BJ. 1984. A quantitative study of intramembrane changes during cell junctional breakdown in the dystrophic rat retinal pigment epithelium. *Exp Cell Res* 150:104-117.
- Calkins DJ, Schein SJ, Tsukamoto Y, Sterling P. 1994. M and L cones in macaque fovea connect to midget ganglion cells by different numbers of excitatory synapses. *Nature* 371:70-72.
- Cammarata PR, Cantu-Crouch D, Oakford L, Morrill A. 1986. Macromolecular organization of bovine lens capsule. *Tissue Cell* 18:83-97.
- Campbell DB, Hess EJ. 1996. Chromosomal localization of the neurological mouse mutations tottering (tg), Purkinje cell degeneration (pcd), and nervous (nr). *Brain Res Mol Brain Res* 37:79-84.
- Carlson MD, Kish PE, Ueda T. 1989. Glutamate uptake into synaptic vesicles: competitive inhibition by bromocriptine. *J Neurochem* 53:1889-1894.
- Chen J, Makino CL, Peachey NS, Baylor DA, Simon MI. 1995. Mechanisms of rhodopsin inactivation in vivo as revealed by a COOH-terminal truncation mutant. *Science* 267:374-377.
- Chen J, Woodford B, Jiang H, Nakayama T, Simon M. 1993. Expression of a C-terminal truncated rhodopsin gene leads to retinal degeneration in transgenic mice. *Invest Ophthalmol Vis Sci* 34:S333.
- Chow AY, Chow VY. 1997. Subretinal electrical stimulation of the rabbit retina. *Neurosci Lett* 225:13-16.
- Coffey PJ, Girman S, Wang SM, Hetherington L, Keegan DJ, Adamson P, Greenwood J, Lund RD. 2002. Long-term preservation of cortically dependent visual function in RCS rats by transplantation. *Nature Neuroscience* 5:53-56.

- Crooks J, Kolb H. 1992. Localization of GABA, glycine, glutamate and tyrosine hydroxylase in the human retina. *J Comp Neurol* 315:287-302.
- D' Cruz PM, Yasumura D, Weir J, Matthes MT, Abderrahim H, LaVail MM, Vollrath D. 2000. Mutation of the receptor tyrosine kinase gene *Mertk* in the retinal dystrophic RCS rat. *Human Molecular Genetics* 9s:645-651.
- Dacey DM, Diller LC, Verweij J, Williams DR. 2000. Physiology of L- and M-cone inputs to H1 horizontal cells in the primate retina. *J Opt Soc Am A Opt Image Sci Vis* 17:589-596.
- Dacey DM, Lee BB. 1994. The 'blue-on' opponent pathway in primate retina originates from a distinct bistratified ganglion cell type. *Nature* 367:731-735.
- Dahl D, Bignami A. 1982. Immunohistological localization of desmin, the muscle-type 100 A filament protein, in rat astrocytes and Muller glia. *J Histochem Cytochem* 30:207-213.
- Davanger S, Ottersen OP, Storm-Mathisen J. 1991. Glutamate, GABA, and glycine in the human retina: an immunocytochemical investigation. *J Comp Neurol* 311:483-494.
- Davson H. 1990. The lens. In: *Physiology of the eye*. New York: Pergamon Press. p 145-149.
- de Raad S, Szczesny PJ, Munz K, Reme CE. 1996. Light damage in the rat retina: glial fibrillary acidic protein accumulates in Müller cells in correlation with photoreceptor damage. *Ophthalmic Res* 28:99-107.
- Derouiche A, Rauen T. 1995. Coincidence of L-glutamate/L-aspartate transporter (GLAST) and glutamine synthetase (GS) immunoreactions in retinal glia: evidence for coupling of GLAST and GS in transmitter clearance. *J Neurosci Res* 42:131-143.
- DeVries SH. 2000. Bipolar cells use kainate and AMPA receptors to filter visual information into separate channels. *Neuron* 28:847-856.
- Dobelle WH, Mladejovsky MG. 1974. Phosphenes produced by electrical stimulation of human occipital cortex, and their application to the development of a prosthesis for the blind. *J Physiol* 243:553-576.

- Dominguez L, Montenegro J, Pasantes-Morales H. 1989. A volume-dependent, chloride-sensitive component of taurine release stimulated by potassium from retina. *J Neurosci Res* 22:356-361.
- Dowling JE, Boycott BB. 1966. Organization of the primate retina: electron microscopy. *Proc R Soc Lond B Biol Sci* 166:80-111.
- Ehinger B, Ottersen OP, Storm-Mathisen J, Dowling JE. 1988. Bipolar cells in the turtle retina are strongly immunoreactive for glutamate. *Proc Natl Acad Sci U S A* 85:8321-8325.
- Eisenfeld AJ, Bunt-Milam AH, Sarthy PV. 1984. Müller cell expression of glial fibrillary acidic protein after genetic and experimental photoreceptor degeneration in the rat retina. *Invest Ophthalmol Vis Sci* 25:1321-1328.
- Erickson PA, Fisher SK, Guerin CJ, Anderson DH, Kaska DD. 1987. Glial fibrillary acidic protein increases in Müller cells after retinal detachment. *Exp Eye Res* 44:37-48.
- Faktorovich EG, Steinberg RH, Yasumura D, Matthes MT, LaVail MM. 1990. Photoreceptor degeneration in inherited retinal dystrophy delayed by basic fibroblast growth factor. *Nature* 347:83-86.
- Famiglietti EV, Jr., Kolb H. 1975. A bistratified amacrine cell and synaptic circuitry in the inner plexiform layer of the retina. *Brain Res* 84:293-300.
- Fariss RN, Li Z-Y, Milam AH. 2000. Abnormalities in rod photoreceptors, amacrine cells, and horizontal cells in human retinas with retinitis pigmentosa. *Am J of Ophthalmol.* 129:215-223.
- Fei Y. 2002. Cone neurite sprouting: An early onset abnormality of the cone photoreceptors in the retinal degeneration mouse. *Mol Vis* 8:306-314.
- Feigenspan A, Gustincich S, Bean BP, Raviola E. 1998. Spontaneous activity of solitary dopaminergic cells of the retina. *J Neurosci* 18:6776-6789.
- Fernandez-Gonzalez A, La Spada AR, Treadaway J, Higdon JC, Harris BS, Sidman RL, Morgan JI, Zuo J. 2002. Purkinje cell degeneration (pcd) phenotypes caused by mutations in the axotomy-induced gene, *Nna1*.

- Science 295:1904-1906.
- Fintz AC, Audo I, Hicks D, Mohand-Said S, Leveillard T, Sahel J. 2003. Partial characterization of retina-derived cone neuroprotection in two culture models of photoreceptor degeneration. *Invest Ophthalmol Vis Sci* 44:818-825.
- Fletcher EL. 2000. Alterations in neurochemistry during retinal degeneration. *Microsc Res Tech* 50:89-102.
- Fletcher EL, Kalloniatis M. 1996. Neurochemical architecture of the normal and degenerating rat retina. *J Comp Neurol* 376:343-360.
- Fletcher EL, Kalloniatis M. 1997. Neurochemical development of the degenerating rat retina. *J Comp Neurol* 388:1-22.
- Frederick JM, Krasnoperova NV, Hoffmann K, Church–Kopish J, Rütther K, Howes K, Lem J, Baehr W. 2001. Mutant rhodopsin transgene expression on a null background. *Invest Ophthalmol Vis Sci* 42:826-833.
- Freed MA, Sterling P. 1988. The ON-alpha ganglion cell of the cat retina and its presynaptic cell types. *J Neurosci* 8:2303-2320.
- Fu KS, Landgrebe DA, Phillips TL. 1969. Information processing of remotely sensed agricultural data. In: *Proceedings of the IEEE*. p 639-653.
- Gadea A, Lopez-Colome AM. 2001. Glial transporters for glutamate, glycine, and GABA: II. GABA transporters. *J Neurosci Res* 63:461-468.
- Gal A, Li Y, Thompson DA, Weir J, Orth U, Jacobson SG, Apfelstedt-Sylla E, Vollrath D. 2000. Mutations in MERTK, the human orthologue of the RCS rat retinal dystrophy gene, cause retinitis pigmentosa. *Nat Genet* 26:270-271.
- Gordon S. 1980. Utilizing Landsat imagery to monitor land use change. *Remote Sensing of Environment* 9:189-196.
- Gouras P, Chader G, Enriques N, Gibbons RC. 1976. Calcium-induced spikes in cultured pigment epithelium of chick retina. *Invest Ophthalmol* 15:62-64.

- Gouras P, Du J, Kjeldbye H, Yamamoto S, Zack DJ. 1994. Long-term photoreceptor transplants in dystrophic and normal mouse retina. *Invest Ophthalmol Vis Sci* 35:3145-3153.
- Green ES, Stubbs JL, Levine EM. 2003. Genetic rescue of cell number in a mouse model of microphthalmia: interactions between Chx10 and G1-phase cell cycle regulators. *Development* 130:539-552.
- Grunert U, Martin PR, Wassle H. 1994. Immunocytochemical analysis of bipolar cells in the macaque monkey retina. *J Comp Neurol* 348:607-627.
- Grunert U, Wassle H. 1990. GABA-like immunoreactivity in the macaque monkey retina: a light and electron microscopic study. *J Comp Neurol* 297:509-524.
- Han Y, Zhang J, Slaughter MM. 1997. Partition of transient and sustained inhibitory glycinergic input to retinal ganglion cells. *J Neurosci* 17:3392-3400.
- Hartveit E, Brandstatter JH, Sassoe-Pognetto M, Laurie DJ, Seeburg PH, Wassle H. 1994. Localization and developmental expression of the NMDA receptor subunit NR2A in the mammalian retina. *J Comp Neurol* 348:570-582.
- Haverkamp S, Wassle H. 2000. Immunocytochemical analysis of the mouse retina. *J Comp Neurol* 424:1-23.
- Hendrickson AE, Koontz MA, Pourcho RG, Sarthy PV, Goebel DJ. 1988. Localization of glycine-containing neurons in the Macaca monkey retina. *J Comp Neurol* 273:473-487.
- Horner PJ, Gage FH. 2000. Regenerating the damaged central nervous system. *Nature* 407:963-970.
- <http://www.sph.uth.tmc.edu/RetNet/>. RetNet. In.
- Huang B, Karwoski CJ. 1992. Light-evoked expansion of subretinal space volume in the retina of the frog. *J Neurosci* 12:4243-4252.
- Humayun MS, de Juane EJ, Dagnelie G, Greenberg RJ, Propst RH, Phillips DH. 1996. Visual perception elicited by electrical stimulation of retina in blind humans. *Arch Ophthalmol* 114:40-46.

- Humayun MS, Prince M, de Juan EJ, Barron Y, Moskowitz M, Klock IB, Milam AH. 1999. Morphometric analysis of the extramacular retina from postmortem eyes with retinitis pigmentosa. *Invest Ophthalmol Vis Sci* 40.
- Humphries MM, Rancourt D, Farrar GJ, Kenna P, Hazel M, Bush RA, Sieving PA, Sheils DM, McNally N, Creighton P, Erven A, Boros A, Gulya K, Capecchi MR, Humphries P. 1997. Retinopathy induced in mice by targeted disruption of the rhodopsin gene. *Nat Genet* 15:216-219.
- Ishida AT, Stell WK, Lightfoot DO. 1980. Rod and cone inputs to bipolar cells in goldfish retina. *J Comp Neurol* 191:315-335.
- Iversen LL. 1984. The Ferrier Lecture, 1983. Amino acids and peptides: fast and slow chemical signals in the nervous system? *Proc R Soc Lond B Biol Sci* 221:245-260.
- Jacoby R, Stafford D, Kouyama N, Marshak D. 1996. Synaptic inputs to ON parasol ganglion cells in the primate retina. *J Neurosci* 16:8041-8056.
- Jean JC, Liu Y, Brown LA, Marc RE, Klings E, Joyce-Brady M. 2002. Gamma-glutamyl transferase deficiency results in lung oxidant stress in normoxia. *Am J Physiol Lung Cell Mol Physiol* 283:L766-776.
- Jeon CJ, Strettoi E, Masland RH. 1998. The major cell populations of the mouse retina. *J Neurosci* 18:8936-8946.
- Ji Q, Luo ZX, Yuan CX, Wible JR, Zhang JP, Georgi JA. 2002. The earliest known eutherian mammal. *Nature* 416:816-822.
- Johnson J, Chen TK, Rickman DW, Evans C, Brecha NC. 1996. Multiple gamma-Aminobutyric acid plasma membrane transporters (GAT-1, GAT-2, GAT-3) in the rat retina. *J Comp Neurol* 375:212-224.
- Jojich L, Pourcho RG. 1996. Glutamate immunoreactivity in the cat retina: a quantitative study. *Vis Neurosci* 13:117-133.
- Jones BW, Baehr W, Frederick JM, Marc RE. 2001. Aberrant remodeling of the neural retina in the GHL transgenic mouse. In: *ARVO Assoc Res Vision & Ophthalmology*. Ft. Lauderdale.
- Jones BW, Marc RE, Watt CB, Shaw MV, Yang JH. 2000. Biochemical Signature

- Analysis of the Human Ganglion Cell Layer. In: ARVO Assoc Res Vision & Ophthalmology. Ft. Lauderdale.
- Jones BW, Watt CB, Frederick JM, Baehr W, Chen CK, Levine EM, Milam AH, LaVail MM, Marc RE. 2003a. Retinal remodeling triggered by photoreceptor degenerations. *J Comp Neurol* 464:1-16.
- Jones BW, Watt CB, Marc RE. 2003b. Retinal remodeling triggered by light damage in the albino rat. In: ARVO Assoc Res Vision & Ophthalmology. Ft. Lauderdale.
- Jones EG, Pons TP. 1998. Thalamic and brainstem contributions to large-scale plasticity of primate somatosensory cortex. *Science* 282:1121-1125.
- Kalloniatis M. 1995. Amino acids in neurotransmission and disease. *J Am Optom Assoc* 66:750-757.
- Kalloniatis M, Fletcher EL. 1993. Immunocytochemical localization of the amino acid neurotransmitters in the chicken retina. *J Comp Neurol* 336:174-193.
- Kalloniatis M, Marc RE, Murry RF. 1996. Amino acid signatures in the primate retina. *J Neurosci* 16:6807-6829.
- Kalloniatis M, Napper GA. 1996. Glutamate metabolic pathways in displaced ganglion cells of the chicken retina. *J Comp Neurol* 367:518-536.
- Kalloniatis M, Tomisich G. 1999. Amino acid neurochemistry of the vertebrate retina. *Prog Retin Eye Res* 18:811-866.
- Kalloniatis M, Tomisich G, Marc RE. 1994. Neurochemical signatures revealed by glutamine labeling in the chicken retina. *Vis Neurosci* 11:793-804.
- Keeler C. 1966. Retinal degeneration in the mouse is rodless retina. *J Hered* 57:47-50.
- Kish PE, Fischer-Bovenkerk C, Ueda T. 1989a. Active transport of gamma-aminobutyric acid and glycine into synaptic vesicles. *Proc Natl Acad Sci U S A* 86:3877-3881.
- Kish PE, Kim SY, Ueda T. 1989b. Ontogeny of glutamate accumulating activity in

- rat brain synaptic vesicles. *Neurosci Lett* 97:185-190.
- Kolb H. 2003. How the retina works. *American Scientist* 91:28-35.
- Kolb H, Fernandez E, Schouten J, Ahnelt P, Linberg KA, Fisher SK. 1994. Are there three types of horizontal cell in the human retina? *J Comp Neurol* 343:370-386.
- Kolb H, Linberg KA, Fisher SK. 1992. Neurons of the human retina: a Golgi study. *J Comp Neurol* 318:147-187.
- Kolb H, Nelson R. 1983. Rod pathways in the retina of the cat. *Vision Res* 23:301-312.
- Kolb H, Nelson R, Mariani A. 1981. Amacrine cells, bipolar cells and ganglion cells of the cat retina: a Golgi study. *Vision Res* 21:1081-1114.
- Kumar-Singh R, Farber DB. 1998. Encapsidated adenovirus mini-chromosome-mediated delivery of genes to the retina: application to the rescue of photoreceptor degeneration. *Hum Mol Genet* 7:1893-1900.
- Lam DM, Li HB, Su YY, Watt CB. 1985. The signature hypothesis: co-localizations of neuroactive substances as anatomical probes for circuitry analyses. *Vision Res* 25:1353-1364.
- Landis SC. 1975. Histochemical demonstration of mitochondrial dehydrogenases in developing normal and nervous mutant mouse Purkinje cells. *J Histochem Cytochem* 23:136-143.
- Lasater EM. 1986. Ionic currents of cultured horizontal cells isolated from white perch retina. *J Neurophysiol* 55:499-513.
- LaVail MM, Sidman RL, Gerhardt CO. 1975. Congenic strains of RCS rats with inherited retinal dystrophy. *J Hered* 66:242-244.
- LaVail MM, White MP, Gorrin GM, Yasumura D, Porrello KV, Mullen RJ. 1993. Retinal degeneration in the nervous mutant mouse. I. Light microscopic cytopathology and changes in the interphotoreceptor matrix. *J Comp Neurol* 333:168-181.

- Lehre KP, Davanger S, Danbolt NC. 1997. Localization of the glutamate transporter protein GLAST in rat retina. *Brain Res* 744:129-137.
- Lem J, Makino CL. 1996. Phototransduction in transgenic mice. *Curr Opin Neurobiol* 6:453-458.
- Levine EM, Fuhrmann S, Reh TA. 2000. Soluble factors and the development of rod photoreceptors. *Cell Mol Life Sci* 57:224-234.
- Levitt JB, Schumer RA, Sherman SM, Spear PD, Movshon JA. 2001. Visual response properties of neurons in the LGN of normally reared and visually deprived macaque monkeys. *J Neurophysiol* 85:2111-2129.
- Lewis GP, Charteris DG, Sethi CS, Fisher SK. 2002. Animal models of retinal detachment and reattachment: identifying cellular events that may affect visual recovery. *Eye* 16:375-387.
- Lewis GP, Erickson PA, Guerin CJ, Anderson DH, Fisher SK. 1989. Changes in the expression of specific Müller cell proteins during long-term retinal detachment. *Exp Eye Res* 49:93-111.
- Li L, Turner JE. 1988. Inherited retinal dystrophy in the RCS rat: prevention of photoreceptor degeneration by pigment epithelial cell transplantation. *Exp Eye Res* 47:911-917.
- Li ZY, Kljavin IJ, Milam AH. 1995. Rod photoreceptor neurite sprouting in retinitis pigmentosa. *J Neurosci* 15:5429-5438.
- Liu IS, Chen JD, Ploder L, Vidgen D, van der Kooy D, Kalnins VI, McInnes RR. 1994. Developmental expression of a novel murine homeobox gene (Chx10): evidence for roles in determination of the neuroretina and inner nuclear layer. *Neuron* 13:377-393.
- Lund RD, Coffey PJ, Sauve Y, Lawrence JM. 1997. Intraretinal transplantation to prevent photoreceptor degeneration. *Ophthalmic Res.* 29:305-319.
- Machida S, Kondo M, Jamison JA, Khan NW, Kononen LT, Sugawara T, Bush RA, Sieving PA. 2000. P23H rhodopsin transgenic rat: correlation of retinal function with histopathology. *Invest Ophthalmol Vis Sci* 41:3200-3208.
- MacNeil MA, Heussy JK, Dacheux RF, Raviola E, Masland RH. 1999. The

- shapes and numbers of amacrine cells: matching of photofilled with Golgi-stained cells in the rabbit retina and comparison with other mammalian species. *J Comp Neurol* 413:305-326.
- MacNeil MA, Masland RH. 1998. Extreme diversity among amacrine cells: implications for function. *Neuron* 20:971-982.
- Malchow RP, Qian HH, Ripps H. 1989. gamma-Aminobutyric acid (GABA)-induced currents of skate Muller (glial) cells are mediated by neuronal-like GABAA receptors. *Proc Natl Acad Sci U S A* 86:4226-4230.
- Marc RE. 1999a. Kainate activation of horizontal, bipolar, amacrine, and ganglion cells in the rabbit retina. *J Comp Neurol* 407:65-76.
- Marc RE. 1999b. Mapping glutamatergic drive in the vertebrate retina with a channel-permeant organic cation. *J Comp Neurol* 407:47-64.
- Marc RE, Cameron D. 2001. A molecular phenotype atlas of the zebrafish retina. *J Neurocytol* 30:593-654.
- Marc RE, Jones BW. 2002a. Molecular phenotyping of retinal ganglion cells. *J Neurosci* 22:412-427.
- Marc RE, Jones BW. 2002b. Molecular phenotyping of retinal ganglion cells. *J Neurosci* 22:413-427.
- Marc RE, Jones BW, Yang JH, Shaw MV, Milam AH. 2001. Molecular phenotyping of the neural retina in retinitis pigmentosa. *Invest Ophthalmol Vis Sci* 42:S117.
- Marc RE, Liu W. 2000. Fundamental GABAergic amacrine cell circuitries in the retina: nested feedback, concatenated inhibition, and axosomatic synapses. *J Comp Neurol* 425:560-582.
- Marc RE, Liu WL, Kalloniatis M, Raiguel SF, van Haesendonck E. 1990. Patterns of glutamate immunoreactivity in the goldfish retina. *J Neurosci* 10:4006-4034.
- Marc RE, Murry RF, Basinger SF. 1995. Pattern recognition of amino acid signatures in retinal neurons. *J Neurosci* 15:5106-5129.

- Marc RE, Murry RF, Fisher SK, Linberg KA, Lewis GP. 1998a. Amino acid signatures in the detached cat retina. *Invest Ophthalmol Vis Sci* 39:1694-1702.
- Marc RE, Murry RF, Fisher SK, Linberg KA, Lewis GP, Kalloniatis M. 1998b. Amino acid signatures in the normal cat retina. *Invest Ophthalmol Vis Sci* 39:1685-1693.
- Marshall GE, Konstas AG, Bechrakis NE, Lee WR. 1992. An immunoelectron microscope study of the aged human lens capsule. *Exp Eye Res* 54:393-401.
- Martin PR, Grunert U. 1992. Spatial density and immunoreactivity of bipolar cells in the macaque monkey retina. *J Comp Neurol* 323:269-287.
- Masland RH. 2001a. The fundamental plan of the retina. *Nat Neurosci* 4:877-886.
- Masland RH. 2001b. Neuronal diversity in the retina. *Current opinion in neurobiology* 11:431-436.
- Massey SC, Mills SL, Marc RE. 1992. All indoleamine-accumulating cells in the rabbit retina contain GABA. *J Comp Neurol* 322:275-291.
- Massey SC, Redburn DA. 1987. Transmitter circuits in the vertebrate retina. *Prog Neurobiol* 28:55-96.
- Masu M, Iwakabe H, Tagawa Y, Miyoshi T, Yamashita M, Fukuda Y, Sasaki H, Hiroi K, Nakamura Y, Shigemoto R, et al. 1995. Specific deficit of the ON response in visual transmission by targeted disruption of the mGluR6 gene. *Cell* 80:757-765.
- Maycox PR, Deckwerth T, Hell JW, Jahn R. 1988. Glutamate uptake by brain synaptic vesicles. Energy dependence of transport and functional reconstitution in proteoliposomes. *J Biol Chem* 263:15423-15428.
- McGuire BA, Stevens JK, Sterling P. 1984. Microcircuitry of bipolar cells in cat retina. *J Neurosci* 4:2920-2938.
- Michal G, Michal G. Michal Gs. 1999. Biochemical pathways an atlas of

- biochemistry and molecular biology. New York: John Wiley & Sons.
- Milam AH, Li ZY, Fariss RN. 1998. Histopathology of the human retina in retinitis pigmentosa. *Prog Ret Eye Res* 17.
- Mills SL, Massey SC. 1995. Differential properties of two gap junctional pathways made by All amacrine cells. *Nature* 377:734-737.
- Mohand-Said S, Deudon-Combe A, Hicks D, Simonutti M, Forster V, Fintz A-C, Lèveillard T, Dreyfus H, Sahel J-A. 1998. Normal retina releases a diffusible factor stimulating cone survival in the retinal degeneration mouse. *Proc. Natl. Acad. Sci.* 95:8357–8362.
- Morin LP, Blanchard JH, Provincio I. 2003. Retinal ganglion cell projections to the hamster suprachiasmatic nucleus, intergeniculate leaflet, and visual midbrain: Bifurcation and melanopsin immunoreactivity. *J Comp Neurol* 465:401-416.
- Mullen RJ, LaVail M. 1975. Two types of retinal degeneration in cerebellar mutant mice. *Nature* 258:528-530.
- Muller JF, Marc RE. 1990. GABA-ergic and glycinergic pathways in the inner plexiform layer of the goldfish retina. *J Comp Neurol* 291:281-304.
- Mural RJ, Adams MD, Myers EW, Smith HO, Miklos GL, Wides R, Halpern A, Li PW, Sutton GG, Nadeau J, Salzberg SL, Holt RA, Kodira CD, Lu F, Chen L, Deng Z, Evangelista CC, Gan W, Heiman TJ, Li J, Li Z, Merkulov GV, Milshina NV, Naik AK, Qi R, Shue BC, Wang A, Wang J, Wang X, Yan X, Ye J, Yooseph S, Zhao Q, Zheng L, Zhu SC, Biddick K, Bolanos R, Delcher AL, Dew IM, Fasulo D, Flanigan MJ, Huson DH, Kravitz SA, Miller JR, Mobarry CM, Reinert K, Remington KA, Zhang Q, Zheng XH, Nusskern DR, Lai Z, Lei Y, Zhong W, Yao A, Guan P, Ji RR, Gu Z, Wang ZY, Zhong F, Xiao C, Chiang CC, Yandell M, Wortman JR, Amanatides PG, Hladun SL, Pratts EC, Johnson JE, Dodson KL, Woodford KJ, Evans CA, Gropman B, Rusch DB, Venter E, Wang M, Smith TJ, Houck JT, Tompkins DE, Haynes C, Jacob D, Chin SH, Allen DR, Dahlke CE, Sanders R, Li K, Liu X, Levitsky AA, Majoros WH, Chen Q, Xia AC, Lopez JR, Donnelly MT, Newman MH, Glodek A, Kraft CL, Nodell M, Ali F, An HJ, Baldwin-Pitts D, Beeson KY, Cai S et al. 2002. A comparison of whole-genome shotgun-derived mouse chromosome 16 and the human genome. *Science* 296:1661-1671.

- Murashima YL, Ishikawa T, Kato T. 1990. gamma-Aminobutyric acid system in developing and degenerating mouse retina. *J Neurochem* 54:893-898.
- Naash MI, Ripps H, Li S, Goto Y, Peachey NS. 1996. Polygenic disease and retinitis pigmentosa: albinism exacerbates photoreceptor degeneration induced by the expression of a mutant opsin in transgenic mice. *J Neurosci* 16:7853-7858.
- Nawy S, Jahr CE. 1990a. Suppression by glutamate of cGMP-activated conductance in retinal bipolar cells. *Nature* 346:269-271.
- Nawy S, Jahr CE. 1990b. Time-dependent reduction of glutamate current in retinal bipolar cells. *Neurosci Lett* 108:279-283.
- Nawy S, Jahr CE. 1991. cGMP-gated conductance in retinal bipolar cells is suppressed by the photoreceptor transmitter. *Neuron* 7:677-683.
- Nelson R, von Litzow A, Kolb H, Gouras P. 1975. Horizontal cells in cat retina with independent dendritic systems. *Science* 189:137-139.
- Newman E, Reichenbach A. 1996. The Müller cell: a functional element of the retina. *Trends Neurosci* 19:307-312.
- Normann RA, Maynard EM, Rousche PJ, Warren DJ. 1999. A neural interface for a cortical vision prosthesis. *Vision Res* 39:2577-2587.
- Okano T, Fukada Y, Yoshizawa T. 1995. Molecular basis for tetrachromatic color vision. *Comp Biochem Physiol B Biochem Mol Biol* 112:405-414.
- Okano T, Kojima D, Fukada Y, Shichida Y, Yoshizawa T. 1992. Primary structures of chicken cone visual pigments: vertebrate rhodopsins have evolved out of cone visual pigments. *Proc Natl Acad Sci U S A* 89:5932-5936.
- Orr HT, Cohen AI, Carter JA. 1976. The levels of free taurine, glutamate, glycine and gamma-amino butyric acid during the postnatal development of the normal and dystrophic retina of the mouse. *Exp Eye Res* 23:377-384.
- Otori Y, Shimada S, Tanaka K, Ishimoto I, Tano Y, Tohyama M. 1994. Marked increase in glutamate-aspartate transporter (GLAST/GluT-1) mRNA

- following transient retinal ischemia. *Brain Res Mol Brain Res* 27:310-314.
- Oyster CW, Simpson JI, Takahashi ES, Soodak RE. 1980. Retinal ganglion cells projecting to the rabbit accessory optic system. *J Comp Neurol* 190:49-61.
- Packer OS, Dacey DM. 2002. Receptive field structure of H1 horizontal cells in macaque monkey retina. *J Vis* 2:272-292.
- Peng YW, Hao Y, Petters RM, Wong F. 2000. Ectopic synaptogenesis in the mammalian retina caused by rod photoreceptor-specific mutations. *Nat Neurosci* 3:1121-1127.
- Piccolino M, Neyton J, Gerschenfeld HM. 1984. Decrease of gap junction permeability induced by dopamine and cyclic adenosine 3':5'-monophosphate in horizontal cells of turtle retina. *J Neurosci* 4:2477-2488.
- Pittler SJ, Keeler CE, Sidman RL, Baehr W. 1993. PCR analysis of DNA from 70-year-old sections of rodless retina demonstrates identity with the mouse rd defect. *Proc Natl Acad Sci U S A* 90:9616-9619.
- Pourcho RG. 1996. Neurotransmitters in the retina. *Curr Eye Res* 15:797-803.
- Pourcho RG, Goebel DJ. 1983. Neuronal subpopulations in cat retina which accumulate the GABA agonist, (3H)muscimol: a combined Golgi and autoradiographic study. *J Comp Neurol* 219:25-35.
- Pow DV, Crook DK. 1996. Direct immunocytochemical evidence for the transfer of glutamine from glial cells to neurons: use of specific antibodies directed against the d-stereoisomers of glutamate and glutamine. *Neuroscience* 70:295-302.
- Pow DV, Robinson SR. 1994. Glutamate in some retinal neurons is derived solely from glia. *Neuroscience* 60:355-366.
- Reh TA, Levine EM. 1998. Multipotential stem cells and progenitors in the vertebrate retina. *J Neurobiol* 36:206-220.
- Reichenbach A, Wohlrab F. 1986. Morphometric parameters of Müller (glial) cells dependent on their topographic localization in the nonmyelinated part of the

- rabbit retina. A consideration of functional aspects of radial glia. *J Neurocytol* 15:451-459.
- Riepe RE, Norenburg MD. 1977. Müller cell localisation of glutamine synthetase in rat retina. *Nature* 268:654-655.
- Robb RM, Silver J, Sullivan RT. 1978. Ocular retardation (or) in the mouse. *Invest Ophthalmol Vis Sci* 17:468-473.
- Rodieck RW, Binmoeller KF, Dineen J. 1985. Parasol and midget ganglion cells of the human retina. *J Comp Neurol* 233:115-132.
- Salceda R, Saldana MR. 1993. Glutamate and taurine uptake by retinal pigment epithelium during rat development. *Comp Biochem Physiol C* 104:311-316.
- Santos A, Humayun MS, de Juan EJ, Greenburg RJ, Marsh MJ, Klock IB, Milam AH. 1997. Preservation of the inner retina in retinitis pigmentosa. A morphometric analysis. *Arch Ophthalmol* 115:511-515.
- Sauve Y, Girman SV, Wang S, Keegan DJ, Lund RD. 2002. Preservation of visual responsiveness in the superior colliculus of RCS rats after retinal pigment epithelium cell transplantation. *Neuroscience* 114:389-401.
- Scarlatis G. 2000. Optical prosthesis: visions of the future. *MSJAMA* 283:2297.
- Schmut O. 1978. The organization of tissues of the eye by different collagen types. *Albrecht Von Graefes Arch Klin Exp Ophthalmol* 207:189-199.
- Schneeweis DM, Schnapf JL. 1995. Photovoltage of rods and cones in the macaque retina. *Science* 268:1053-1056.
- Smith RG, Freed MA, Sterling P. 1986. Microcircuitry of the dark-adapted cat retina: functional architecture of the rod-cone network. *J Neurosci* 6:3505-3517.
- Steinberg R, Flannery J, Naash M, Oh P, Matthes M, Yasumura D, Lau-Villacorta C, Chen J, LaVail M. 1996. Transgenic rat models of inherited retinal degeneration caused by mutant opsin genes. *Invest Ophthalmol Vis Sci* 37.
- Stone JL, Barlow WE, Humayun MS, de Juan EJ, Milam AH. 1992. Morphometric analysis of macular photoreceptors and ganglion cells in retinas with retinitis

- pigmentosa. *Arch Ophthalmol* 110:1634-1639.
- Storm-Mathisen J, Leknes AK, Bore AT, Vaaland JL, Edminson P, Haug FM, Ottersen OP. 1983. First visualization of glutamate and GABA in neurones by immunocytochemistry. *Nature* 301:517-520.
- Strettoi E, Dacheux RF, Raviola E. 1990. Synaptic connections of rod bipolar cells in the inner plexiform layer of the rabbit retina. *J Comp Neurol* 295:449-466.
- Strettoi E, Masland RH. 1995. The organization of the inner nuclear layer of the rabbit retina. *J Neurosci* 15:875-888.
- Strettoi E, Pignatelli V. 2000. Modifications of retinal neurons in a mouse model of retinitis pigmentosa. *Proc Natl Acad Sci* 97:11020-11025.
- Strettoi E, Pignatelli V, Rossi C, Porciatti V, Falsini B. 2003. Remodeling of second-order neurons in the retina of rd/rd mutant mice. *Vision Res* 43:867-877.
- Strettoi E, Porciatti V, Falsini B, Pignatelli V, Rossi C. 2002. Morphological and functional abnormalities in the inner retina of the rd/rd mouse. *J Neurosci* 22:5492-5504.
- Strettoi E, Raviola E, Dacheux RF. 1992. Synaptic connections of the narrow-field, bistratified rod amacrine cell (All) in the rabbit retina. *J Comp Neurol* 325:152-168.
- Sullivan R, Penfold P, Pow DV. 2003. Neuronal migration and glial remodeling in degenerating retinas of aged rats and in nonneovascular AMD. *Invest Ophthalmol Vis Sci* 44:856-865.
- Taxt T, Lundervold A. 1994. Multispectral analysis of the brain in magnetic resonance imaging. In: *IEEE Workshop on Biomedical Image Analysis*. PAMI. p 33-42.
- Terada N, Hamazaki T, Oka M, Hoki M, Mastalerz DM, Nakano Y, Meyer EM, Morel L, Petersen BE, Scott EW. 2002. Bone marrow cells adopt the phenotype of other cells by spontaneous cell fusion. *Nature* 415:429-434.

- Thomas JW, Touchman JW, Blakesley RW, Bouffard GG, Beckstrom-Sternberg SM, Margulies EH, Blanchette M, Siepel AC, Thomas PJ, McDowell JC, Maskeri B, Hansen NF, Schwartz MS, Weber RJ, Kent WJ, Karolchik D, Bruen TC, Bevan R, Cutler DJ, Schwartz S, Elnitski L, Idol JR, Prasad AB, Lee-Lin SQ, Maduro VV, Summers TJ, Portnoy ME, Dietrich NL, Akhter N, Ayele K, Benjamin B, Cariaga K, Brinkley CP, Brooks SY, Granite S, Guan X, Gupta J, Haghighi P, Ho SL, Huang MC, Karlins E, Laric PL, Legaspi R, Lim MJ, Maduro QL, Masiello CA, Mastrian SD, McCloskey JC, Pearson R, Stantripop S, Tiongson EE, Tran JT, Tsurgeon C, Vogt JL, Walker MA, Wetherby KD, Wiggins LS, Young AC, Zhang LH, Osoegawa K, Zhu B, Zhao B, Shu CL, De Jong PJ, Lawrence CE, Smit AF, Chakravarti A, Haussler D, Green P, Miller W, Green ED. 2003. Comparative analyses of multi-species sequences from targeted genomic regions. *Nature* 424:788-793.
- Tian N, Copenhagen DR. 2001. Visual deprivation alters development of synaptic function in inner retina after eye opening. *Neuron* 32:439-449.
- Trexler EB, Li W, Mills SL, Massey SC. 2001. Coupling from All amacrine cells to ON cone bipolar cells is bidirectional. *J Comp Neurol* 437:408-422.
- Tsukamoto Y, Masarachia P, Schein SJ, Sterling P. 1992. Gap junctions between the pedicles of macaque foveal cones. *Vision Res* 32:1809-1815.
- Tsukamoto Y, Morigiwa K, Ueda M, Sterling P. 2001. Microcircuits for night vision in mouse retina. *J Neurosci* 21:8616-8623.
- van Nie R, Ivanyi D, Demant P. 1978. A new H-2-linked mutation, *rds*, causing retinal degeneration in the mouse. *Tissue Antigens* 12:106-108.
- Vaney DI. 1980. A quantitative comparison between the ganglion cell populations and axonal outflows of the visual streak and periphery of the rabbit retina. *J Comp Neurol* 189:215-233.
- Vaney DI, Young HM. 1988. GABA-like immunoreactivity in cholinergic amacrine cells of the rabbit retina. *Brain Res* 438:369-373.

- Villegas-Perez MP, Lawrence JM, Vidal-Sanz M, Lavail MM, Lund RD. 1998. Ganglion cell loss in RCS rat retina: a result of compression of axons by contracting intraretinal vessels linked to the pigment epithelium. *J Comp Neurol* 392:58-77.
- Von Noorden GK, Crawford MLJ. 1978. Morphological and physiological changes in the monkey visual system after short-term lid suture. *Investigative Ophthalmology and Visual Science* 17:762-768.
- Wagner HJ, Wagner E. 1988. Amacrine cells in the retina of a teleost fish, the roach (*Rutilus rutilus*): a Golgi study on differentiation and layering. *Philos Trans R Soc Lond B Biol Sci* 321:263-324.
- Wassle H, Grunert U, Chun MH, Boycott BB. 1995. The rod pathway of the macaque monkey retina: identification of All-amacrine cells with antibodies against calretinin. *J Comp Neurol* 361:537-551.
- Waterston RH, Lindblad-Toh K, Birney E, Rogers J, Abril JF, Agarwal P, Agarwala R, Ainscough R, Alexandersson M, An P, Antonarakis SE, Attwood J, Baertsch R, Bailey J, Barlow K, Beck S, Berry E, Birren B, Bloom T, Bork P, Botcherby M, Bray N, Brent MR, Brown DG, Brown SD, Bult C, Burton J, Butler J, Campbell RD, Carninci P, Cawley S, Chiaromonte F, Chinwalla AT, Church DM, Clamp M, Clee C, Collins FS, Cook LL, Copley RR, Coulson A, Couronne O, Cuff J, Curwen V, Cutts T, Daly M, David R, Davies J, Delehaunty KD, Deri J, Dermitzakis ET, Dewey C, Dickens NJ, Diekhans M, Dodge S, Dubchak I, Dunn DM, Eddy SR, Elnitski L, Emes RD, Eswara P, Eyas E, Felsenfeld A, Fewell GA, Flicek P, Foley K, Frankel WN, Fulton LA, Fulton RS, Furey TS, Gage D, Gibbs RA, Glusman G, Gnerre S, Goldman N, Goodstadt L, Grafham D, Graves TA, Green ED, Gregory S, Guigo R, Guyer M, Hardison RC, Haussler D, Hayashizaki Y, Hillier LW, Hinrichs A, Hlavina W, Holzer T, Hsu F, Hua A, Hubbard T, Hunt A, Jackson I, Jaffe DB, Johnson LS, Jones M, Jones TA, Joy A, Kamal M, Karlsson EK et al. 2002. Initial sequencing and comparative analysis of the mouse genome. *Nature* 420:520-562.
- Weleber R, Gregory-Evans K. 2001. Retinitis pigmentosa and allied disorders. In: Ogden TE, Hinton DR, Editors. *Retina: basic science, inherited disease and tumors*. St Louis: Mosby. p 362-460.

- Wu SM, Yang XL. 1988. Electrical coupling between rods and cones in the tiger salamander retina. *Proc Natl Acad Sci U S A* 85:275-278.
- Xin D, Bloomfield SA. 1997. Tracer coupling pattern of amacrine and ganglion cells in the rabbit retina. *J Comp Neurol* 383:512-528.
- Xu J, Dodd RL, Makino CL, Simon MI, Baylor DA, Chen J. 1997. Prolonged photoresponses in transgenic mouse rods lacking arrestin. *Nature* 389:505-509.
- Yazulla S, Studholme KM, Pinto LH. 1997. Differences in the retinal GABA system among control, spastic mutant and retinal degeneration mutant mice. *Vision Res* 37:3471-3482.
- Young MJ, Ray J, Whiteley SJO, Klassen H, Gage FH. 2000. Neuronal differentiation and morphological integration of hippocampal progenitor cells transplanted to the retina of immature and mature dystrophic rats. *Mol Cell Neurosci* 16:197-205.
- Yu DY, Cringle SJ. 2001. Oxygen distribution and consumption within the retina in vascularised and avascular retinas and in animal models of retinal disease. *Prog Retin Eye Res* 20:175-208.
- Zrenner E. 2002. Will retinal implants restore vision? *Science* 295:1022-1025.
- Zrenner E, Gabel VP, Haemmerle H, Hoefflinger B, Shubert M. 1998. Subretinal implants. *Ophthalmic Res*. 30:197-198.
- Zwas F, Alpern M. 1976. The density of human rhodopsin in the rods. *Vision Res* 16:121-127.